A Thesis for the Degree of Doctor of Philosophy in Pharmacy

Structure Determination of Secondary Metabolites from Marine-Derived *Aspergillus* and *Penicillium* Fungi

August 2021

by
Sung Chul Park

Natural Products Science Major, College of Pharmacy
Doctoral Course in the Graduate School
Seoul National University

Structure Determination of Secondary Metabolites from Marine-Derived *Aspergillus* and *Penicillium* Fungi

해양 유래 진균 *Aspergillus* 와 *Penicillium*의
이차대사물질에 대한 연구

지도교수 신 종 헌

이 논문을 약학박사학위논문으로 제출함

2021 년 8월

서울대학교 대학원
약학대학 약학과
박 성 철

박성철의 박사학위논문을 인준함

2021 년 6월

위 원 장	오 동 찬
부 위 원 장	오 기 봉
위 원	심 상 희
위 원	남 상 집
위 원	신 종 헌

Abstract

Structure Determination of Secondary Metabolites from Marine-Derived *Aspergillus* and *Penicillium* Fungi

Sung Chul Park
Natural Products Science Major
College of Pharmacy
Doctoral Course in the Graduate School
Seoul National University

Bioactive natural products produced by microbes have been playing a key role in drug discovery. At the same time, due to the increment in drug resistance, chemical compounds with new carbon skeletons are urgently required. Today, the most impressive remaining frontiers are largely microbial, and exploring unique and uninvestigated environments with suitably improved microbiological and chemical techniques.

Among them, marine fungi have been recognized as a new source of bioactive secondary metabolites, since 1990s. Nowadays, fungi becomes one of the dominant group of prolific source of novel compounds. While the microbial and chemical techniques are improving, the unique and uninvestigated environment is exploring. Because the marine has wide variation of environmental conditions, the marine-derived microbes also produce unique bioactive secondary metabolites to adapt to the environment. Thus, the marine-derive fungi become promising sources for structurally novel bioactive compounds.

The purpose of this study is to investigate new marine-derived fungal bioactive natural products and determine their physical, chemical, and biological properties.

During the course of searching for novel bioactive secondary metabolites from marine-derived fungi, over 600 fungal strains were collected from the marine environments. *Aspergillus ochraceopetalifumis*, *Penicillium herquei*, and *Aspergillus* sp. (strain F452) were selected for chemical investigation based on chemical analyses and bioassay screening of the crude extracts and the partitioned fractions. Secondary metabolites from the selected fungal strains were isolated through chromatographic

methods. As a result, 9 new compounds and 14 known compounds were structurally determined using combined spectroscopic analyses and chemical, computational approaches. The structures of 23 compounds belonged to various structural classes with diverse biogenetic origins: a mixed-biogenetic salt and its components, phenalenones, polyketides, alkaloids, and fumiquinazolines. All isolated compounds have been examined under various bioactivities: cytotoxicity, anti-angiogenic activity, antimicrobial activities, adiponectin secretion- stimulating activity, and inhibition against the enzymes isocitrate lyase (ICL) and sortase A (SrtA). Some of the isolated compounds showed potent bioactivities.

1. Ochraceopetalin, a Mixed-Biogenic Salt of Polyketide and Amino Acid Origins from a Marine-Derived *Aspergillus ochraceopetaliformis* Fungus

Ochraceopetalin (**1**), a mixed-biogenetic salt compound, and its component **2** were isolated from the culture broths of a marine-derived fungus, *Aspergillus ochraceopetaliformis*. Based on combined spectroscopic and chemical analyses, the structure of **1** was determined to be a sulfonated diphenylether-aminol-amino acid ester guanidinium salt of an unprecedented structural class, while **2** was determined to be the

corresponding sulfonated diphenylether. Ochraceopetaguanidine (**3**), the other guanidine-bearing aminol amino acid ester component, was also prepared and structurally elucidated. Compound **1** exhibited significant cytotoxicity against K562 and A549 cells.

2. Phenalenones from a Marine-Derived *Penicillium* sp. Fungus

Six new phenalenone derivatives (**5**-**10**) along with five known compounds (**11**-**15**) of the herqueinone class were isolated from a marine-derived *Penicillium* sp. fungus. The absolute configurations of these compounds were assigned based on chemical modifications and their specific rotations. 4-Hydroxy-sclerodin (**10**) and an acetone adduct of triketone (**11**) exhibited moderate anti-angiogenetic and anti-inflammatory activities, respectively, while *ent*-peniciherqueinone (**5**) and isoherqueinone (**13**) exhibited moderate abilities to induce adipogenesis without cytotoxicity.

3. Sortase A-Inhibitory Metabolites from a Marine-Derived Fungus *Aspergillus* sp.

Seven alkaloidal compounds (**17**–**23**) and one polyketide (**16**) were isolated from a semisolid rice culture of the marine-derived fungus *Aspergillus* sp. F452. Structures of the isolated compounds were elucidated based on spectroscopic data and comparisons with previously reported data. The alkaloidal compounds (**17**–**23**) displayed weak to moderate inhibitory activities against *Staphylococcus aureus*-derived sortase A (SrtA), a transpeptidase responsible for anchoring surface proteins to the peptidoglycan cell wall in Gram-positive bacteria, without affecting cell viability. Aspermytin A (**16**) strongly inhibited SrtA activity, with an IC_{50} value of 146.0 μM, and significantly reduced bacterial adherence to fibronectin-coated surfaces. The present results indicate that the underlying mechanism of action of compound **16** is associated with the inhibition of SrtA-mediated *S. aureus* adhesion to fibronectin, thus potentially serving as an SrtA inhibitor.

Key words: marine natural products, marine-derived fungi, *Aspergillus* sp., *Penicillium* sp., structure determination

Student number: 2015-23182

List of Contents

List of Tables

List of Figures

I. Introduction

Bioactive natural products produced by microbes have been playing a key role in drug discovery.[1] At the same time, due to the increment in drug resistance, chemical compounds with new carbon skeletons are urgently required. Today, the most impressive remaining frontiers are largely microbial, and exploring unique and uninvestigated environments with suitably improved microbiological and chemical techniques.

Among them, marine fungi have been recognized as a new source of bioactive secondary metabolites, since 1990s. According to the marine natural products review from *Natrual Product Reports*, more than 400 novel compounds were isolated from marine fungi between 1985 and 2014.[2,3] (Figure 1) Nowadays, fungi becomes one of the dominant group of prolific source of novel compounds.

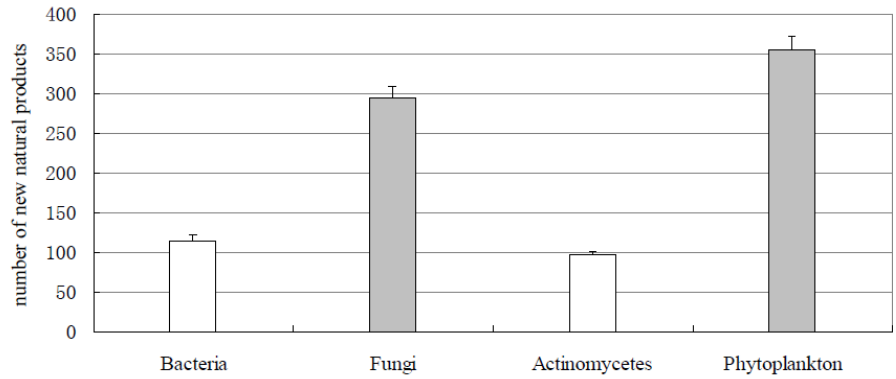

Figure 1. Number of novel compounds isolated from marine microorganisms between 1985 and 2008.[2]

From the search with the keyword ‘marine fungi’ in SciFinder, the number of papers related to marine fungi is dramatically increasing (Figure 2). While the microbial and chemical techniques are improving, the unique and uninvestigated environment is exploring. Because the marine has wide variation of environmental conditions, the marine-derived microbes also produce unique bioactive secondary metabolites to adapt to the environment. Thus, the marine-derive fungi become promising sources for structurally novel bioactive compounds.

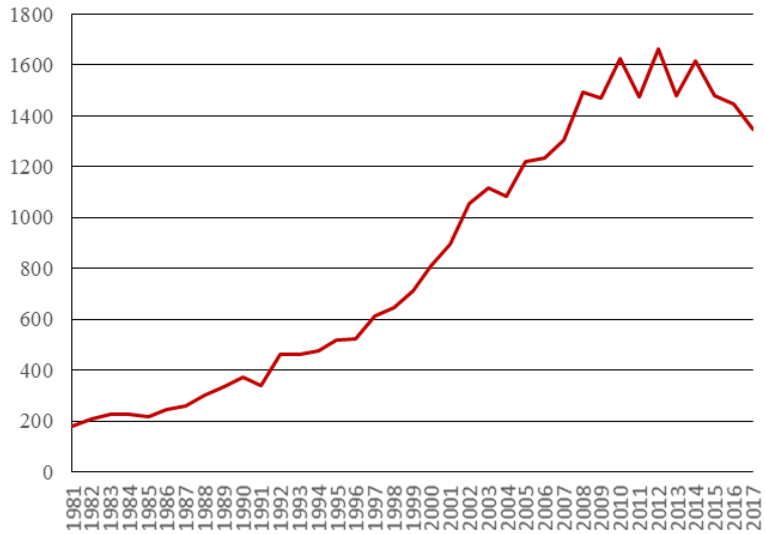

Figure 2. Number of papers found in SciFinder with the keyword 'marine fungi.'

To date, there are some examples of bioactive secondary metabolites derived from marine fungi (Figure 3). Cephalosporin C, isolated from *Acremonium chrysogenum* is an antibiotic drug. It is widely used as penicillin substitute to treat bacterial infection. Plinaculin, isolated from *Aspergillus* sp., is an anticancer drug for non-small cell lung cancer. It is in phase 3 clinical trial. Halovir A, *Scytalidium* sp., has an antiviral activity against HSV-1 and HSV-2. Asperphenin, which is a lipopeptidyl benzophenone, has an antitumor activity against human colorectal cancer cell.

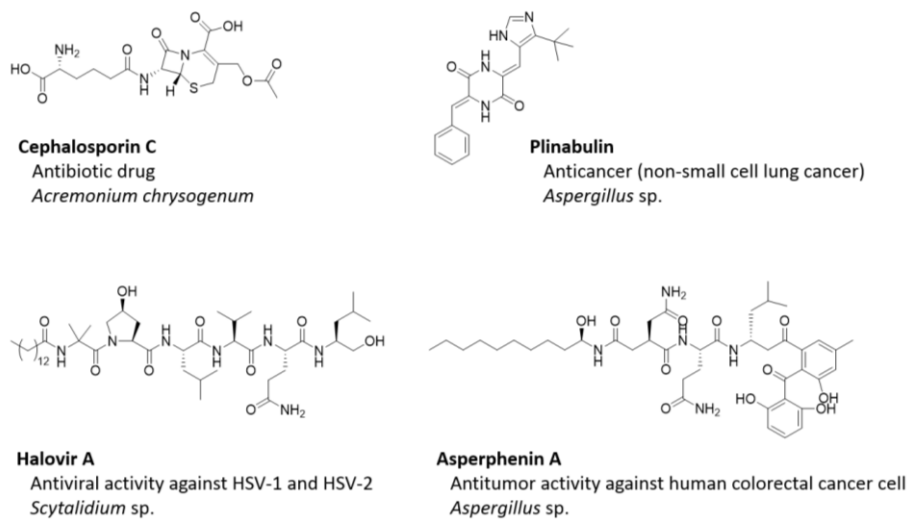

Figure 3. Examples of bioactive secondary metabolites derived from marine fungi.

The purpose of this study is to investigate new marine-derived fungal bioactive natural products and determine their physical, chemical, and biological properties.

During the course of searching for novel bioactive secondary metabolites from marine-derived fungi, over 600 fungal strains were collected from the marine environments. *Aspergillus ochraceopetalifumis*, *Penicillium herquei*, and *Aspergillus* sp. (strain F452) were selected for chemical investigation based on chemical analyses and bioassay screening of the crude extracts and the partitioned fractions. Secondary metabolites

from the selected fungal strains were isolated through chromatographic methods. As a result, 9 new compounds and 14 known compounds were structurally determined using combined spectroscopic analyses and chemical, computational approaches. The structures of 23 compounds belonged to various structural classes with diverse biogenetic origins: a mixed-biogenetic salt and its components, phenalenones, polyketides, alkaloids, and fumiquinazolines. All isolated compounds have been examined under various bioactivities: cytotoxicity, anti-angiogenic activity, antimicrobial activities, adiponectin secretion- stimulating activity, and inhibition against the enzymes isocitrate lyase (ICL) and sortase A (SrtA). Some of the isolated compounds showed potent bioactivities.

II. Ochraceopetalin, a Mixed-Biogenetic Salt of Polyketide and Amino Acid Origins from a Marine-Derived *Aspergillus ochraceopetaliformis* Fungus

1-1. Introduction

Metabolites of polyketide pathways are widely recognized as an important class of fungal natural products due to their significant structural and functional diversities, as well as their wide taxonomical distribution.[4,5] Attributed from the potent bioac-tivity, several fungal polyketides have been used as lead compounds in the pharma-ceutical industry, which culminates to occupy 20% of the major commercial drugs by these compounds, such as lovastatin and griseofulvin.[6–8] Tetraketide-derived diphenyl ethers are structurally distinctive from other subclasses of fungal polyketides in terms of their formation by the condensation of two polyketide derivatives.[9] Amidst their wide natural distribution, diphenyl ethers are frequently obtained from marine microorganisms, especially from filamentous fungi of the genera *Aspergillus* and *Penicillium*.[10,11] These compounds possess diverse bioactivities, including antibacterial, cytotoxic, enzyme inhibitory and antiviral activities.[12] Accordingly, these compounds are increasingly applied in cosmetics, pharmaceutical

intermediates and chemical products, which in turn have led to extensive studies on their biosynthesis.[12] Recently, a detailed biosynthetic pathway with the gene cluster and key enzyme sys-tem was unveiled for diorcinol, which is a representative of fungal diphenyl ethers, in a marine-derived *A. nidulans* strain.[9,12]

In the process of searching for bioactive compounds from marine-derived fungi, my group recently reported the structures of two new sortase A-inhibitory depsihexapeptides from an *Aspergillus ochraceopetaliformis* fungus, collected from underwater sediment off the coast of Jeju-do, Korea.[13] However, LC–UV and LC–ESI–MS analyses, aided by an in-house spectral library of fungal extracts, revealed the presence of a natural product with distinct structural motifs in a liquid culture broth of this strain. More interestingly, the same analyses of this strain from a rice-based semi-solid culture broth revealed the presence of a structurally related but fragmented compound, prompting an extensive chemical investigation.

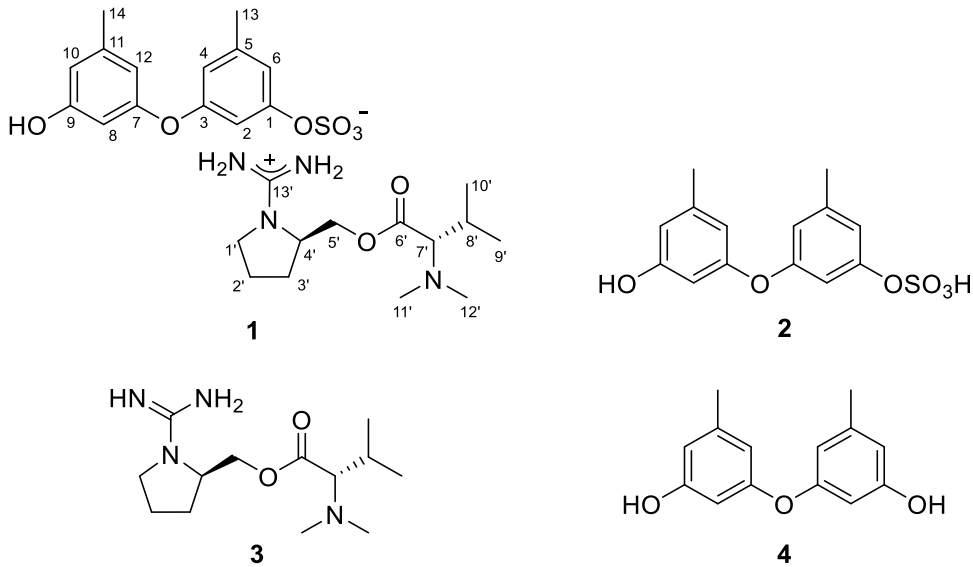

Figure 4. Chemical structures of compounds **1**–**4**.

Herein, I report the structures of ochraceopetalin (**1**), a novel sulfonated diphenylether-aminol-amino acid guanidinium salt and its aromatic component (**2**) (Figure 4). In the process of isolation and structure determination, ochraceopetaguanidine (**3**), a guanidine-bearing aminol amino acid, was structurally elucidated as the other component of **1**. Organic salts coupled with organic counterions are occasionally found in marine organisms: psammaplins, bromotyrosines and dihydroxystyrenes, from an association of *Poecillastra* sp. and *Jaspis* sp. sponges[14–16]; suvanines, from a *Coscinoderma mathewsi* sponge[17]; sesterterpene sulfates, from a *Ircinia* sp. sponge[18]; iodotyramine derivative, from the *Didemnum rubem* ascidian.[19,20] To the best of my knowledge, **1**

would be the first of this kind to be obtained from marine-derived fungi. Furthermore, its mixed-biogenetic salt formation, that is derived from polyketide and amino acid pathways, would be remarkably unprecedented. Compound **1** exhibited noticeably stronger cytotoxicity toward the human cancer cell lines K562 and A549 than the other compounds.

1-2. Results and discussion

The molecular formula of compound **1** obtained from the YMM liquid culture broth was deduced to be $C_{27}H_{40}N_4O_8S$, with 11 degrees of unsaturation, by positive HR–ESI–MS analysis ($[M + H]^+$ *m/z* 581.2628, calcd 581.2640). This positive mode MS analysis also gave a highly conspicuous cluster of $C_{13}H_{27}N_4O_2$ (*m/z* 271.2123, calcd 271.2129), while a similar analysis in negative mode gave a conspicuous cluster of $C_{14}H_{13}O_6S$ (*m/z* 309.0433, calcd 309.0427), whose sum corresponded well with the molecular formula of **1**. This phenomenon of significant discrepancy attributed from the opposite MS ionization modes strongly suggested the presence of ionized partial structures, thus the salt nature of **1**. In addition, a strong absorption band was observed in the IR spectrum at 1456 cm^{-1}, which corresponds with a sulfate group, as suggested by the

MS-indicated sulfur atom.

The ^{13}C NMR data of compound **1** showed signals of a carbonyl carbon (δ_C 170.5) and thirteen sp^2 carbons (δ_C 160.2–102.7) (Table 1). Based on the combined ^1H NMR and HSQC data, the chemical shifts and splitting patterns (δ_H 6.74–6.16, all s) of corresponding protons were indicative of aromatic moieties. In addition, the odd numbers of sp^2 carbons suggested the presence of an electron-deficient functionality, such as an imine or guanidine. The NMR data of **1** also contained three sp^3 methines (δ_C/δ_H 73.3/2.74, 53.0/3.63 and 26.8/1.94), of which the former two carbons would bear nitrogen, according to their carbon and proton chemical shifts. Among the remaining four aliphatic methylene and six methyl signals in the NMR data, the carbon and proton chemical shifts indicated the presence of an oxymethylene (δ_C/δ_H 64.4/4.19 and 4.12), a nitrogenous methylene (δ_C/δ_H 42.7/3.30 and 3.05) and two nitrogenous methyls (δ_C/δ_H 41.0/2.21 × 2).

The gross structure of **1** was determined by combined ^1H–^1H COSY and HMBC experiments. First, all of the aromatic protons (δ_H 6.74–6.16, all s) lacked direct proton–proton couplings, placing them at meta- or para-positions to each other. The HMBC correlations of these and

two benzylic methyl protons (δ_H 2.23, H_3-13 and δ_H 2.18, H_3-14) with neighboring carbons readily constructed two 1,3-dioxygenated-5-methyl-benzene moieties (C-1–C-6 and C-13, C-7–C-12 and C-14), accounting for eight degrees of unsaturation (Figure 5). Despite the identical proton–carbon correlations, the noticeable differences in both the ^{1}H and ^{13}C chemical shifts revealed different oxygenated functionalities between aromatic rings. Aided by the negative mode ESI–MS cluster of $C_{14}H_{13}O_6S$ and the IR absorption band of the sulfate group at 1456 cm^{-1}, the partial structure was interpreted as 9-hydroxy-1-(sulfooxy)-3,7-diphenylether, which is discussed later.

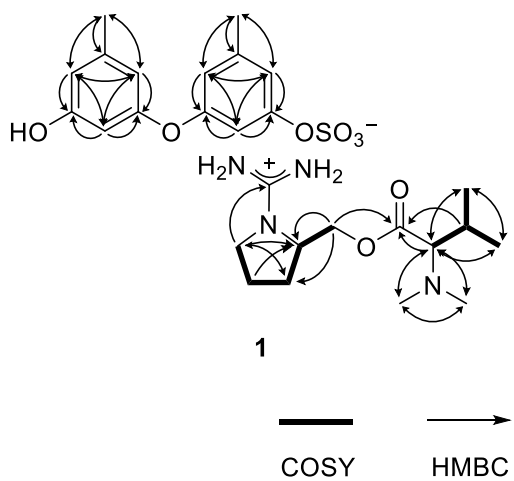

Figure 5. Key correlations of COSY (bold) and HMBC (arrows) experiments for **1**.

Meanwhile, the COSY data showed the proton spin couplings of an isobutyl group (δ_C/δ_H 73.3/2.74, 26.8/1.94, 19.0/0.82 and 19.5/0.92; C-7′–C-10′) which was confirmed by the HMBC correlations among these. Then, additional proton–carbon correlations of the C-7′ methine and C-8′ methine groups placed a carbonyl (δ_C 170.5, C-6′) and two methyl groups (δ_C/δ_H 41.0/2.21 × 2, C-11′ and C-12′) at the adjacent positions. Because the latter methyl groups were determined to be N-CH_3 by their chemical shifts, nitrogen must be connected to the methyl groups and C-7′. Thus, an *N*,*N*-dimethyl-valine residue was identified. The COSY data also showed a linear array of four methylenes and a methine (δ_C/δ_H 42.7/3.30 and 3.05, 24.8/1.78 and 1.57, 29.0/1.78 and 1.57, 53.0/3.63 and 64.4/4.19 and 4.12; C-1′–C-5′). Aided by their ^{1}H and ^{13}C NMR chemical shifts and the crucial HMBC correlation at H_2-1′/C-4′, a pyrrolidine moiety was identified for C-1′–C-4′. Similarly, the C-5′ methylene was connected to the C-6′ carbonyl by an ester linkage, according to the HMBC correlation at H_2-5′/C-6′. Thus, a prolinol moiety was defined for the C-1′–C-5′ portion.

The ^{13}C NMR data of **1** had a remaining nonprotonated carbon (δ_C 160.2), which was placed at the prolinol nitrogen (C-13′) by the crucial HMBC correlation with H_2-1′. The significant deshielding of this carbon must be attributed to the remaining two nitrogen atoms from the MS data. Thus, in conjunction with the $C_{13}H_{27}N_4O_2$ cluster observed in the positive ESI–MS analysis, the functionality of C-13′ was assigned to the guanidinium group. Thus, the C-1′–C-13′ portion was defined as 1-(aminoiminomethyl)-prolinol, *N*,*N*-dimethylvaline ester and the overall structure of **1**, designated as ochraceopetalin, was determined to be a mixed-biogenetic salt.

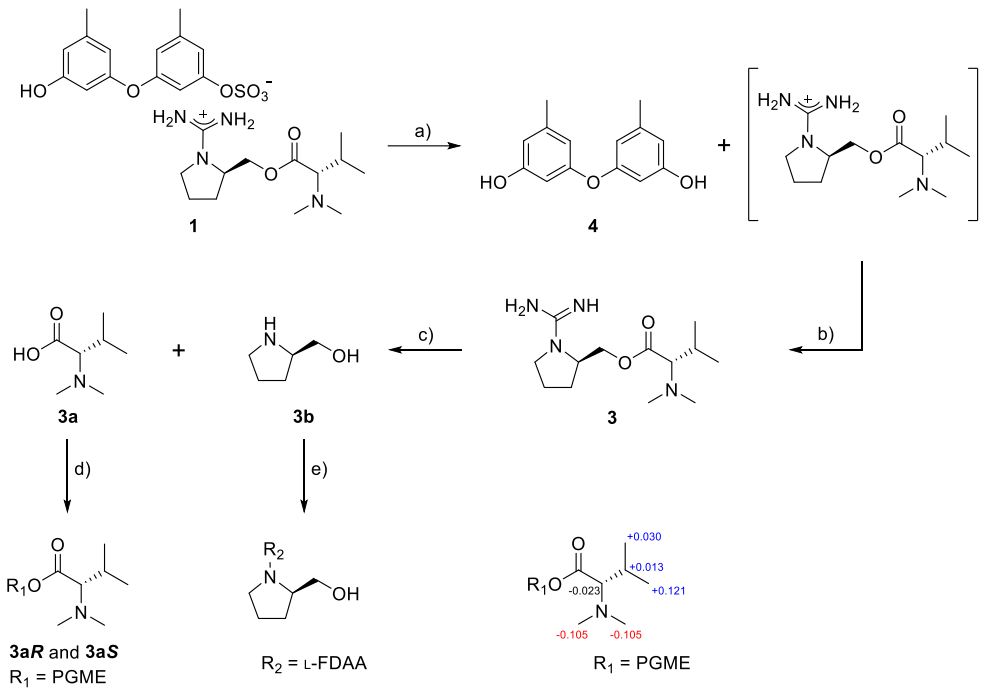

Figure 6. Sequential degradation and configurational assignments of **1**. *Reagents and conditions*: a) H_2O, TFA, rt, 3 h; b) NH_4OH, rt, 10 min; c) NaOH, 100 °C, 3 h; d) PGME, PyBOP, HOBT, *N*-methylmorpholine, rt, 3 h; e) $NaHCO_3$, L-FDAA, acetone, 80 °C, 15 min; Δδ values [$\Delta\delta = \delta_S - \delta_R$] obtained for (*S*)- and (*R*)-PGME amide derivatives **3a*S*** and **3a*R***.

The proposed structure of **1**, including the salt nature, was confirmed by a series of pH-dependent degradations (Figure 6). When **1** was placed in a mildly acidic solution, a compound separated into an organic layer (*n*-BuOH). A combination of HR–ESI–MS and 1D- and 2D-

NMR analyses readily identified this compound as diorcinol (**4**), a well-known 3,3′-oxybis [5-methylphenol] of diverse fungal origins.[7,9,11] Changing the pH of the remaining aqueous solution to basic conditions brought another compound (**3**) into an organic layer. The molecular formula of this compound was deduced to be $C_{13}H_{26}N_4O_2$ by HR–FAB–MS analysis ($[M + H]^+$ *m/z* 271.2135, calcd 271.2129) and the positive mode MS analysis of **3** was identical to that of **1**. Furthermore, the combined 1D- and 2D-NMR data of **3** were identical to those of the cation portion of **1**, which was designated as ochraceopetaguanidine and identified as 1-(aminoiminomethyl)-prolinol, *N*,*N*-dimethylvaline ester. Thus, the structure of **1** was unambiguously defined as a mixed-biogenetic salt derived from polyketide and amino acid pathways. The sulfate[21,22] and guanidinium salts of **1** was also supported by the comparison of ^{13}C NMR data between the simple salts bearing these functionalities and corresponding neutral groups (Figure B1). Compound **1** as a single salt compound was also supported by extensive HPLC analyses, in which **1** was always eluted as single peak under diverse chromatographic conditions (Figure B2).

The production of **1** was further investigated under different

culture conditions. After culturing the same strain in a static semi-solid YMM-rice medium, chromatographic separation of the culture broth yielded compound **2**. The molecular formula of **2** was defined to be $C_{14}H_{14}O_6S$ by HR–ESI–MS analysis ($[M - H]^-$ *m/z* 309.0433, calcd 309.0427), which was identical to the data of **1** in the negative mode MS analysis. Furthermore, the 1D- and 2D-NMR data of **2** were identical to the negative ion portion of **1** (Table 1). In addition, **2** was slowly converted to diorcinol (**4**) during prolonged storage, emphasizing their structural relationship. Thus, the structure of **2** was determined to be 1-(sulfooxy)-diorcinol, a sulfate-bearing diphenyl ether of polyketide origin.

Ochraceopetalin (**1**) and ochraceopetaguanidine (**3**) commonly bear two stereogenic centers in the amino acid portion. For the configurational assignments of these, firstly, a basic hydrolysis of **3** gave *N*,*N*-dimethylvaline and prolinol. The absolute configuration at C-7′ of the valine residue was assigned using the PGME method.[23] Treatments with (*S*)- and (*R*)-PGME produced the corresponding PGME amides, respectively. The $\Delta\delta_H$ values between these unambiguously assigned a D-configuration (Figure 6). For the C-4′ center of prolinol, the absolute configuration was assigned by using the Marfey reaction.[24] After the L-

FDAA-prolinol adduct was prepared by condensation with L-FDAA, its HPLC retention time was compared with those of authentic L-FDAA-L-prolinol and L-FDAA-D-prolinol, which resulted in assigning the D-configuration. Thus, both amino acid-derived units of **1** were found to possess D-configurations. In addition, the guanidinium salt of **1** was supported by the ^{13}C NMR data of **3c**, the TFA salt of **3**, whose guanidinium bearing C-13′ showed very similar chemical shift with 3 (δ_C 161.47 and 160.39 for **3c** and **3**, respectively) (Figure B3). At the same time, the carbon chemical shifts of C-13′ of **1** and **3** also showed similarity with 0.15 ppm and 0.13 ppm differences in DMSO-d_6 (δ_C 160.24 and δ_C 160.39 for **1** and **3**, respectively) and MeOH-d_4 solvent (δ_C 161.95 and δ_C 162.08 for **1** and **3**, respectively), respectively (Figures B4–B5, Table B1).

In addition to the structure determination, the structure of **1** and **2** led to an interesting argument. Diorcinol (**4**) is widely recognized as a natural product of diverse fungi, such as *Aspergillus versicolor* GH-2,[25] *A. tennesseensis*[26] and *Cordyceps* sp.[27] The detailed biosynthesis via orsellinic acid, including the gene cluster and enzymatic reactions, was recently determined for a marine-derived *A. nidulans*.[9,12] However, the

results of finding **1** and **2** consecutively (eight times of cultivation) raise the possibility that, in the case of this strain (strain number FJ120) of *A. ochraceopetaliformis*, the natural product of the fungus is not diorcinol (**4**), but 1-(sulfooxy)-diorcinol (**2**), or its salt (**1**). Alternatively, it would be possible that naturally produced **4** was sulfonated to **1** or **2** by a biotransformation during the cultivation. It would be also possible to transform **1** by an abiotic process during the cultivation or isolation procedures. To clarify this, time-dependent cultivation and ESI–MS analyses of the broths revealed two interesting phenomena. The first is that **1** and **2** were independently produced after 8 and 6 weeks of cultivation, respectively, under given culturing conditions, while the production of **4** was undetected by LC–ESI–MS analysis (Figures B6 and B7). The second interesting phenomenon is that distinct products according to the culturing conditions could be attributed to the differences in pH in the culture media, **1**, pH 9.0, and **2**, pH 5.0. This question of biosynthesis of diorcinol derivatives would be fully answered only by the extensive biosynthetic study on this strain.

Compounds **1**–**4** were tested using a number of bioassays. In cytotoxicity tests, all four compounds were either significantly inhibitory (**1**, IC_{50} 9.5 and 6.8 μM), or less active (**2**–**4**, IC_{50} 11–25 μM) against the

human cancer cell lines K562 and A549 (Figure B8 and Table B2). Although its cytotoxicity was not remarkable, **1** was noticeably more potent than its components **2**–**4**. These microbial compounds failed to inhibit both Gram-positive and Gram-negative bacteria and pathogenic fungi (MIC > 128 μg/mL). They were also inactive against the microbial enzymes sortase A (SrtA), a transpeptidase responsible for the anchoring of surface proteins to the cell wall envelope of Gram-positive bacteria and isocitrate lyase (ICL), a key enzyme in the glyoxylate cycle.

1-3. Experimental section

General Experimental Procedures. Optical rotations were measured on a JASCO P1020 polarimeter (Jasco, Tokyo, Japan) using a 1 cm cell. UV spectra were acquired with a Hitachi U-3010 spectrophotometer (Hitachi High-Technologies, Tokyo, Japan). IR spectra were recorded on a JASCO 4200 FT-IR spectrometer (Jasco, Tokyo, Japan) using a ZnSe cell. ^{1}H and ^{13}C NMR spectra were measured in DMSO-d_6, $CDCl_3$, or MeOH-d_4 solutions on Bruker Avance -400, -500, -600, or -800 instruments (Bruker, Billerica, MA, USA), with solvent peaks at δ_H 2.50/δ_C 39.50, δ_H 7.26/δ_C 77.16 and δ_H 3.31/δ_C 49.00, respectively, as

their internal standards. High-resolution ESI mass spectrometric data were obtained at the National Instrumentation Center for Environmental Management (Seoul, Korea) and were acquired using an AB Sciex 5600 QTOF HR–MS instrument (Sciex, Washington, DC, USA). High-resolution FAB mass spectrometric data were obtained at the Korea Basic Science Institute (Daegu, Korea) and were acquired using a JEOL JMS 700 mass spectrometer (Jeol, Tokyo, Japan) with *meta*-nitrobenzyl alcohol (NBA) as the matrix. Low-resolution ESI–MS data were recorded on an Agilent Technologies 6130 quadrupole mass spectrometer with an Agilent Technologies 1200 series HPLC. Semi-preparative and analytical HPLC separations were performed on a Spectrasystem p2000 equipped with a Spectrasystem RI-150 refractive index detector and a UV-Vis-151 detector (Gilson, Middleton, WI, USA). All the solvents used were of spectroscopic grade or distilled from glass prior to use.

Fungal Material. The fungal strain *Aspergillus ochraceopetaliformis* (strain number FJ120) was isolated from marine sediments collected from Jeju-do, Korea, in July 2007.[13] The isolate was identified using standard molecular biology protocols by DNA amplification and sequencing of the ITS region. Genomic DNA extraction was performed using Intron's i-genomic BYF DNA Extraction Mini Kit,

according to the manufacturer's protocol. The nucleotide sequence was deposited in the GenBank database under accession number KF384187. The 18S rDNA sequence of this strain exhibited 100% identity (588/588) with that of *Aspergillus ochraceopetaliformis* strain RKI08-134 (GenBank accession number FJ797698).

Fermentation. The fungal strain was cultured on solid YPG medium (5 g of yeast extract, 5 g of peptone, 10 g of glucose, 24.8 g of sea salt and 16 g of agar in 1 L of distilled water) for 7 days. An agar plug (1 cm × 1 cm) was inoculated in 250 mL flask containing 100 mL of YPG medium. After 7 days of growth, 10 mL of each culture was transferred to 2.8 L Fernbach flasks containing YMM medium (5 g of yeast extract, 5 g of malt extract, 10 g of mannitol and 24.8 g of sea salt in 1000 mL of distilled water). In total, 30 L of YMM medium was prepared and cultivated under static conditions for 8 weeks at 30 °C.

The large-scale cultivation of YPG-based seed culture was also performed on semi-solid YMM-rice media (1 g of yeast extract, 1 g of malt extract, 2 g of mannitol and 200 g of rice in 200 mL of artificial seawater) in 2.8 L Fernbach flasks at 30 °C in the static condition for 6 weeks.

Extraction and Isolation. The entire culture was filtered and extracted with EtOAc (20 L × 3). The solvent was evaporated in vacuo to afford a brown organic gum (4.3 g). The extract was separated by C_{18} reversed-phase vacuum flash chromatography using sequential mixtures of H_2O and MeOH (five fractions of H_2O-MeOH, gradient from 80:20 to 0:100), acetone and, finally, EtOAc as the eluents. Based on the results of ^{1}H NMR and LR–ESI–MS analyses, the fraction eluted with H_2O-MeOH 40:60 (850 mg) was subjected to semi-preparative reversed-phase HPLC (YMC-ODS-A column, 250 × 10 mm; H_2O-MeOH, 50:50, 1.7 mL/min), affording compound **1** (t_R = 29.1 min). Compound **1** was further purified by analytical HPLC (YMC-ODS-A column, 250 × 4.6 mm; H_2O-MeCN, 75:25, 0.7 mL/min; t_R = 22.0 min; 11.1 mg).

The broth (4.2 kg) from semi-solid YMM-rice medium was extracted with methanol (21 L × 3) and dichloromethane (21 L × 3). The combined extracts (111.1 g) were dried in vacuo and partitioned between H_2O (84.6 g) and *n*-BuOH (26.4 g). The organic layer was repartitioned between H_2O-MeOH (15:85, 14.2 g) and *n*-hexane (12.2 g). The H_2O-MeOH layer was evaporated to obtain an organic extract (14.2 g). The extract was fractionated by C_{18} reversed-phase vacuum flash chromatography using a sequential mixture of MeCN and H_2O as eluents

(H_2O-MeCN, from 80:20 to 50:50), MeOH, acetone and, finally, EtOAc. On the basis of the result of ^1H NMR and LC–MS profile, the fraction (1240 mg) eluted with H_2O-MeCN (70:30) was purified by semi-preparative reversed-phase HPLC (YMC-ODS-A column, 250 × 10 mm; H_2O-MeOH, 55:45, 1.7 mL/min) to yield compound **2** (t_R = 34.5 min). Compound **2** was further purified by analytical HPLC (YMC-ODS-A column, 250 × 4.6 mm; H_2O-MeCN, 80:20, 0.7 mL/min; t_R = 15.6 min; 13.7 mg).

Ochraceopetalin (**1**): white amorphous solid; $[\alpha]_D^{25}$ -5 (*c* 0.4, MeOH); UV (MeOH) λ_{max} (log ε) 209 (3.17), 275 (2.01) nm; IR (ZnSe) ν_{max} 3347 (br), 2946, 1456, 1031 cm^{-1}; ^1H and ^{13}C NMR data, Table 1; HR−ESI−MS *m/z* 581.2628 $[M + H]^+$ (calcd for $C_{27}H_{41}N_4O_8S$, 581.2640).

1-(Sulfooxy)-diorcinol (**2**): yellow amorphous solid; UV (MeOH) λ_{max} (log ε) 210 (3.16), 275 (2.19) nm; IR (ZnSe) ν_{max} 3359 (br), 2833, 1455, 1033 cm^{-1}; ^1H and ^{13}C NMR data, Table 2; HR−ESI−MS *m/z* 309.0437 $[M - H]^-$ (calcd for $C_{14}H_{13}O_6S$, 309.0438).

pH-Dependent Hydrolysis of Compound 1. Firstly, compound **1** (9.7 mg) was dissolved in water (0.05% TFA, 5 mL). The solution was stood at room temperature for 3 h. The aqueous solution was partitioned

with *n*-BuOH (5 mL) through a separate funnel. Removal of *n*-BuOH in vacuo yielded pure compound **4** (3.5 mg). To the aqueous fraction, 0.05% of NH_4OH (5 mL) was added. After removing water, purification by analytical HPLC (YMC-ODS-A column, 250 × 4.6 mm; 0.7 mL/min; H_2O-MeCN, 70:30) afforded compound **3** (t_R = 21.1 min; 4.2 mg).

Ochraceopetaguanidine (3): white amorphous solid; $[\alpha]_D^{25}$ -4 (*c* 0.4, MeOH); UV (MeOH) λ_{max} (log ε) 205 (2.39) nm; IR (ZnSe) ν_{max} 3362 (br), 2360, 1636 cm^{-1}; ^1H and ^{13}C NMR data, Table 3; HR–FAB–MS *m/z* 271.2135 $[M + H]^+$ (calcd for $C_{13}H_{27}N_4O_2$, 271.2129).

Diorcinol (4): colorless gum; ^1H and ^{13}C NMR spectra, Figures B9–B10; HR–ESI–MS *m/z* 231.1012 $[M + H]^+$ (calcd for $C_{14}H_{15}O_3$, 231.1016).

Basic Hydrolysis of Compound 3. Compound **3** (3.5 mg) was dissolved in 1 N NaOH (1 mL) and the solution was stirred at 100 °C for 3 h. The separation by analytical HPLC (YMC-ODS-A column, 250 × 4.6 mm; 0.7 mL/min; H_2O-MeCN, 65:35) afforded compounds **3a** (*N*,*N*-dimethylvaline, t_R = 15.4 min; 2.2 mg) and **3b** (prolinol, t_R = 23.8 min; 2.8 mg) as pure compounds.

N,N-Dimethylvaline (3a): white amorphous solid; ^{1}H NMR (DMSO-d_6, 400 MHz) δ_H 3.16 (1H, br s, 6′-OH), 2.66 (1H, d, *J* = 9.1 Hz, H-7′), 2.29 (6H, s, H-11′, H-12′), 1.90 (1H, dhep, *J* = 9.1, 6.8 Hz, H-8′), 0.92 (3H, d, *J* = 6.6 Hz, H-10′), 0.83 (3H, d, *J* = 6.6 Hz, H-9′); LR–ESI–MS *m/z* 146.2 $[M + H]^+$.

Prolinol (3b): pale yellow oil; ^{1}H NMR ($CDCl_3$, 400 MHz) δ_H 3.81 (2H, OH, NH), 3.37 (1H, dd, *J* = 11.0, 4.0 Hz, H-5′), 3.20 (1H, dd, *J* = 11.0, 7.0 Hz, H-5′), 3.02 (1H, m, H-4′), 2.71 (1H, m, H-1′), 2.68 (1H, m, H-1′), 1.63-1.52 (3H, m, H-2′,3′), 1.22 (1H, m, H-2′); LR–ESI–MS *m/z* 102.1 $[M + H]^+$.

Preparation of (*S*)- and (*R*)-PGME Amides of 3a. To a dry DMF solution (500 μL) of compound **3a** (0.5 mg, 6.9 mM) and (*S*)-PGME (1.5 mg, 33 mM), PyBOP (8.5 mg, 33 mM), HOBT (2.2 mg, 33 mM) and *N*-methylmorpholine (100 μL) were added. After stirring the mixture for 3 h at room temp, a 5% HCl solution and EtOAc were added to the reaction mixture. The EtOAc layer was subsequently washed with saturated $NaHCO_3$ solution and brine. The organic layer was dried over anhydrous Na_2SO_4. After removing the solvent under vacuum, the residue was purified by reversed-phase HPLC (YMC-ODS column, 250 × 4.6 mm;

H_2O-MeCN, 25:75) to give (*S*)-PGME amide **3a*S*** (0.2 mg). Compound **3a*R*** (0.2 mg), the (*R*)-PGME amide of **3a**, was prepared from (*R*)-PGME in a similar fashion. The molecular formulae of **3a*S*** and **3a*R*** were confirmed as $C_{16}H_{24}N_2O_3$ based on LR–ESI–MS data.

(S)-PGME Amide of 3a (**3a*S***): white amorphous solid; ^{1}H NMR (CD_3OD, 800 MHz) δ_H 7.393-7.338 (5H, m, PGME-Ar), 5.495 (1H, s, PGME-H-1), 3.697 (3H, s, PGME-OMe), 2.716 (1H, d, *J* = 9.0 Hz, H-7′), 2.240 (6H, s, H-11′, H-12′), 2.050 (1H, dhep, *J* = 9.3, 6.7 Hz, H-8′), 0.975 (3H, d, *J* = 6.7 Hz, H-10′), 0.931 (3H, d, *J* = 6.7 Hz, H-9′); LR–ESI–MS *m/z* 293.4 $[M + H]^+$.

(R)-PGME Amide of 3a (**3a*R***): white amorphous solid; ^{1}H NMR (CD_3OD, 800 MHz) δ_H 7.373-7.335 (5H, m, PGME-Ar), 5.481 (1H, s, PGME-H-1), 3.704 (3H, s, PGME-OMe), 2.739 (1H, d, *J* = 9.2 Hz, H-7′), 2.345 (6H, s, H-11′, H-12′), 2.037 (1H, dhep, *J* = 9.4, 6.7 Hz, H-8′), 0.945 (3H, d, *J* = 6.7 Hz, H-10′), 0.810 (3H, d, *J* = 6.7 Hz, H-9′); LR–ESI–MS *m/z* 293.4 $[M + H]^+$.

Marfey's Analysis of 3b. Compound **3b** (0.5 mg) was dissolved in 12 N HCl (0.5 mL) and heated at 110 °C for 16 h. The solution and traces of HCl were removed by repeated drying under vacuum with

distilled water. To the hydrolysate, 1 N $NaHCO_3$ (100 μL) and 1% L- or D-FDAA (50 μL) in acetone were added. The mixture was stirred at 80 °C for 15 min. After quenching the reaction by the addition of 2 N HCl (50 μL), the residue was analyzed using HPLC with an analytical column (YMC-ODS-A column, 250 × 4.6 mm; H_2O-MeCN, 60:40). As standard compounds, L- and D-prolinol were also prepared using this method. The retention times of the L-FDAA-derivatized L-prolinol was 19.686 min and that of L-FDAA-derivatized D-prolinol was 20.160 min. The retention time of the L-FDAA-derivatized **3b** was 20.222 min, leading to assignment of the D-configuration.

Antibacterial Activity Assays. To investigate the antibacterial activity of isolated compounds, a series of minimal inhibitory concentration (MIC) tests was performed according to the Clinical and Laboratory Standards Institute (CLSI) guide methods.[28] Three species of Gram-positive bacteria (*S. aureus* strain Newman, *E. faecalis* ATCC19433 and *E. faecium* ATCC19434) and three species of Gram-negative bacteria (*K. pneumoniae* ATCC10031, *S. enterica* ATCC14028 and *E. coli* ATCC25922) were selected as test strains. The MIC of each test compound against six bacterial strains was determined in liquid culture using Mueller–Hinton broth (inoculum concentration, 5×10^4 cfu/mL)

with the compounds (concentration range of 0.06–128 μg/mL) after 24 h incubation at 37 °C. Ampicillin and tetracycline were used as reference compounds.

Antifungal Activity Assays. The antifungal activity of isolated compounds was estimated against *C. albicans* ATCC10231, *A. fumigatus* HIC6094, *T. rubrum* NBRC9185 and *T. mentagrophytes* IFM40996 according to the guidelines in CLSI document M38.[29] The growth of test fungi was monitored in RPMI 1640 broth (inoculum concentration: 10^4 cells/mL) with the compound concentration range of 0.06–128 μg/mL. Amphotericin B was used as a positive control.

ICL Inhibition Assays. The preparation of recombinant SrtA from *S. aureus* ATCC6538p and the evaluation of the effect of isolated compounds on SrtA were performed according to a previously described procedure.[30] The enzyme reaction was carried out at 37 °C for 1 h with 300 μL of buffer (50 mM Tris–HCl, 150 mM NaCl, 5 mM $CaCl_2$, pH 7.5), 55 μg of purified SrtA, 0.75 μg of synthetic peptide dabcyl-QALPETGEE-edans and test samples at various concentrations. The increase in the fluorescence intensity was recorded by a fluorescence spectrophotometer (excitation, 350 nm; emission, 495 nm). Curcumin and

berberine chloride were used as positive controls.

(Antibacterial activity, antifungal activity and ICL inhibition assays were performed by Prof. Ki-Bong Oh's laboratory)

Cytotoxic Assays. The effects of compounds **1**–**4** on cell viability were analyzed by MTT assay.[30] A549 (lung cancer) and K562 (leukemia) cells were purchased from the Korean Cell Line Bank (KCLB), Seoul, Korea. Both cell lines were cultured in RPMI-1640 medium with L-glutamine, 10% fetal bovine serum and 1% penicillin/streptomycin. All the cells were cultured at 37 °C in a humidified atmosphere with 5% CO_2. For the assay, each cell (5×10^4 cells/mL) was seeded in 96-well plates (100 μL/well). After 24 h, they were treated with various concentrations of compounds **1**–**4**. After 24 h of compound treatment, MTT (250 μg/mL) was added to each well and incubated for 4 h. The formazan product was dissolved with 250 μL of DMSO. Absorbances of each well were detected at the wavelength of 595 nm using an ELISA microplate reader (BioTek, Winooski, VT, USA) to determine the cell viability by quantifying the production of formazan. The IC_{50} values were calculated using a nonlinear regression analysis (percent survival versus concentration). Doxorubicin was used as a positive control.

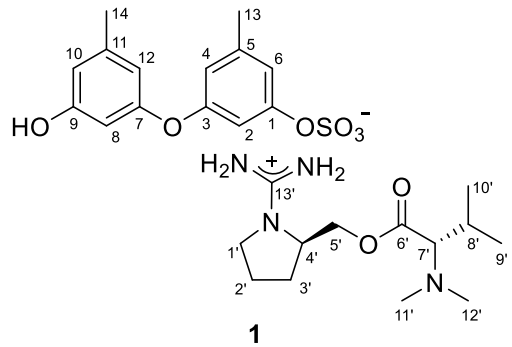

1

Table 1. ^{13}C and ^{1}H NMR assignment for compound **1** in DMSO-d_6

Position	δ_C, type	δ_H (J in Hz)	Position	δ_C, type	δ_H (J in Hz)
1	154.5, C		1′	42.7, CH_2	3.30, m, 3.05, m
2	108.1, CH	6.61, s	2′	24.8, CH_2	1.78, m, 1.57, m
3	156.6, C		3′	29.0, CH_2	1.78, m, 1.57, m
4	113.9, CH	6.49, s	4′	53.0, CH	3.63, d (7.0)
5	139.3, C		5′	64.4, CH_2	4.19, dd (11.5, 5.0)
6	115.8, CH	6.74, s			4.12, dd (11.5, 6.5)
7	157.6, C		6′	170.5, C	
8	102.7, CH	6.16, s	7′	73.3, CH	2.74, d (10.5)
9	158.4, C		8′	26.8, CH	1.94, dhep (10.5, 6.5)
10	109.8, CH	6.25, s	9′	19.0, CH_3	0.82, d (6.5)
11	140.1, C		10′	19.5, CH_3	0.92, d (6.5)
12	111.2, CH	6.34, s	11′	41.0, CH_3	2.21, s
13	21.0, CH_3	2.23, s	12′	41.0, CH_3	2.21, s
14	21.1, CH_3	2.18, s	13′	160.2, C	
9-OH		9.47, s			

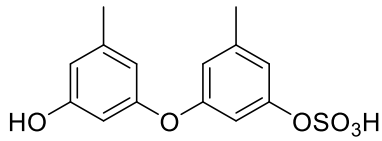

Table 2. ^{13}C and ^{1}H NMR assignment for compound **2** in DMSO-d_6

Position	δ_C, type	δ_H (J in Hz)
1	154.5, C	
2	108.1, CH	6.61, s
3	156.7, C	
4	113.9, CH	6.49, s
5	139.3, C	
6	116.0, CH	6.74, s
7	157.6, C	
8	102.8, CH	6.16, s
9	158.6, C	
10	109.9, CH	6.25, s
11	140.1, C	
12	111.2, CH	6.34, s
13	21.1, CH_3	2.23, s
14	21.1, CH_3	2.18, s
9-OH		9.49, br s

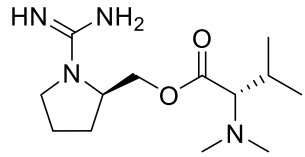

Table 3. ^{13}C and ^{1}H NMR assignment for compound **3** in DMSO-d_6

Position	δ_C, type	δ_H (J in Hz)
1′	42.7, CH_2	3.30, m, 3.05, m
2′	24.8, CH_2	1.78, m, 1.57, m
3′	29.0, CH_2	1.78, m, 1.57, m
4′	52.9, CH	3.63, m
5′	64.6, CH_2	4.19, dd (11.5, 4.5)
		4.12, dd (11.5, 6.5)
6′	170.4, C	
7′	73.2, CH	2.74, d (10.5)
8′	26.8, CH	1.94, dhep (10.5, 6.5)
9′	19.2, CH_3	0.82, d (6.5)
10′	19.2, CH_3	0.92, d (6.5)
11′	41.0, CH_3	2.21, s
12′	41.0, CH_3	2.21, s
13′	160.4, C	

III. Phenalenones from a Marine-Derived *Penicillium* sp. Fungus

2-1. Introduction

Fungi produce a wide variety of polyketide-derived metabolites. Among these, phenalenones are a class of hexa- or heptaketides bearing a perinaphtenone-type tricyclic system.[31] As summarized in a recent comprehensive review, these compounds can have immense structural variations, such as homo- and heterodimerization, the incorporation of additional carbon frameworks, and a high degree of oxygenation and nitrogenation as well as being complexed with metals.[32] A frequently occurring variation is the incorporation of an isoprene unit by forming either a linear ether or a trimethylhydrofuran moiety, and this variation is well-represented in the herqueinones from *Penicillium* sp.[33–35] Fungi-derived phenalenone compounds have attracted significant interest due to their chemical structures, bioactivities, and biosynthesis.[31] With their diverse phylogenic origins, phenalenones are widely recognized as a representative group of fungal polyketides.[31–32]

During the course of search for novel compounds from marine-

derived fungi, the structures of herqueiazole and herqueioxazole, unusual pyrrole- and oxazole-containing phenalenones from a *Penicillium* sp. strain, were reported.[36] Herqueidiketal, a cytotoxic sortase A inhibitory congener, also possessed a novel skeleton containing a highly oxidized naphthoquinone moiety.[36] Despite its carbon skeleton being different from typical phenalenones, the presence of naphthalene and dihydrofuran moieties in herqueidiketal may further emphasize the wide structural variations of phenalenones. In my continuing search for such compounds, I isolated several structurally related phenalenones from a large-scale cultivation of this *Penicillium* sp. strain. Here, I report the isolation of eleven compounds (**5**–**15**) as well as the structure determination of six new compounds (**5**–**10**) in the herqueinone subclass. 4-Hydroxysclerodin (**10**) exhibited moderate anti-angiogenic activity on human umbilical vascular endothelial cells (HUVECs). The acetone adduct of a triketone (**11**) exhibited moderate anti-inflammatory activity in mouse macrophage RAW 264.7 cells. In addition, *ent*-peniciherqueinone (**5**) and isoherqueinone (**13**) moderately induced adipogenesis in human bone marrow-mesenchymal stem cells (hBM-MSCs). All of these bioactivities were found to occur without cytotoxicity.

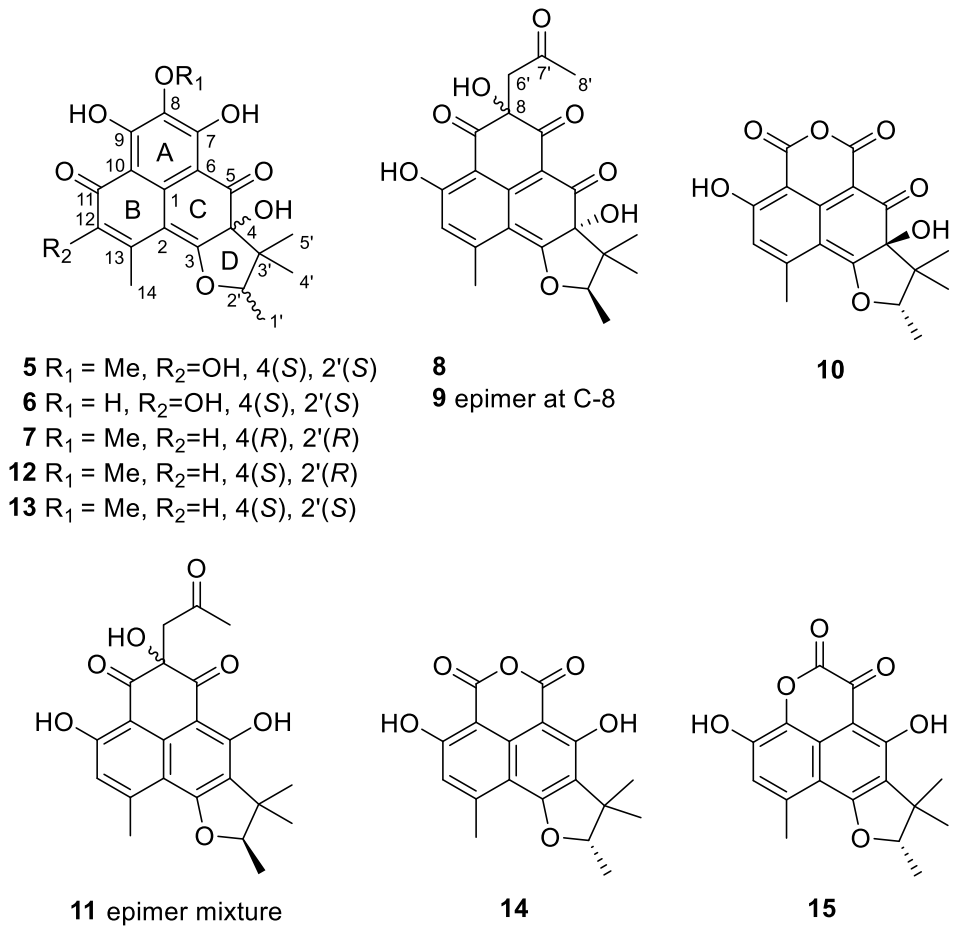

5 R_1 = Me, R_2=OH, 4(*S*), 2'(*S*)
6 R_1 = H, R_2=OH, 4(*S*), 2'(*S*)
7 R_1 = Me, R_2=H, 4(*R*), 2'(*R*)
12 R_1 = Me, R_2=H, 4(*S*), 2'(*R*)
13 R_1 = Me, R_2=H, 4(*S*), 2'(*S*)

8
9 epimer at C-8

10

11 epimer mixture

14

15

Figure 7. Chemical structures of compounds **5**–**15**.

2-2. Results and discussion

The molecular formula of **5** was deduced to be $C_{20}H_{20}O_8$ with 11 degrees of unsaturation by HR–FAB–MS analysis. The ^{13}C NMR data of

this compound showed a signal of a ketone carbon at δ_C 197.6 (Table 4). The signals at δ_C 178.1 and 174.6 could belong to either carbonyl or highly deshielded olefinic carbons. The ^{13}C NMR spectrum, in combination with DEPTs and HSQC spectra, displayed nine nonprotonated sp^2 carbon signals in the δ_C 103.5–162.8 region. The deshielded carbons must be one carbonyl carbon and one olefinic carbon, accounting therefore for seven degrees of unsaturation. The ^{13}C NMR data also showed two oxygen-bearing quaternary sp^3 carbons (δ_C 89.5 and 79.0), one methoxy carbon (δ_C 60.9), one shielded quaternary sp^3 carbon (δ_C 46.9), and four shielded methyl carbons (δ_C 16.4, 16.4, 14.9, and 13.3) (Table 4). Combining the NMR data and the degrees of unsaturation, **5** must possess four rings featuring the herqueinone class of phenalenones.

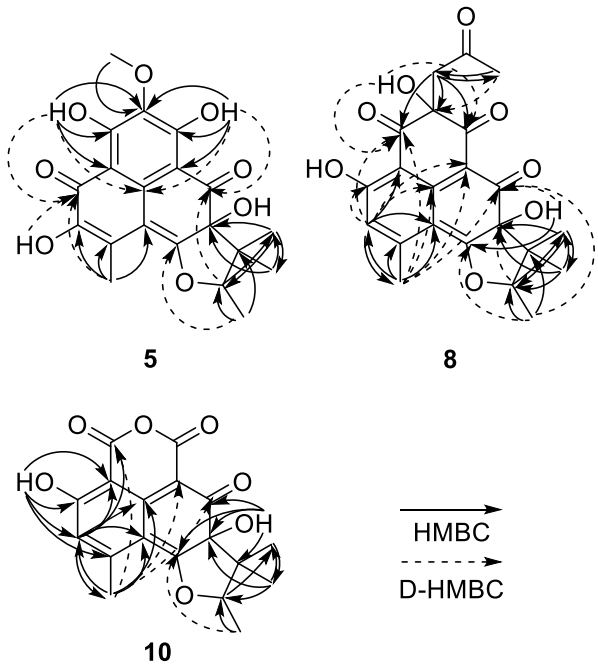

Figure 8. Key correlations of HMBC (arrows) and D-HMBC (dashed arrows) experiments for compounds **5**, **8** and **10**.

Due to the lack of COSY correlations except for that from the methyl doublet at δ_H 1.40 (Me-1′) to the quartet at δ_H 4.99 (H-2′), the structure determination of **5** had to be carried out through extensive HMBC analyses under diverse measuring conditions (Figure 8). First, the long-range couplings from OH-7 (δ_H 13.23) to C-6 (δ_C 103.5), C-7 (δ_C 162.8), and C-8 (δ_C 131.6); from OCH_3-8 (δ_H 3.92) to C-8 (δ_C 131.6); and

OH-9 (δ_H 13.99) to C-8 (δ_C 131.6), C-9 (δ_C 161.7), and C-10 (δ_C 108.7) lead to a delineation of the C-6 to C-10 fragment. Aided by the four-bond couplings from OH-7 (δ_H 13.23) to C-1 (δ_C 137.3) and OH-9 (δ_H 13.99) to C-1 (δ_C 137.3) by decoupled HMBC (D-HMBC)[37] experiments, the presence of a hexa-substituted benzene ring (C-1, C-6–C-10; ring A) was confirmed. In addition, the combined HMBC and D-HMBC correlations from OH-12 (δ_H 6.66) and H_3-14 (δ_H 2.47) to neighboring carbons revealed the presence of an *α*-hydroxy-*β*-methyl-*α*,*β*-unsaturated ketone group (OH-12 (δ_H 6.66) to C-11 (δ_C 178.1), C-12 (δ_C 143.7), and C-13 (δ_C 124.0); H_3-14 (δ_H 2.47) to C-2 (δ_C 103.7), C-11 (δ_C 178.1), C-12 (δ_C 143.7), and C-13 (δ_C 124.0)), which was directly connected to the benzene ring based on the D-HMBC correlation from OH-7 (δ_H 13.23) to C-11 (δ_C 178.1).

In addition to the correlation from H_3-14 (δ_H 2.47) to C-2 (δ_C 102.7), a correlation from H_3-14 (δ_H 2.47) to a highly deshielded C-3 (δ_C 175.4) in the D-HMBC spectrum was crucial evidence for the attachment of an electron-withdrawing oxygen at this position. Subsequently, long-range correlations from OH-4 (δ_H 7.23) to C-3 (δ_C 8), C4 (δ_C 8), and C5 (δ_C 8) defined not only its connectivity to the C-2 double bond but also placed a carbonyl carbon (δ_C 198.2) at C-5. These carbon–proton

correlations constructed an *α*,*β*-dioxycyclohexadienone moiety (C-1–C-6; ring C). The assignment of ring C also secured the formation of the conjugated carbonyl group to another six-membered ring (C-1, C-2, C-10–C-13; ring B).

The remaining C_5 fragment (C-1′–C-5′) of **5** was readily defined as a 2,3-disubstituted 2-methylbutane moiety by a combination of COSY and HMBC data (Figure 8). The cyclization of this moiety to the three-ring system was also accomplished by a series of long-range carbon–proton correlations. That is, the connection between C-4 and C-5′ was confirmed by the HMBC correlations from H_3-4′ (δ_H 1.43) and H_3-5′ (δ_H 0.86) to C-4 (δ_C 79.0) as well as a long-range correlation from H-2′ to C-5. The diagnostic chemical shifts of the CH-2′ methine group (δ_C 89.3, δ_H 4.91) suggested its attachment to C-3 via an ethereal bridge. This interpretation was corroborated by the correlation from H_3-1′ (δ_H 1.40) to C-3 (δ_C 174.6), which established a hydrofuran moiety (C-3, C-4, C-2′, and C-4′; ring D). Thus, the structure of **5** was defined as a herqueinone-type tetracyclic phenalenone.

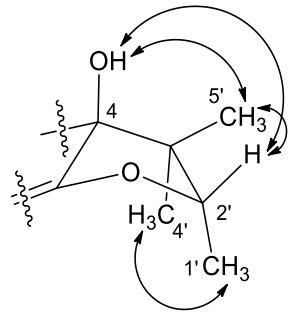

Figure 9. NOESY correlations of the hydrofuran moiety of compound **5.**

The planar structure of **5** was found to be the same as that of the recently reported peniciherqueinone from the fungus *Penicillium herquei.*[38] In my study of the configurations of the C-4 and C-2′ stereogenic centers by NOESY analysis (Figure 9), the OH-4, H-2′, and H_3-5′ protons were oriented toward the same face of the hydrofuran ring based on their mutual cross-peaks. The opposite face was occupied by H_3-1′ and H_3-4′ based on the cross peak between the methyl protons, suggesting that **5** has the same relative configuration (4*S** and 2′*S**) as peniciherqueinone. Interestingly, despite the same signs of optical rotations, there was a remarkable difference in their values of the specific rotations: $[\alpha]_D^{25}$ ($CHCl_3$) +203 (**5**) and +92 (peniciherqueinone). Since the absolute configurations at C-4 and C-2′ of herqueinones have been the

subject of comprehensive investigations,[39,40] the discrepancy in the specific rotations of **5** and herqueinones needed to be justified. Using a pre-established chemical modification technique,[41–43] **5** was reduced to **5a**, which showed a negative specific rotation ($[\alpha]_D^{25}$ ($CHCl_3$) −23); thus, the 2′*S* configuration was confirmed. The absolute configuration was further evaluated via the acetylation of **5a** to corresponding 9,11,12-triacetyl derivative **5b** (Figure 10). The sign of the specific rotation of **5b** ($[\alpha]_D^{25}$ (MeOH) −42) was opposite to that of herqueinone (**12**) but the same as that of isoherqueinone (**13**), which proved a 2′*S* configuration.[39,40] Therefore, the absolute configuration of **5** was assigned as 4*S* and 2′*S*. Thus, **5**, designated as *ent*-peniciherqueinone, is a new herqueinone-type phenalenone.

The molecular formula of **6** was deduced to be $C_{19}H_{18}O_8$ based on HR–FAB–MS analysis. The NMR data of this compound were very similar to those of **5**, with the absence of a methyl group. A detailed examination of the ^{13}C and ^{1}H NMR data revealed that the OMe-8 of **5** (δ_C 60.9, δ_H 3.92) was replaced by a hydroxyl group (δ_H 8.96) in **6**, and this assignment was confirmed by a combination of 2D-NMR analyses. The NOESY data and specific rotation of the reduction product **6a** indicated the same 4*S* and 2′*S* configuration as in **5**. Thus, **6**, designated as 12-

hydroxynorherqueinone, was determined to be 8-demethyl-*ent*-peniciherqueinone.

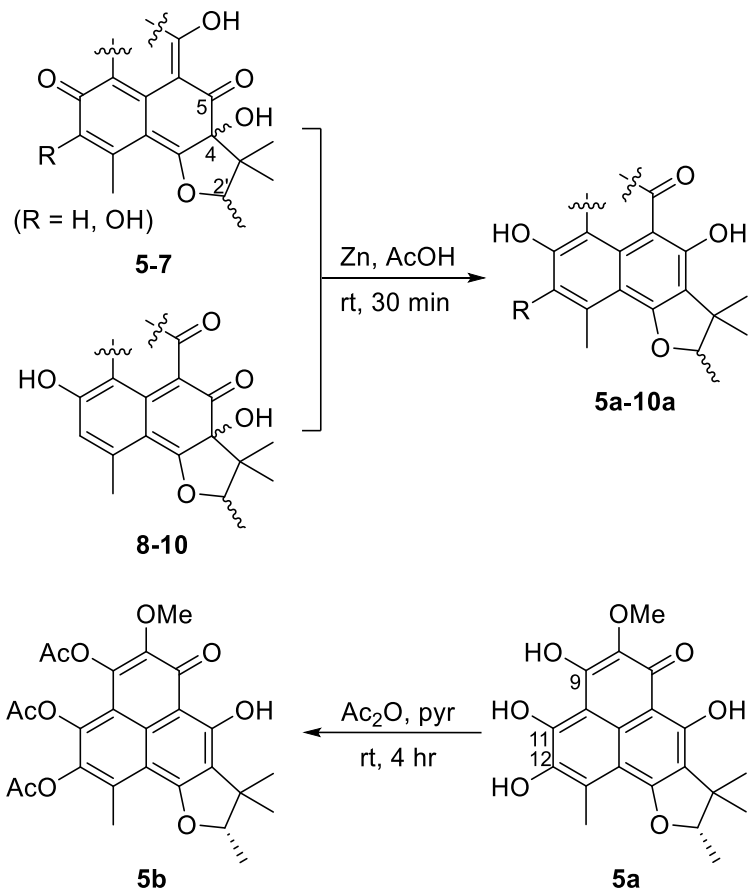

Figure 10. Phenolic derivatization of herqueinones.

Compound **7** was isolated as an orange amorphous solid with a molecular formula of $C_{20}H_{20}O_7$, based on HR–FAB–MS analysis. The ^{13}C and ^{1}H NMR data of this compound were similar to those obtained for **7**. The most noticeable difference was the replacement of a hydroxyl-bearing olefinic carbon with the sp^2 methine carbons (δ_C 122.8, δ_H 6.36). The structural difference was found to be at C-12 based on the HMBC correlations from H-12 (δ_H 6.36) to C-2 (δ_C 103.0), C-10 (δ_C 109.2), and C-14 (δ_C 23.8) as well as from H_3-14 (δ_H 2.48) to C-2 (δ_C 103.0), C-12 (δ_C 122.8), and C-13 (δ_C 150.9). However, the sign of the specific rotation of **7** ($[\alpha]_D^{25}$ (MeOH) −69) was opposite to those of **5** and **6**, implying a configurational difference. Since the NOESY spectrum showed the same cross-peaks for the hydrofuran moiety as those in the congeners, **7** was proposed to possess the opposite absolute configuration at C-4 and C-2′. As the reduction product of **7** (**7a**) is dextrorotatory (specific rotation ($[\alpha]_D^{25}$ (MeOH) +39)), the configuration of C-4 and C-2′ are 4*R*, 2′*R*, respectively. Thus, **7**, designated as *ent*-isoherqueinone, is a new herqueinone-type phenalenone derivative.

The molecular formula of **8** was also established as $C_{22}H_{22}O_8$ by HR–FAB–MS analysis. Although its spectroscopic data resembled those of **5**–**7**, several differences were found in both ^{13}C and ^{1}H NMR data. First,

aided by the HSQC data, it was found that three additional carbons, i.e., one carbonyl (δ_C 206.9), one methylene sp^2 (δ_C 48.5, δ_H 3.30), and one methyl (δ_C 29.8, δ_H 2.09), were present in this compound (Table 7). In the ^{13}C NMR spectrum, resonances of three ketone groups (δ_C 200.6, 193.1, and 189.9) were found for **8**, unlike **5**–**7**. In addition, an aromatic or olefinic carbon had been replaced by an oxygen-bearing nonprotonated sp^3 carbon (δ_C 76.9). A detailed examination of its NMR data revealed that **8** contained the same B and D rings as **5**–**7**, and the structural differences were located in the remaining portion of the molecule.

The planar structure of **8** was established by extensive HMBC experiments (Figure 8). Several HMBC correlations were found from an aromatic proton (δ_H 6.75, H-12) and a benzylic methyl proton (δ_H 2.57, H_3-14) to their neighboring carbons (H-12 (δ_H 6.75) to C-2 (δ_C 116.3), C-10 (δ_C 109.4), and C-14 (δ_C 23.5); H_3-14 (δ_H 2.57) to C-2 (δ_C 116.3), C-12 (δ_C 117.5), and C-13 (δ_C 152.3)). Aided by the D-HMBC correlations from H-12 (δ_H 6.75) to C-1 (δ_C 142.7) and C-11 (δ_C 165.6) and from H_3-14 (δ_H 2.57) to C-1 (δ_C 142.7), the long-range carbon–proton correlations led to the establishment of a hydroxyl- and methyl-bearing pentasubstituted benzene as ring B. Additional D-HMBC correlations from these protons to the conspicuous H_3-1′ at δ_H 1.30 (H-12 (δ_H 6.75) to C-6 (δ_C 101.2); H_3-14

(δ_H 2.57) to C-3 (δ_C 175.1), C-5 (δ_C 193.1), and C-6 (δ_C 101.2); H_3-1′ (δ_H 1.30) to C-3 (δ_C 175.1) and C-5 (δ_C 193.1)) defined ring C as a hydroxyl-bearing cyclohexadienone. The ring D was found to be the same as that in other herqueinones by a 2D-NMR spectrum.

The remaining portion of **8** consists of three ketone carbonyl (δ_C 206.9, 200.6, and 189.9) and one nonprotonated sp^3 (δ_C 76.9), one methylene sp^3 (δ_C 48.5), and one methyl (δ_C 29.8) carbons. These carbons were initially assembled into a 2-keto-propyl group (C-6′–C-8′) by the HMBC correlations from the methylene and methyl protons to their neighboring carbons (H_2-6′ (δ_H 3.30) to C-7′ (δ_C 206.9) and C-8′ (δ_C 29.8); H_3-8′ (δ_H 2.09) to C-6′ (δ_C 48.5), and C-7′ (δ_C 206.9)) (Figure 8). Then, this fragment was connected to the core structure by the HMBC correlations from H_2-6′ (H_2-6′ (δ_H 3.30) to C-7 (δ_C 189.9), C-8 (δ_C 76.9), and C-9 (δ_C 200.6)). The confirmation of this assignment as well as the linkage with the B-ring was accomplished by the key D-HMBC correlations from OH-8 (δ_H 6.68) to C-7 (δ_C 189.9) and C-9 (δ_C 200.6); from H-12 (δ_H 6.75) to C-9 (δ_C 200.6); from H_3-14 (δ_H 2.57) to C-9 (δ_C 200.6); and from H_3-8′ (δ_H 2.09) to C-8 (δ_C 76.9). Although it could not be confirmed by 2D-NMR-based carbon–proton correlations, the presence of the four rings, required by the molecular formula and NMR data, directly

connected C-6 and C-7 carbonyl carbons to be part of a diketo-bearing six-membered ring as ring A. Thus, the structure of **8** was determined to be a phenalenone related to an acetone adduct of a triketone.[44,45]

The molecular formula of **9** was the same as that of **8**, $C_{22}H_{22}O_8$. Moreover, the ^{13}C and ^{1}H NMR data of these compounds were very similar (Table 8). Two-dimensional NMR analyses showed the same carbon–proton correlations throughout the entire molecule, indicating that they have the same planar structure. Therefore, **9** could be an epimer of **8**.

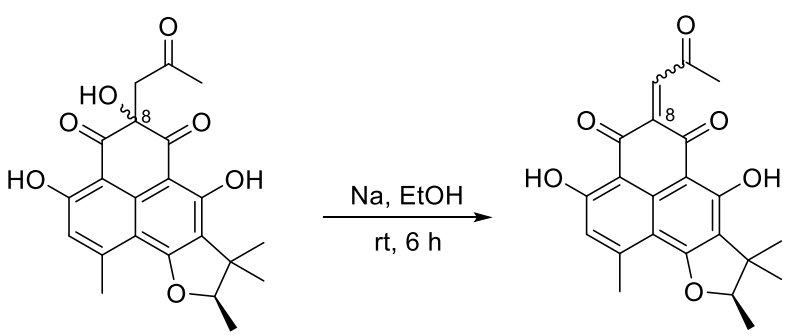

8a, 9a, 11 **8b, 9b, 11a**

Figure 11. Dehydrations of compounds **8a**, **9a** and **11**.

In order to clarify the difference in stereochemistry between **8** and **9**, NOESY experiments were carried out. The NOESY spectra of both compounds showed the same cross-peaks around the D ring as those observed in other herqueinones, suggesting the 4*R*,2′*R* or 4*S*,2′*S* configurations. Then, by chemical conversions to remove the other two stereogenic centers, the absolute configurations at C-4 were determined. That is, **8** and **9** were reduced to **8a** and **9a**, respectively (Figure 10), then the compounds were dehydrated to yield 8,15-unsaturated derivatives **8b** and **9b**, respectively (Figure 11), and the MS and NMR data of these compounds were identical. Furthermore, their specific rotations were also very similar ($[\alpha]_D^{25}$ ($CHCl_3$) +27 and +26 for **8b** and **9b**, respectively), implying that these were indeed the same compound. The negative specific rotations allow me to confidently assign the 2′*R* configuration for both natural products. Thus, **8** and **9**, designated as oxopropylisoherqueinones A and B respectively, were elucidated as new phenalenones possessing C_3 side chains. These compounds possessed 4*R*, 2′*R* configurations. However, the configurations at C-8 remain unassigned despite various chemical and spectroscopic analyses.

In order to determine the absolute configurations at C-8 of **8** and **9**, a comparison of the experimental and calculated ECD spectra was carried

out. Initially, the experimental CD profiles of these compounds showed opposite signs in the region of 285–340 nm, possibly reflecting the different configuration at C-8. Despite all the efforts, however, the calculated ECD profiles based on the postulated conformational populations failed to assign the absolute configurations satisfactorily (Figure B11 and B12). This could be due to a weak contribution of a single and remote stereogenic center to the ECD in the molecule possessing several UV chromophores and stereogenic centers.

The molecular formula of **10** was deduced to be $C_{18}H_{16}O_7$, which corresponds to 11 degrees of unsaturation, by HR–FAB–MS analysis. The ^{13}C and ^{1}H NMR data of this compound revealed that it is a phenalenone derivative based on the presence of signals for two aromatic rings and a trimethylhydrofuran moiety, which account for eight degrees of unsaturation (Table 9). However, only the carbon signals of two nonprotonated quaternary sp^2 carbons (δ_C 164.4 and 155.4) had replaced the NMR signals of the A ring of the other compounds. Therefore, in addition to satisfying the three remaining degrees of unsaturation, the C_2O_3 portion must account for two carbonyls and a cyclic ether or ester group.

The planar structure of **10** was determined with the aid of HMBC experiments (Figure 8). First, the long-range couplings of key protons, such as the four methyl groups [H_3-14 (δ_H 2.58), H_3-1′ (δ_H 1.36), H_3-4′ (δ_H 0.78), and H_3-5′ (δ_H 1.26)], an aromatic proton [H-12 (δ_H 6.81)], and two hydroxy protons [OH-4 (δ_H 7.41) and OH-11 (δ_H 11.43)], with their neighboring carbons confirmed the presence of the same B-D polycyclic moiety as in **8** and **9**. An additional coupling to OH-11 placed a carbonyl carbon (δ_C 164.4) at C-9, which was supported by the key D-HMBC correlation from H_3-14 (δ_H 2.58) to C-9 (δ_C 164.4). The other carbon (δ_C 155.5) must be located at C-7 due to the shielding of C-6 (δ_C 92.3). Although it was not directly proved by NMR spectra, both the MS data and the shielded chemical shifts of the C-7 and C-9 carbonyls were indicative of an oxygen bridge between these positions, leading to a six-membered cyclic acid anhydride moiety as ring A. The NMR data of the ring portion of **10** were similar to those of sclerodin (**14**), which was previously reported from the fungus *Gremmeniella abietina* thus supporting the structure of **10**.[44,46]

The NOESY correlations of **10** placed the OH-4, H-2′, and H_3-5′ on one side and H_3-1′ and H_3-4′ on the other side of the hydrofuran moiety, leading to the same relative configuration (4*S** and 2′*S**) as that in **5**–**7**.

Then, the specific rotation of **10** was similar to that of **7** ($[\alpha]_D^{25}$ −69 and −52 for **7** and **10**, respectively), suggesting they have the same absolute configuration (4*R* and 2′*R*). However, to remove the effect of structural differences in ring A, the reduction of **10** produced the 4-deoxy derivative **10a** (=**14**), which possessed only the C-2′ stereogenic center (Figure 10). Interestingly, the specific rotation of **10a** showed the same sign as those of **5a** and **6a** but opposite to those of **7a** ($[\alpha]_D^{25}$ +34 and −18 for **7a** and **10a**, respectively), confirming the 2′*S* configuration. My results were in good agreement with the specific rotations of natural **10a** (**14**) and 2′-*epi*-**10a**, which are levorotatory and dextrorotatory, respectively.[44] Overall, the configuration of this compound was assigned as 4*S*,2′*S*. Notably, changing the phenolic A ring to an acid anhydride inverted the sign of the specific rotation of the herqueinone. Thus, **10**, designated as 4-hydroxysclerodin, is a new phenalenone derivative and structurally related to sclerodin (**14**).

In addition to **5**–**10**, five previously reported phenalenones (**11**–**15**) were also isolated. Based on a combination of spectroscopic analyses and a literature survey, these compounds were identified as an acetone adduct of the triketone (**11**),[44] herqueinone (**12**),[33,47,48] isoherqueinone (**13**),[49,50] sclerodin (**14**),[44] and scleroderolide (**15**).[51] The NMR data of these compounds were in good agreement with the reported values in the

literature. Compound **11** was obtained as an unseparated epimeric mixture, which was consistent with the literature.[44,45] Compound **11** was dehydrated to **11a** by the same method used for **8** and **9**, and the 2′*R* configuration was thus assigned. In this way, the epimerization of **11** was found to occur not at C-2′ (in the hydrofuran moiety) but at the hydroxy-bearing C-8 stereogenic center.

Compounds **8**, **9**, and **11** possessed a C_3 oxopropyl moiety (C-6′–C-8′) whose structural resemblance raised the hypothesis that **11** could be the acetone adduct formed during the separation process. This hypothesis has a reliable experimental basis of chemical transformation of a triketone to **11**.[44] In order to verify if **11** is an acetone adduct or a true natural compound biosynthesized by the fungus, the production of these compounds was monitored by time-scale cultivation and LC–ESI–MS analysis. Weekly mass analysis of the culture media showed that the major metabolite **11** was clearly detected after 6 weeks without using acetone. Thus, these compounds were unambiguously proved to be the natural products produced by the *Penicillum* sp. fungus.

Although fungal phenalenones exhibit diverse bioactivities,[31,32] herqueinone-type compounds have not frequently shown remarkable

bioactivities. The mild antioxidant and radical scavenging activities of isoherqueinone (**13**),[39] the antibacterial activity of scleroderolide (**15**),[52] and human leukocyte elastase inhibition of atrovenetinone can be considered exceptions.[53] Regarding the bioactivities of herqueinones, it is interesting to note that the presence of both OH-5 and OH-11 groups are required for the antibacterial activity.[31] The cytotoxicity assay revealed that **5**–**15** were inactive (IC_{50} > 10 μM) against the K562 (human chronic myeloid leukemia) and A549 (adenocarcinomic human alveolar basal epithelial) cancer cell lines. These compounds were also inactive (MIC > 128 μM) against various bacterial and fungal strains, which was consistent with the report on the structure-activity relationships of herqueinones.[31]

Compound **11** moderately inhibited NO production in RAW 264.7 cells with an IC_{50} value of 3.2 μM, while the rest of the isolated compounds were inactive (IC_{50} > 20 μM). In the angiogenesis assay, **10** inhibited tube formation in HUVECs with an IC_{50} of 20.9 μM, while **5** and **13** induced adipogenesis through PPARγ binding and adiponectin secretion-promoting activity in hBM-MSCs and in a concentration-dependent manner, which was determined by adiponectin secretion-promoting effects with their IC_{50} values of 57.5 μM and 39.7 μM, respectively. All of these bioactivities were found to occur without

significant cytotoxicity.

2-3. Experimental section

General Experimental Procedures. Optical rotations were measured on a JASCO P-1020 polarimeter (Easton, MD, USA) using a cell with a 1-cm path length. UV spectra were acquired using a Hitachi U-3010 spectrophotometer (Tokyo, Japan). CD spectra were recorded on an Applied Photophysics Ltd. Chirascan plus CD spectrometer (Applied Photophysics Ltd., Leatherhead, Surrey, UK). IR spectra were recorded on a JASCO 4200 FT-IR spectrometer (Easton, MD, USA) using a ZnSe cell. NMR spectra were recorded in DMSO-d_6 or $CDCl_3$ solutions on Bruker Avance-400, -500, or -600 instruments (Billerica, MA, USA). High-resolution FAB–MS data were acquired using a JEOL JMS 700 mass spectrometer (Tokyo, Japan) with 6 keV-energy, emission current 5.0 mA, xenon as inert gas, and meta-nitrobenzyl alcohol (NBA) as the matrix at the Korea Basic Science Institute (Daegu, Korea). Low-resolution ESI–MS data were recorded on an Agilent Technologies 6130 quadrupole mass spectrometer (Santa Clara, CA, USA) with an Agilent Technologies 1200 series HPLC (Santa Clara, CA, USA). HPLC separations were performed

on a SpectraSYSTEM p2000 equipped with a refractive index detector (SpectraSYSTEM RI-150 (Waltham, MA, USA)) and a UV-Vis detector (Gilson UV-Vis-151 (Middleton, WI, USA)). All solvents used were of spectroscopic grade or were distilled prior to use.

Fungal Material. The fungal strain *Penicillium* sp. was isolated from marine sediments collected from Gagudo, Korea, in October 2008. The isolate was identified using standard molecular biological protocols by DNA amplification and sequencing of the ITS region. Genomic DNA extraction was performed using Intron's i-genomic BYF DNA Extraction Mini Kit according to the manufacturer's protocol. The nucleotide sequence was deposited in the GenBank database under the accession number JF901804. The 18S rDNA sequence of this strain showed 99% identity with *Penicillium herquei* GA4 (GenBank accession number EF536027).

Extraction and Isolation. The fungus was cultivated on YPG medium (5 g of yeast extract, 5 g of peptone, 10 g of glucose in 1 L of artificial seawater) in 2.8 L Fernbach flasks at 30 °C under static conditions in the dark for 6 weeks. The mycelia and culture broth were separated by filtration, and the broth (20 L) was extracted with EtOAc (20

L × 3). The solvent was evaporated under reduced pressure to afford a crude EtOAc extract (6.2 g), which was fractionated by C18 reversed-phase vacuum flash chromatography using mixtures of H_2O-MeOH, from 50:50 to 0:100, and acetone and EtOAc as the eluents.

Based on the ^{1}H NMR and LC–MS analyses, the moderately polar fractions (30:70–10:90 H_2O-MeOH) were chosen for further separation. The fraction (220 mg) that eluted with H_2O-MeOH (30:70) was separated by a semi-preparative reversed-phase HPLC (YMC-ODS-A column, 10 × 250 mm; H_2O-MeOH, 45:55; 1.7 mL/min) to yield **8** (t_R = 18.4 min, 5.5 mg) and **9** (t_R = 18.9 min, 7.7 mg). The fraction (570 mg) that eluted with H_2O-MeOH (20:80) was separated by a semi-preparative reversed-phase HPLC (H_2O-MeOH, 32:68; 1.7 mL/min) to afford **5** (t_R = 37.5 min), **6** (t_R = 27.8 min), **7** (t_R = 29.1 min), **12** (t_R = 25.1 min), and **13** (t_R = 21.8 min). Compounds **5** (311.5 mg), **7** (5.6 mg), **12** (16.5 mg), and **13** (4.4 mg) were purified by an analytical HPLC (YMC-ODS-A column, 4.6 × 250 mm; H_2O-MeOH, 37:63; 0.7 mL/min; t_R = 38.8, 34.5, 30.9, and 27.1 min, respectively). Compound **6** (1.7 mg) was also purified by an analytical HPLC (H_2O-MeCN, 48:52; 0.7 mL/min; t_R = 35.0 min). The fraction (230 mg) eluted with H_2O-MeOH (10:90) was separated by a semi-preparative reversed-phase HPLC (H_2O-MeOH, 22:78; 1.7 mL/min) to yield **11** (t_R =

19.7 min, 73.4 mg), **14** (t_R = 22.8 min), and **15** (t_R = 23.5 min). Compounds **14** (3.9 mg) and **15** (3.3 mg) were further purified by an analytical HPLC (H_2O-MeOH, 26:74; 0.7 mL/min; t_R = 26.8 and 30.1 min, respectively).

***ent*-Peniciherqueinone** (**5**): red, amorphous solid; $[\alpha]_D^{25}$ +203 (*c* 1.7, $CHCl_3$), +254 (*c* 1.0, MeOH); UV (MeOH) λ_{max} (log ε) 217 (4.32), 248 (4.27), 311 (4.20), 427 (3.75) nm; IR (ZnSe) ν_{max} 3413 (br), 1629, 1590, 1385 cm^{-1}; ^1H and ^{13}C NMR data, Table 4; HR–FAB–MS *m/z* 389.1239 $[M + H]^+$ (calcd for $C_{20}H_{21}O_8$, 389.1239).

12-Hydroxynorherqueinone (**6**): red, amorphous solid; $[\alpha]_D^{25}$ +124 (*c* 0.1, MeOH); UV (MeOH) λ_{max} (log ε) 217 (4.32), 248 (4.31), 311 (4.36), 430 (3.80) nm; IR (ZnSe) ν_{max} 3445 (br), 1629, 1579, 1461 cm^{-1}; ^1H and ^{13}C NMR data, Table 5; HR–FAB–MS *m/z* 375.1079 $[M + H]^+$ (calcd for $C_{19}H_{19}O_8$, 375.1080).

***ent*-Isoherqueinone** (**7**): orange, amorphous solid; $[\alpha]_D^{25}$ −69 (*c* 0.2, MeOH); UV (MeOH) λ_{max} (log ε) 217 (4.32), 248 (4.29), 311 (4.22), 428 (3.79) nm; IR (ZnSe) ν_{max} 3422 (br), 1631, 1460 cm^{-1}; ^1H and ^{13}C NMR data, Table 6; HR–FAB–MS *m/z* 373.1285 $[M + H]^+$ (calcd for $C_{20}H_{21}O_7$, 373.1283).

Oxopropylisoherqueinone A (**8**): brown, amorphous solid; $[\alpha]_D^{25}$ +92 (*c* 0.2, MeOH); UV (MeOH) λ_{max} (log ε) 224 (4.36), 274 (4.30), 357 (3.57) nm; IR (ZnSe) ν_{max} 3382 (br), 1678, 1639, 1297 cm^{-1}; ^{1}H and ^{13}C NMR data, Table 7; HR–FAB–MS *m/z* 415.1396 $[M + H]^+$ (calcd for $C_{22}H_{23}O_8$, 415.1393).

Oxopropylisoherqueinone B (**9**): brown, amorphous solid; $[\alpha]_D^{25}$ +43 (*c* 0.2, MeOH); UV (MeOH) λ_{max} (log ε) 224 (4.36), 274 (4.30), 357 (3.57) nm; IR (ZnSe) ν_{max} 3415 (br), 1679, 1640, 1297 cm^{-1}; ^{1}H and ^{13}C NMR data, Table 8; HR–FAB–MS *m/z* 415.1396 $[M + H]^+$ (calcd for $C_{22}H_{23}O_8$, 415.1393).

4-Hydroxysclerodin (**10**): yellow, amorphous solid; $[\alpha]_D^{25}$ −52 (*c* 0.2, MeOH); UV (MeOH) λ_{max} (log ε) 213 (3.94), 280 (4.21), 312 (3.68) nm; IR (ZnSe) ν_{max} 3424 (br), 3069, 1729, 1460, 1286 cm^{-1}; ^{1}H and ^{13}C NMR data, Table 9; HR–FAB–MS *m/z* 345.0977 $[M + H]^+$ (calcd for $C_{18}H_{17}O_7$, 345.0974).

Reduction of Herqueinones (**5**–**10**). To a solution of 44.3 mg (114 μM) of **5** in 0.5 mL of glacial acetic acid was added 100.0 mg (1.53 mM) of zinc dust under nitrogen atmosphere. The mixture was stirred at room temperature for 30 min and filtered through cotton with 1.0 mL of distilled

water. The filtrate was left to stand for 45 min and extracted with 1.5 mL of ethyl acetate. Purification by analytical HPLC (YMC-ODS-A column, 4.6 × 250 mm; H_2O-MeCN (50:50); 0.7 mL/min) afforded the 4-deoxy derivative (**5a**, 6.8 mg) (t_R = 15.8 min) as a pure compound. Compounds **6**–**10** were reduced in a similar manner.

4-Deoxy-*ent*-peniciherqueinone (**5a**): $[\alpha]_D^{25}$ −23 (*c* 0.5, $CHCl_3$); ^1H NMR ($CDCl_3$, 400 MHz) δ_H 13.14 (1H, s), 13.10 (1H, s), 13.07 (1H, s), 4.57 (1H, q, *J* = 6.5 Hz), 3.99 (3H, s), 2.71 (3H, s), 1.50 (3H, s), 1.44 (3H, d, *J* = 6.5 Hz), 1.25 (3H, s); ESI–MS *m/z* 373.1 $[M + H]^+$ (calcd for $C_{20}H_{21}O_7$, 373.1).

4-Deoxy-12-hydroxynorherqueinone (**6a**): $[\alpha]_D^{25}$ −20 (*c* 0.3, $CHCl_3$); ^1H NMR (DMSO-d_6, 400 MHz) δ_H 14.32 (1H, s), 13.52 (1H, s), 9.28 (1H, s), 8.72 (1H, s), 4.64 (1H, q, *J* = 6.5 Hz), 2.66 (3H, s), 1.49 (3H, s), 1.38 (3H, d, *J* = 6.5 Hz), 1.26 (3H, s); ESI–MS *m/z* 359.1 $[M + H]^+$ (calcd for $C_{19}H_{19}O_7$, 359.1).

4-Deoxy-*ent*-isoherqueinone (**7a**): $[\alpha]_D^{25}$ +34 (*c* 0.5, $CHCl_3$); ^1H NMR (DMSO-d_6, 400 MHz) δ_H 13.52 (1H, s), 8.13 (1H, s), 7.48 (1H, br s), 7.14 (1H, br s), 4.69 (1H, q, *J* = 6.5 Hz), 3.13 (3H, s), 2.66 (3H, s), 1.47 (3H, s), 1.42 (3H, d, *J* = 6.5 Hz), 1.22 (3H, s); ESI–MS *m/z* 357.3 [M +

H]$^+$ (calcd for $C_{20}H_{21}O_6$, 357.3).

4-Deoxy-oxopropylisoherqueinone A (**8a**): $[\alpha]_D^{25}$ +8 (*c* 0.5, $CHCl_3$), +10 (*c* 0.5, MeOH); ^{1}H NMR (DMSO-d_6, 400 MHz) δ_H 13.27 (1H, s), 8.48 (1H, s), 6.18 (1H, s), 5.73 (1H, s), 4.13 (1H, q, *J* = 6.5 Hz), 3.16 (2H, s), 2.80 (3H, s), 2.05 (3H, s), 1.35 (3H, s), 1.25 (3H, d, *J* = 6.5 Hz), 1.05 (3H, s); ESI–MS *m/z* 399.1 [M + H]$^+$ (calcd for $C_{22}H_{23}O_7$, 399.1).

4-Deoxy-oxopropylisoherqueinone B (**9a**): $[\alpha]_D^{25}$ +3 (*c* 0.5, $CHCl_3$), +5 (*c* 0.5, MeOH); ^{1}H NMR (DMSO-d_6, 400 MHz) δ_H 13.27 (1H, s), 8.47 (1H, s), 6.18 (1H, s), 5.71 (1H, s) 4.10 (1H, q, *J* = 6.5 Hz), 3.16 (2H, s), 2.80 (3H, s), 2.05 (3H, s), 1.34 (3H, s), 1.26 (3H, d, *J* = 6.5 Hz), 1.05 (3H, s); ESI–MS *m/z* 399.1 [M + H]$^+$ (calcd for $C_{22}H_{23}O_7$, 399.1).

Sclerodin (**10a** = **14**): $[\alpha]_D^{25}$ −18 (*c* 0.5, $CHCl_3$); ^{1}H NMR ($CDCl_3$, 400 MHz) δ_H 11.5 (1H, s), 6.75 (1H, s), 5.06 (1H, q, *J* = 6.5 Hz), 2.69 (3H, s), 1.48 (3H, d, *J* = 6.5 Hz), 1.41 (3H, s), 0.92 (3H, s); ESI–MS *m/z* 329.1 [M + H]$^+$ (calcd for $C_{18}H_{17}O_6$, 329.1).

Acetylation of 4-Deoxy-*ent*-peniciherqueinone (5a). To a solution of 3.0 mg (2.7 mM) of **5a** in 3.0 mL of pyridine was added 0.4 mL of Ac_2O. After stirring the mixture for 4 h at room temperature, the

pyridine and excess Ac_2O were removed under vacuum. Purification by analytical HPLC (YMC-ODS column, 4.6 × 250 mm; 0.7 mL/min; H_2O-MeCN (40:60)) yielded 4-deoxy-9,11,12-triacetyl-*ent*-peniciherqueinone (**5b**) (t_R = 35.8 min): $[\alpha]_D^{25}$ −35 (*c* 0.5, $CHCl_3$), −42 (*c* 0.5, MeOH); ^1H NMR ($CDCl_3$, 400 MHz) δ_H 4.72 (1H, q, *J* = 6.5 Hz), 4.05 (3H, s), 2.71 (3H, s), 2.404 (3H, s), 2.401 (3H, s), 2.39 (3H, s), 1.59 (3H, s), 1.50 (3H, d, *J* = 6.5 Hz), 1.35 (3H, s); ESI–MS m/z 499.5 $[M + H]^+$ (calcd for $C_{26}H_{27}O_{10}$, 499.5).

Dehydration of Herqueinones (8a, 9a, and 11). To a solution of 0.5 mg (44 mM) of Na in 500 μL of anhydrous ethanol was added 1.5 mg (7.5 mM) of **8a** under nitrogen atmosphere. After stirring the mixture for 6 h at room temperature, the solvent was removed under vacuum. Purification by analytical HPLC (YMC-ODS column, 4.6 × 250 mm; 0.7 mL/min; H_2O-MeCN (40:60)) afforded the 8(6′)-dehydroxy derivative (**8b**) (t_R = 12.2 min) as a pure compound. Compounds **9a** and **11** were dehydrated to **9b** and **11a**, respectively, in the same manner.

4-Deoxy-8(6′)-dehydroxyoxopropylisoherqueinone A (**8b**): $[\alpha]_D^{25}$ +27 (*c* 0.5, $CHCl_3$); ^1H NMR ($CDCl_3$, 400 MHz) δ_H 13.31 (1H, s), 12.79 (1H, s), 6.33 (1H, s), 5.61 (1H, s) 4.42 (1H, q, *J* = 6.5 Hz), 2.56 (3H, s),

2.38 (3H, s), 1.46 (3H, s), 1.38 (3H, d, *J* = 6.5 Hz), 1.20 (3H, s); ESI–MS *m/z* 381.1 $[M + H]^+$ (calcd for $C_{22}H_{21}O_6$, 381.1).

4-Deoxy-8(6′)-dehydroxyoxopropylisoherqueinone B (**9b**): $[\alpha]_D^{25}$ +26 (*c* 0.5, $CHCl_3$); ^1H NMR ($CDCl_3$, 400 MHz) δ_H 13.31 (1H, s), 12.79 (1H, s), 6.33 (1H, s), 5.61 (1H, s) 4.42 (1H, q, *J* = 6.5 Hz), 2.56 (3H, s), 2.38 (3H, s), 1.46 (3H, s), 1.38 (3H, d, *J* = 6.5 Hz), 1.20 (3H, s); ESI–MS *m/z* 381.1 $[M + H]^+$ (calcd for $C_{22}H_{21}O_6$, 381.1).

8(6′)-Dehydroxy derivative of 11 (**11a**): $[\alpha]_D^{25}$ +26 (*c* 0.5, $CHCl_3$); ^1H NMR ($CDCl_3$, 400 MHz) δ_H 13.31 (1H, s), 12.79 (1H, s), 6.33 (1H, s), 5.61 (1H, s) 4.42 (1H, q, *J* = 6.5 Hz), 2.56 (3H, s), 2.38 (3H, s), 1.46 (3H, s), 1.38 (3H, d, *J* = 6.5 Hz), 1.20 (3H, s); ESI–MS *m/z* 381.1 $[M + H]^+$ (calcd for $C_{22}H_{21}O_6$, 381.1).

ECD Calculations. The conformational searches for the C-8 position of **8** and **9** were performed using Macromodel (Version 9.9, Schrodinger LLC.) software with “Mixed torsional/Low Mode sampling” in the GAFF force field. The experiments were conducted in the gas phase with a 50 kJ/mol energy window limit and a maximum of 10,000 steps to thoroughly examine all low-energy conformers. The Polak–Ribiere conjugate gradient (PRCG) method was utilized for minimization

processes with 10,000 maximum iterations and a 0.001 kJ (mol Å)$^{-1}$ convergence threshold on the RMS gradient. Conformers within 10 kJ/mol of each global minimum for *R* and *S* form of **8** and **9** were used for gauge-independent atomic orbital (GIAO) shielding constant calculations without geometry optimization employing TmoleX Version 4.2.1 (COSMOlogic GmbH & Co. KG, Leverkusen, Germany) at the B3LYP/6-31G(d,p) level in the gas phase. The ECD spectra were simulated by overlapping each transition, where σ is the width of the band at 1/*e* height. ΔE_i and R_i are the excitation energies and rotatory strengths, respectively, for transition *i*. In the current work, the value was 0.10 eV.

$$\Delta \in (E) = \frac{1}{2.297 \times 10^{-39}} \frac{1}{\sqrt{2\pi}\sigma} \sum_{i}^{A} \Delta E_i R_i e^{[-(E-\Delta E_i)^2/(2\sigma)^2]}$$

Cytotoxicity and Antibacterial Assay. The cytotoxicity assay was performed in accordance with the published protocols.[54] The antimicrobial assay was performed according to the method described previously.[55]

iNOS Assay. Mouse macrophage RAW 264.7 cells obtained from the American Type Culture Collection (ATCC, Rockville, MD, USA) were cultured in Dulbecco's modified Eagle's medium (DMEM) supplemented with 10% heat-inactivated fetal bovine serum (FBS) with antibiotics-

antimycotics (PSF; 100 units/mL penicillin G sodium, 100 ng/mL streptomycin, and 250 ng/mL amphotericin B).[56,57] The cells were seeded in 24-well plates (2×10^5 cells/mL). The next day, the culture media was changed to 1% FBS-DMEM, and the samples were treated with the test compounds. After pretreatment with the drug for 1 h, 1 μg/mL lipopolysaccharides (LPS) was added to stimulate NO production. The cells were incubated for an additional 18 h, and the amount of NO produced in the supernatant was determined by Griess reaction. Then, the absorbance was measured at 540 nm, and the nitrite concentration was determined by comparison with a sodium nitrite standard curve. The percent inhibition was calculated using the following formula: [1 − (NO level of test samples/NO levels of vehicle-treated control)] × 100. The IC_{50} values were calculated through nonlinear regression analysis using TableCurve 2-D v5.01 (Systat Software Inc., San Jose, CA, USA). At the same time, MTT assays were also performed to test cell viability. MTT solution (final concentration of 500 μg/mL) was added to the cells, and they were incubated for 4 h at 37 °C. The culture media was removed, and the remaining dyes were dissolved in DMSO. The absorbance of each well was measured at 570 nm using a VersaMax ELISA microplate reader (Molecular Devices, Sunnyvale, CA, USA). The percent survival was

determined by comparison with a control group (LPS+).

Tube Formation Assay. Human umbilical vascular endothelial cells (HUVECs) were purchased from the American Type Culture Collection (ATCC, Rockville, MD, USA), and cultured in EGM-2 (Lonza, Walkerswille, MD, USA) supplemented with 10% FBS and antibiotics-antimycotics (PSF).[58,59] The cells were maintained at 37 °C under a humidified atmosphere containing 5% CO_2. A 96-well plate was coated with Matrigel (Corning) for 30 min at 37 °C under a humidified atmosphere containing 5% CO_2. HUVECs (1.8×10^4 cells/well) were mixed with the test compounds in 0.5% FBS EBM-2 medium with VEGF (50 ng/mL) or 0.5% FBS EBM-2 medium only for the VEGF negative control. The cells were incubated for 6 h and photographed using an inverted microscope (Olympus Optical Co. Ltd., Tokyo, Japan). Images were quantified with an angiogenesis analyzer using ImageJ software. Tube formation activity was calculated using the following formula: [(Total segment # (tested compound) − Total segment # (VEGF−)]/[Total segment # (VEGF+) − Total segment # (VEGF−)] × 100 (# stands for tubule segment number). The IC_{50} values were calculated through nonlinear regression analysis using TableCurve 2-D v5.01 (Systat Software Inc., San Jose, CA, USA). Cell viabilities were evaluated with

the MTT assay. HUVECs (0.8×10^4 cells/well) were seeded into a 96-well plate and indicated for 1 day. The culture medium was replaced with serum-free medium, and the cells were incubated overnight. After starvation, the cells were treated with the test compounds and VEGF (50 ng/mL) in 2% FBS EBM-2 medium. Cells were incubated for a further 24 h, and MTT solution (final concentration of 500 μg/mL) was added to the cells to measure the cell viability. The formazan products were dissolved in DMSO. The absorbance of each well was measured at 570 nm using a VersaMax ELISA microplate reader (Molecular Devices, Sunnyvale, CA, USA).

Adiponectin Production Assay. Human bone marrow-mesenchymal stem cells (hBM-MSCs) were purchased from Lonza, Inc. (Walkersville, MD, USA) and cultured in low-glucose (1 g/L) DMEM supplemented with 10% FBS, penicillin-streptomycin, and Glutamax™ (Invitrogen, Carlsbad, CA, USA). To induce adipogenesis, the cell growth medium was replaced with high-glucose (4.5 g/L) DMEM supplemented with 10% FBS, penicillin-streptomycin, 10 μg/mL insulin, 0.5 μM dexamethasone, and 0.5 mM 3-isobutyl-1-methylxanthine (IBMX) (IDX conditions).[60] IBMX, pioglitazone, and aspirin were purchased from Sigma-Aldrich (St. Louis, MO, USA). hBM-MSCs were stained with

0.2% oil red O (ORO) reagent for 10 min at 24 °C, and then washed with H_2O four times. Following a 10-min elution with isopropanol, the absorbance was measured at 500 nm using a spectrophotometer. To visualize the nucleus, the hBM-MSCs were counterstained with hematoxylin reagent for 2 min and then washed twice with H_2O. The level of adipocyte differentiation was observed and counted using an inverted phase microscope. A Quantikine immunoassay kit (R&D Systems, Minneapolis, MN, USA) was used for quantitative determination of adiponectin in the cell culture supernatants.

Receptor Binding Assay. The time-resolved fluorescence resonance energy transfer (TR-FRET)-based nuclear receptor binding assay to evaluate binding of the ligand to PPARγ was performed using Lanthanscreen^{TM} competitive binding assay kits (Invitrogen).[60] All assay measurements were performed using a CLARIOstar instrument (BMG LABTECH, Ortenberg, Germany) with the settings described in the TR-FRET manufacturer's instructions.

(Bioactivity experiments were performed by Prof. Minsoo Noh's and Prof. Sang Kook Lee's laboratory)

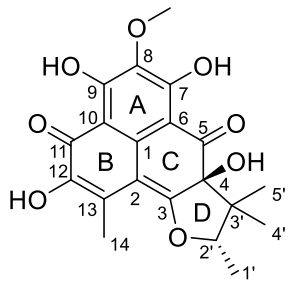

Table 4. ^{13}C and ^{1}H NMR assignment for compound **5** in $CDCl_3$

Position	δ_C, type	δ_H (*J* in Hz)	Position	δ_C, type	δ_H (*J* in Hz)
1	137.3, C		1′	13.3, CH_3	1.40, d (6.6)
2	103.7, C		2′	89.5, CH	4.99, q (6.6)
3	174.6, C		3′	46.9, C	
4	79.0, C		4′	16.4, CH_3	1.43, s
5	197.6, C		5′	16.4, CH_3	0.86, s
6	103.5, C		4-OH		7.23, s
7	162.8, C		7-OH		13.23, s
8	131.6, C		9-OH		13.99, s
9	161.7, C		12-OH		6.66, s
10	108.7, C				
11	178.1, C				
12	143.7, C				
13	124.0, C				
14	14.9, CH_3	2.47, s			
15	60.9, CH_3	3.92, s			

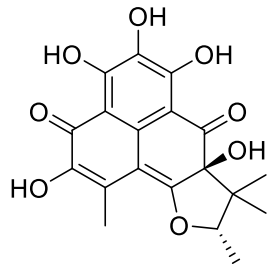

Table 5. ^{13}C and ^{1}H NMR assignment for compound **6** in DMSO-d_6

Position	δ_C, type	δ_H (J in Hz)	Position	δ_C, type	δ_H (J in Hz)
1	133.5, C		1′	12.9, CH_3	1.34, d (6.4)
2	102.9, C		2′	88.7, CH	4.88, q (6.4)
3	173.9, C		3′	45.9, C	
4	78.2, C		4′	15.9, CH_3	1.30, s
5	198.3, C		5′	16.1, CH_3	0.75, s
6	102.6, C		4-OH		7.28, s
7	157.2, C		7-OH		13.14, s
8	129.2, C		8-OH		8.96, s
9	156.2, C		9-OH		14.55, s
10	108.4, C		12-OH		9.00, s
11	178.7, C				
12	143.9, C				
13	123.8, C				
14	14.4, CH_3	2.39, s			
15					

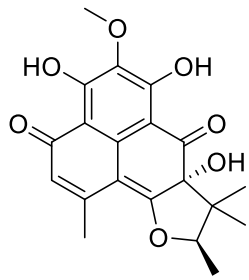

Table 6. ^{13}C and ^{1}H NMR assignment for compound **7** in DMSO-d_6

Position	δ_C, type	δ_H (J in Hz)	Position	δ_C, type	δ_H (J in Hz)
1	139.0, C		1′	12.9, CH_3	1.37, d (6.5)
2	103.0, C		2′	90.6, CH	4.99, q (6.5)
3	178.2, C		3′	46.0, C	
4	78.5, C		4′	15.9, CH_3	0.78, s
5	197.7, C		5′	16.1, CH_3	1.32, s
6	102.6, C		4-OH		7.52, s
7	161.9, C		7-OH		13.26, s
8	131.2, C		9-OH		15.73, s
9	163.0, C				
10	109.2, C				
11	186.4, C				
12	122.8, CH	6.36, s			
13	150.9, C				
14	23.8, CH_3	2.48, s			
15	60.0, CH_3	3.77, s			

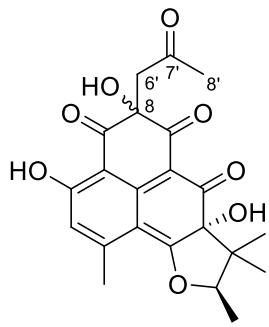

Table 7. ^{13}C and ^{1}H NMR assignment for compound **8** in DMSO-d_6

Position	δ_C, type	δ_H (J in Hz)	Position	δ_C, type	δ_H (J in Hz)
1	142.7, C		1′	12.7, CH_3	1.30, d (6.4)
2	116.3, C		2′	88.6, CH	4.77, q (6.4)
3	175.1, C		3′	45.6, C	
4	78.5, C		4′	16.1, CH_3	0.79, s
5	193.1, C		5′	16.3, CH_3	1.25, s
6	101.2, C		6′	48.5, CH_2	3.30, s
7	189.9, C		7′	206.9, C	
8	76.9, C		8′	29.8, CH_3	2.09, s
9	200.6, C		4-OH		7.15, s
10	109.4, C		8-OH		6.68, s
11	165.6, C		11-OH		12.80, s
12	117.5, CH	6.75, s			
13	152.3, C				
14	23.5, CH_3	2.57, s			
15					

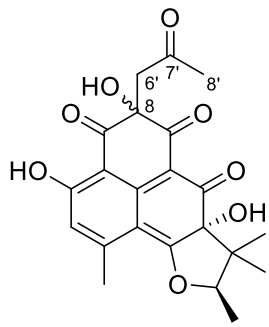

Table 8. ^{13}C and ^{1}H NMR assignment for compound **9** in DMSO-d_6

Position	δ_C, type	δ_H (J in Hz)	Position	δ_C, type	δ_H (J in Hz)
1	142.9, C		1′	12.8, CH_3	1.29, d (6.5)
2	116.7, C		2′	88.8, CH	4.79, q (6.5)
3	175.6, C		3′	45.3, C	
4	78.5, C		4′	16.1, CH_3	0.78, s
5	193.3, C		5′	16.3, CH_3	1.25, s
6	101.4, C		6′	48.6, CH_2	3.38, s
7	189.3, C		7′	207.1, C	
8	75.8, C		8′	29.7, CH_3	2.12, s
9	200.3, C		4-OH		7.23, s
10	109.4, C		8-OH		6.82, s
11	165.8, C		11-OH		12.75, s
12	117.5, CH	6.76, s			
13	152.2, C				
14	23.4, CH_3	2.55, s			
15					

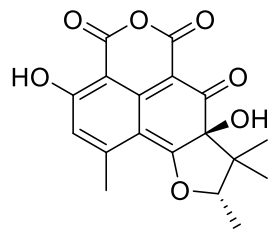

Table 9. ^{13}C and ^{1}H NMR assignment for compound **10** in DMSO-d_6

Position	δ_C, type	δ_H (J in Hz)
1	141.8, C	
2	115.4, C	
3	180.4, C	
4	78.9, C	
5	192.2, C	
6	92.3, C	
7	155.5, C	
8		
9	164.4, C	
10	102.0, C	
11	164.0, C	
12	117.3, C	6.81, s
13	152.4, C	
14	23.2, CH_3	2.58, s
15		
1′	12.8, CH_3	1.36, d (6.5)
2′	90.8, CH	4.92, q (6.5)
3′	45.7, C	
4′	16.0, CH_3	0.78, s
5′	16.3, CH_3	1.26, s
4-OH		7.41, s
11-OH		11.43, br s

IV. Sortase A-Inhibitory Metabolites from a Marine-Derived Fungus *Aspergillus* sp.

3-1. Introduction

Antibiotic-resistant bacteria are the most prominent limitation in conventional antimicrobial treatment.[61] Microorganisms can acquire antibiotic resistance when their survival is at risk. Whereas antibiotics have a long-standing history of success in treatment of bacterial infections, recent increasing antimicrobial resistance has stimulated the search for anti-virulence drugs as an alternative to conventional antibiotics, despite their high importance, for counteracting bacterial pathogens.[62,63]

The pathogenesis of bacterial infections is initiated with bacterial adhesion to host tissue surfaces mediated via specific interactions between host ligands and bacterial surface proteins.[64] In particular, in Gram-positive bacteria including *Staphylococcus aureus*, this fundamental stage of infection proceeds through sortase-mediated anchoring of surface proteins in host cells to the bacterial cell wall envelope.[65] In *S. aureus*, sortase A (SrtA) cleaves surface proteins between threonine and glycine

residues in LPXTG sorting signals at their C-termini and is subsequently incorporated into the bacterial cell wall envelope via a transpeptidation reaction.[66,67] Numerous knockout studies have revealed that SrtA plays a critical role in the pathogenesis of Gram-positive bacterial infections, including those of *S. aureus*, by modulating bacterial adhesion to host tissues.[68–70] SrtA decorates the surfaces of Gram-positive bacteria with a diverse array of proteins that enable each microbe to effectively interact with its environment and is not required for bacterial growth or viability.[62,63] It is thus considered a promising target for the development of anti-virulence drugs that aim to interfere with important virulence mechanisms, such as adhesion to host tissues.

The secondary metabolites of marine fungi including polyketides, alkaloids, terpenes, lactones, and peptides are a rich source of bioactive natural products.[71] Many bioactive compounds with varying degrees of action, such as antibiotic, antiviral, antimicrobial, and anticancer properties, have been isolated from marine fungal sources. Recent investigations of marine fungal metabolites looking for bioactive compounds indicate their potential as a source of new medicines.[72,73] Previously, I reported several novel natural products isolated from marine-derived fungi; polyaromatic metabolites from *Penicillium* sp. exhibited

moderate cytotoxicity and significant inhibitory activity against *S. aureus* SrtA,[36] asperphenins from *Aspergillus* sp. induced significant cytotoxicity in diverse cancer cells,[74] and peptides from *A. allahabadii* and *A. ochraceopetaliformis* displayed SrtA inhibitory activity.[13]

In further study, chemical investigation of *Aspergillus* sp. F452 was performed,[74] whose crude extract inhibited *S. aureus*-derived SrtA (63% inhibition at 100 μg/mL). Bioassay-guided separation of the extract yielded seven alkaloidal (**17**–**23**) and one polyketide (**16**) compound, whose structures were analyzed through combined spectroscopic methods. This study describes the structures and biological activities of these compounds. Among them, compound **16** (aspermytin A) significantly inhibited *S. aureus*-derived SrtA. The *in vivo* bioactivity and underlying mechanism of action were also found to be associated with the inhibition of SrtA-mediated *S. aureus* adhesion to the eukaryotic cell matrix protein fibronectin.

3-2. Results and discussion

The fungal strain F452[74] was cultured in semisolid rice medium

and extracted with MeOH and CH_2Cl_2. Following solvent evaporation, the combined extract was separated by solvent partitioning followed by reversed-phase C_{18} vacuum flash chromatography and semi-preparative HPLC to yield eight compounds. Compounds **16**–**23** were identified as aspermytin A (**16**),[75] versicomide A (**17**),[76] versicoloid A (**18**),[77] isochaetominines A–C (**19**–**21**),[78,79] 14-*epi*-isochaetominine C (**22**),[79] and fumiquinazoline K (**23**),[80] respectively, via combined spectroscopic analyses, including high-resolution fast atom bombardment mass spectroscopy, ^{1}H- and ^{13}C-NMR, 2-D NMR, and UV spectroscopy (Figure 12).[70] The spectroscopic data for these compounds were in good agreement with those in the literature.

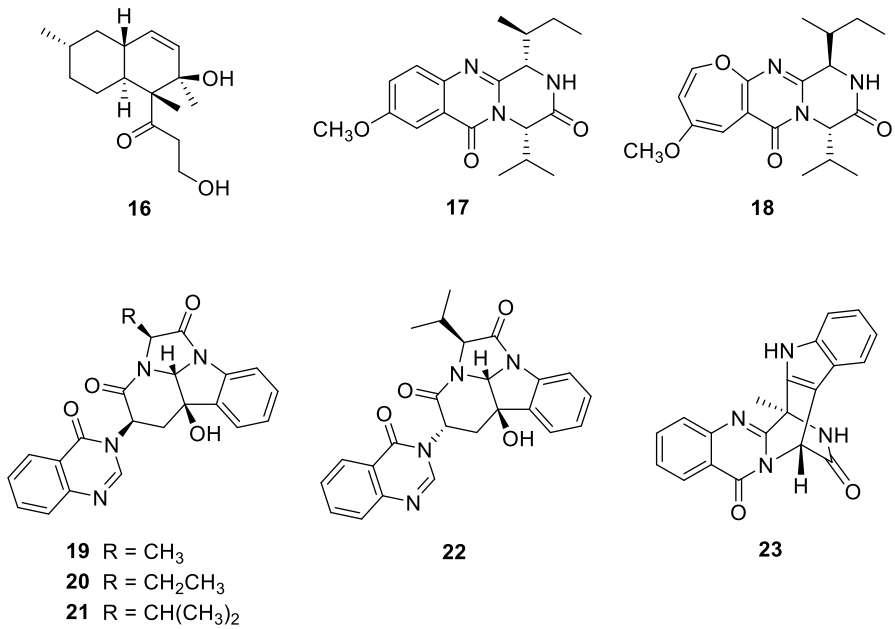

Figure 12. Chemical structures of compounds **16**–**23**.

Recombinant SrtA derived from *S. aureus* ATCC6538p was purified from *Escherichia coli* extracts using metal chelate-affinity chromatography.[81] The enzyme activity was determined from the fluorescence intensity upon cleavage of a peptide substrate containing the LPETG motif.[82] Throughout the separation process, the crude extract and chromatographic fractions containing fungal metabolites of strain F452 inhibited the activity of SrtA. Accordingly, the same bioassay was

performed using pure compounds. The inhibitory potencies of the pure compounds against recombinant SrtA, expressed as IC_{50} values, are shown in Table 10 and are compared to those of the known SrtA inhibitors berberine chloride (IC_{50} = 85.9 μM) and *para*-hydroxymercuribenzoic acid (*p*HMB) (IC_{50} = 112.5 μM). The pure compounds **16**–**23** displayed weak to significant SrtA inhibition (IC_{50} values of 269.4–146.0 μM). Among them, compound **16** exhibited the most potent inhibitory activity.

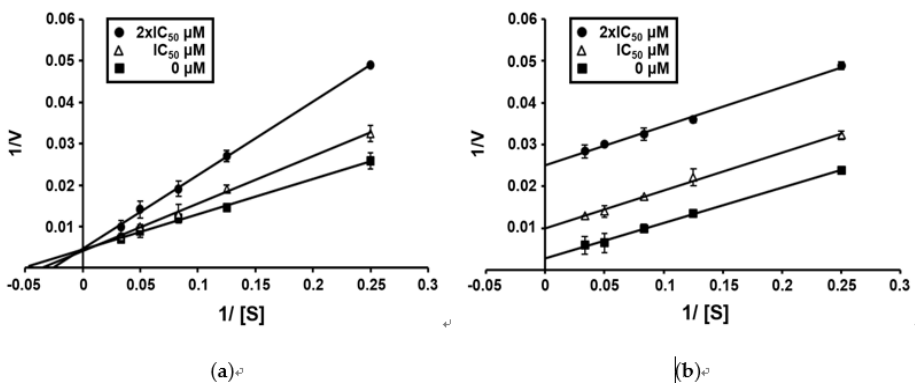

(**a**) (**b**)

Figure 13. Lineweaver-Burk plot of SrtA inhibition by compounds **16** (**a**) and **18** (**b**). [S], substrate concentration [μM]; *V*, reaction velocity (Δabsorbance unit/min). Each data point represents the mean of three experiments.

Table 10. Inhibitory activity of compounds **16**–**23** toward the activity of the SrtA enzyme and bacterial growth of *S. aureus* ATCC6538p.

Compounds	SrtA IC_{50} μM (μg/mL)	MIC μM (μg/mL)
16	146.0 ± 2.3 (38.9 ± 0.6)	>480.5 (>128)
17	269.4 ± 3.9 (92.5 ± 1.4)	>372.7 (>128)
18	193.5 ± 2.5 (69.5 ± 0.9)	>356.1 (>128)
19	267.9 ± 4.1 (107.8 ± 1.5)	>318.1 (>128)
20	232.5 ± 3.7 (96.8 ± 1.4)	>307.4 (>128)
21	216.4 ± 2.5 (93.1 ± 1.1)	>297.4 (>128)
22	237.1 ± 3.8 (102.1 ± 1.2)	>297.4 (>128)
23	235.1 ± 2.6 (83.8 ± 0.9)	>359.2 (>128)
Berberine chloride	85.9 ± 1.2 (31.9 ± 0.4)	>332.2 (>128)
*p*HMB	112.5 ± 1.7 (33.1 ± 0.5)	ND[1]
Ampicillin	ND	0.4 (0.1)

[1]ND means not determined. *para*-Hydroxymercuribenzoic acid (*p*HMB) and berberine chloride were used as reference inhibitors of SrtA. Ampicillin was used as a standard antibacterial drug.

To determine the type of inhibition, kinetic studies were performed with compounds **16** and **18** at IC_{50} or twofold IC_{50} based on Lineweaver and Burk plot (Figure 13).[83] Inhibitor constants were obtained by Dixon plot. Inhibitory kinetics show that compound **16** behaved as a mixed inhibitor (Ki = 265.0 μM). In contrast, compound **18** behaved as an

uncompetitive inhibitor (*K*i = 83.0 μM). Moreover, the binding of compounds **16** and **18** to SrtA were reversible because the enzyme activity was indeed recovered by dialysis within 2 h, excluding the possible existence of a covalent bond between inhibitor and enzyme.

Because SrtA inhibitors are expected to serve as anti-infective agents and inhibit bacterial pathogenesis without affecting cell viability,[68] the minimum inhibitory concentrations (MICs) of these compounds were also measured to exclude the possible effects of test compounds on *S. aureus* cell adhesion to the eukaryotic cell matrix protein fibronectin owing to the inhibition of cell growth. The compounds did not exhibit inhibitory activity against *S. aureus* ATCC6538p (MIC > 128 μg/mL) (Table 10). In the cytotoxicity assay against A549 (lung cancer) and K562 (leukemia) cell lines, compounds **16**–**23** displayed weak (**17**–**22**: IC_{50} > 13–50 μM) to no inhibitory activity (**16** and **23**: IC_{50} > 100 μM), comparable to etoposide (IC_{50} = 0.5 μM).

An active SrtA enzyme is required for the attachment of *S. aureus* to eukaryotic cell matrix proteins, such as fibronectin and fibrinogen, thus accelerating bacterial adhesion to host tissues and subsequent invasion.[84] The *srtA*$^-$ mutant strain cannot bind these proteins. Thus, SrtA inhibitors

should inhibit SrtA activity *in vivo* and in turn reduce fibronectin-binding protein surface display. Initially, the SrtA-mediated fibronectin-binding capacities of *S. aureus* strain Newman (wild-type) and its isogenic *srtA* knockout mutant (*srtA*$^-$) to fibronectin were evaluated. As shown in Figure 14a, the fibronectin-binding activity of the *srtA* knockout mutant was significantly reduced compared to that of the wild type. Based on SrtA inhibition intensity, compound **16** was selected. The results of the inhibition of *S. aureus* adhesion to fibronectin via fibronectin-binding protein by compound **16** are shown in Figure 14b. As expected, treatment of strain Newman with 0-, 1-, 2-, or 4-fold the SrtA IC_{50} of compound **16** significantly reduced bacterial adherence to fibronectin-coated surfaces. The onset and magnitude of inhibition of Newman strain adhesion to fibronectin by compound **16** with 4× the SrtA IC_{50} value was comparable to the behavior of the untreated *srtA* knockout mutant, as shown in Figure 14a. The results of a fibronectin-binding assay suggested the potential of this compound in treating *S. aureus* infections through inhibition of SrtA activity.

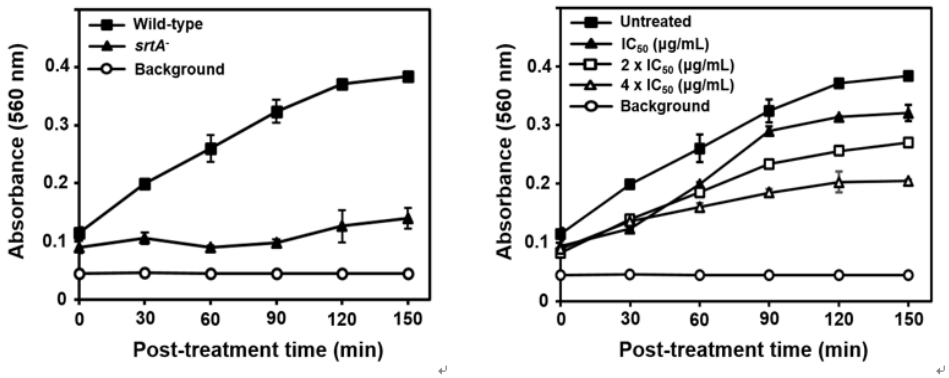

(**a**) (**b**)

Figure 14. Adhesion of *S. aureus* strain Newman (wild type) and the isogenic *srtA* knockout mutant (*srtA*$^-$) to fibronectin (**a**), and inhibition of Newman strain adhesion to fibronectin by compound **16** (**b**) with 0×, 1×, 2×, or 4× the SrtA IC_{50} value. The results are presented as the mean ± standard deviation of three replicates.

3-3. Experimental section

General Experimental Procedures. The UV spectra were acquired with a Hitachi U-3010 spectrophotometer. The NMR spectra were recorded in DMSO-d_6 solution using Bruker Avance (400, 500, or 600) instruments. Low-resolution ESI–MS data were recorded on an

Agilent Technologies 6130 quadrupole mass spectrometer with an Agilent Technologies 1200 series HPLC system. HPLC analyses were performed on a Spectrasystem p2000 equipped with a refractive index detector (Spectrasystem RI-150). All of the solvents used were spectroscopic grade or distilled from glass prior to use.

Fungal Material. The isolation and identification of *Aspergillus* sp. (strain number F452) have previously been reported.[74] The fungal strain was isolated from submerged, decaying wood off the shore of Jeju Island, Korea, and identified using standard molecular biological protocols by DNA amplification and sequencing of the ITS region. The nucleotide sequence of F452 has been deposited in the GenBank database under accession number KF384188.

Extraction and Isolation. The isolated strain was cultivated on a YPG agar plate (5 g of yeast extract, 5 g of peptone, 10 g of glucose, and 16 g of agar in 1 L of artificial seawater) at 30°C for 4 days. The agar plugs (1 cm × 1 cm, 5 pieces each) were inoculated into 100 mL YPG medium in a 250 mL Erlenmeyer flask for 5 days, then separately transferred to 2.8 L glass Fernbach flasks with rice medium (200 g of rice, 2 g of peptone, and 2 g of yeast extract with 200 mL of artificial seawater

in each flask, boiled in an autoclave for 20 min at 120°C; 50 flasks in total).

Fermentation in rice medium was conducted under static conditions for 6 weeks followed by extraction of each flask with MeOH (1 L × 3) and CH_2Cl_2 (1 L × 3). The solvent was combined and evaporated to obtain an organic extract. The combined extracts (247.33 g) were successively partitioned between *n*-BuOH (177.12 g) and H_2O (70.05 g); the former fraction was repartitioned using H_2O-MeOH (15:85) (83.31 g) and *n*-hexane (93.18 g). The H_2O-MeOH fraction was separated by C_{18} reversed-phase vacuum flash chromatography using a sequential mixture of MeOH and H_2O as eluents (five fractions in the gradient, H_2O-MeOH, from 60:40 to 0:100), acetone, and finally EtOAc.

Based on the results of ^{1}H NMR analyses and bioactivity tests, the 30:70 H_2O-MeOH fraction (9.20 g) was separated by semi-preparative reversed-phase HPLC (YMC-ODS-A column, 10 × 250 mm; H_2O-MeOH, 50:50; 1.7 mL/min) and yielded compounds **16** (t_R = 46.1 min), **17** (t_R = 22.2 min), **18** (t_R = 13.5 min), **19** (t_R = 37.2 min), **20** (t_R = 40.5 min), **21** (t_R = 66.9 min), **22** (t_R = 74.1 min), and **23** (t_R = 15.4 min). Compounds **16**, **19**, and **20** were further purified by analytical HPLC (YMC-ODS-A column,

4.6 × 250 mm; H_2O-MeCN, 65:35; 0.7 mL/min; t_R = 18.2, 11.9, and 14.5 min, respectively). The purified metabolites were isolated at the following yields: 5.5, 3.4, 4.4, 2.9, 5.1, 9.3, 1.9, and 7.9 mg for **16**–**23**, respectively.

SrtA Inhibition Assay. The *srtA* gene from *S. aureus* ATCC6538p was expressed and recombinant SrtA was purified as previously described.[81] The SrtA inhibition test was carried out by analyzing the increased fluorescence intensity resulting from the cleavage of synthetic peptide substrate dabcyl-LPETG-edans (AnaSpec, Inc., Fremont, CA, USA)[67,82] with slight modification. The reaction was carried out with 100 μL buffer (50 mM Tris-HCl, 5 mM $CaCl_2$, and 150 mM NaCl, pH 7.5), 7.5 μM synthetic peptide, 7.5 μM purified SrtA, and test samples at various concentrations. Each sample was dissolved in DMSO and diluted with reaction buffer to obtain a final concentration of 1% DMSO, which did not influence enzyme activity. The SrtA inhibition assay was conducted at 37°C for 1 h, and inhibition was quantified fluorometrically using a microplate reader (FLx800, BioTek Instruments, Winooski, VT, USA) at excitation and emission wavelengths of 350 nm and 495 nm, respectively. *p*HMB and berberine chloride were used as reference inhibitors of SrtA.

Enzyme Kinetics. All sortase (SrtA) assays were performed at

37°C in SrtA enzyme buffer as described above. The inhibitors **16** and **18** were dissolved in DMSO and immediately diluted to the desired working concentration with the same SrtA buffer. The enzymatic inhibition measurements by the inhibitor were carried out at different substrate concentrations in the presence and absence of a given concentration of inhibitor, and their kinetics were evaluated by the Lineweaver and Burk plot method.[74] For the dialysis kinetic studies, a solution of enzyme (0.96 mL, 75 μM) and fixed inhibitor concentration (0.04 mL) was prepared and dialyzed against 100 mL buffer at 37ºC for 2 h using regenerated cellulose dialysis membranes SPECTRAPOR®. Aliquots of 100 μL of the enzyme-inhibitor mixture were taken in time intervals of 0, 30, 60, 90, 120 min and added to 0.020 mL of substrate (7.5 μM), and after an hour of incubation the enzyme activity was measured. A control solution prepared with enzyme and buffer (SrtA buffer, 100 μL; SrtA, 7.5 μM) was treated similarly.

Antibacterial Activity Assay. The MICs of test compounds were determined as previously described.[85] *S. aureus* ATCC6538p (5 mL) was cultured in tryptic soy broth to saturation at 37°C and diluted to an OD_{600} of 0.01. The culture was incubated for an additional 2 h and diluted to an OD_{600} of 0.005. In each well of a 96-well plate, 180 μL cells was mixed

with 20 μL a concentrated test compound solution in 10% DMSO (final concentration, 1% DMSO). Culture plates were incubated overnight at 37°C, and the OD_{600} was measured spectrophotometrically. MIC values were defined as the lowest concentration of the test compounds inhibiting cell growth. Ampicillin was used as a positive control.

Cytotoxicity Assay. The effect of compounds (**16**–**23**) on cell proliferation was measured by the sulforhodamine B (SRB) cellular protein-staining method.[86] In brief, A549 (lung cancer) and K562 (leukemia) cells (1×10^4 cells in 190 μL of complete DMEM) were seeded in 96-well plates with various concentrations of compounds (**16**–**23**) and incubated at 37°C in a humidified atmosphere with 5% CO_2. After 72 h of compound (**16**–**23**) treatment, the cells were fixed with 10% TCA solution for 1 h, and cellular proteins were stained with a solution of 0.4% SRB in 1% acetic acid. The stained cells were dissolved in 10 mM Tris buffer (pH 10.0). The effect of compounds (**16**–**23**) on cell viability was calculated as a percentage relative to a solvent-treated control, and the IC_{50} values were calculated using a nonlinear regression analysis (percent survival versus concentration). Etoposide was used as a positive control.

Fibronectin Binding Assay. *S. aureus* strains used were Newman

(wild-type) and the isogenic *srtA* knockout mutant (*srtA*$^-$).[86] These strains were cultured in tryptic soy broth at 37°C at 200 rpm up to mid-log phase (OD_{600} = 0.5). The fibronectin-binding assay was performed as described previously.[82,87] Cells were treated with test compounds at their indicated concentrations. Every 30 min for 2.5 h, a 0.65 mL cell suspension was centrifuged at 10,000 × *g* for 10 min, and the supernatant was eliminated. Following incubation overnight at -20°C, pellets were resuspended in 0.65 mL phosphate-buffered saline (PBS) and distributed as a 100 μL scale in fibronectin-coated flat-bottomed 96-well plates (Corning Life Sciences, Tewksbury, MA, USA). The cell suspension was removed and washed with PBS following incubation at 37°C for 2 h. Bound cells were fixed via incubation with 2% (v/v) glutaraldehyde for 30 min. After a second wash with PBS, cells were stained for 15 min with 100 μL crystal violet dye (12.5 g/L). Each well was washed with PBS and covered with aluminum foil. Plates were dried overnight and absorbance was measured at 560 nm using a microplate reader.

(Bioactivity experiments were performed by Prof. Ki-Bong Oh's laboratory)

V. Conclusion

The purpose of this work is the investigation of novel bioactive secondary metabolites from marine-derived fungal strains, *Aspergillus* sp. and *Penicillium* sp. Based upon chemical analysis and bioassay, novel substances from marine-derived fungi have been isolated, structure elucidated, and demonstrated the biomedical potential as new drug candidates.

Chemical studies of selected three fungal strains lead to isolation of 9 new compounds, 14 known compounds. These compounds have been structurally elucidated by combined spectroscopic methods and chemical analyses. The structures of these 23 compounds are a mixed-biogenetic salt and its components, 11 phenalenone-class, 1 polyketide-class, 2 alkaloid-class, and 5 fumiquinazoline-class.

To the best of my knowledge, ochraceopetalin (**1**), a mixed-biogenetic salt compound, would be the first of the organic salt consisting of both organic counterions to be obtained from marine-derived fungi. Furthermore, its mixed-biogenetic salt formation that is derived from polyketide and amino acid pathways, would be remarkably unprecedented.

Also, the result that amino acid components of **1** are in D-form gives a value for the discovery. Since compounds **1** and **2** were isolated independently without existence of diorcinol (**4**), well-known fungal diphenylether, the results suggest a possibility that naturally produced **4** was sulfonated to **1** or **2** by a biotransformation during the cultivation.

According to diverse chemical reactions, the absolute configuration on the hydrofuran moiety of novel herqueinone type compounds (**5**–**10**) could be completely determined. At the same time, the unknown absolute configuration at C-8 of compounds **8**, **9** and **11** were partially suggested through CD experiment and ECD calculation.

Diverse bioassay tests related to cytotoxicity, antimicrobial, enzyme-inhibitory activities, and adiponectin secretion-stimulating activity have been performed. Some of the isolated compounds showed potent bioactivities in cytotoxicity, adiponectin secretion-stimulating activity, and inhibiting SrtA activity.

This study has successfully demonstrated the biomedical potential of the marine-derived fungi. Compounds and fungal strains, obtained during research, as well as techniques developed throughout the research, will be valuable assets for related works in the future.

Summary

During the six years of the Doctor of Philosophy studies, effort is focused on the study of structure determination of novel bioactive secondary metabolites from marine-derived fungi, *Aspergillus* sp. and *Penicillium* sp.

To achieve isolation and structure determination of novel substances, *Aspergillus* sp. and *Penicillium* sp. were isolated from marine sediments, collected at Korea. The fungal strains were selected for chemical investigation on the basis of combined results of bioactivity tests and NMR analysis of the crude organic extracts. From three selected fungal strains, 23 compounds have been isolated and 9 new ones among these have been structurally elucidated by combined spectroscopic and chemical analysis. The structures of these 23 compounds belonged to diverse structural classes with various biogenetic origins. Diverse bioassay tests related to cytotoxicity, antimicrobial, enzyme-inhibitory activities, and adiponectin secretion-stimulating activity have been performed. Some of the isolated compounds showed potent bioactivities.

1. Ochraceopetalin, a Mixed-Biogenetic Salt of Polyketide and Amino Acid Origins from a Marine-Derived *Aspergillus ochraceopetaliformis* Fungus

Ochraceopetalin (**1**), a mixed-biogenetic salt compound, and its component **2** were isolated from a marine-derived fungus *Aspergillus ochraceopetaliformis*. Based on the results of combined spectroscopic and chemical analyses, the structure of **1** was determined to be a sulfonated diphenylether-aminol-amino acid guanidinium of an unprecedented structural class. Compounds **2** and **3**, obtained from the different culturing condition and chromatographic processes, respectively, were defined to be the corresponding components of **1**, 1-(sulfooxy)-diorcinol and 1-(aminoiminomethyl)-prolinol, *N*,*N*-dimethylvaline ester, respectively. Compound **1** exhibited weak cytotoxicity against K562 and A549 cells.

2. Phenalenones from a Marine-Derived *Penicillium* sp. Fungus

Eleven polyketide-derived phenalenones, including six previously unreported phenalenones, were isolated from the culture broth of a marine-derived *Penicillium* sp. The absolute configurations of the

stereogenic centers in the hydrofuran moiety were assigned by chemical modifications and measurements of specific rotations. Compounds **5**, **10**, **11** and **13** exhibited diverse bioactivities such as anti-inflammatory, anti-angiogenetic, and adipogenesis-inducing activities.

3. Sortase A-Inhibitory Metabolites from a Marine-Derived Fungus *Aspergillus* sp.

Seven alkaloidal compounds (**17**–**23**) and one polyketide (**16**) were isolated from a semisolid rice culture of the marine-derived fungus *Aspergillus* sp. F452. The structures of these compounds were obtained through a combination of spectroscopic analyses, and their data were in good agreement with previous reports. Bioactivity studies have revealed that compound **16** from a marine-derived fungus *Aspergillus* sp., separated from the mussel *Mytilus edulis*, shows significant neurotrophic effects on PC-12 cells. Compound **18** from the deep sea-derived *A. versicolor* SCSIO 05879 exhibits antifungal activity against the phytopathogenic fungus *Colletotrichum acutatum* (minimum inhibitory concentration (MIC) of 1.6 μg/mL). Compounds **19**–**22** from a marine-derived fungus *Aspergillus* sp. F452 exhibit weak inhibition against Na^+/K^+-ATPase (IC_{50} values of 20–

78 μM). Compound **21** also displays weak inhibition against *Bacillus subtilis*, and compound **22** from *A. fumigatus*, an endophytic fungus, shows weak cytotoxic activity against the human prostate cancer cell line PC3. In the measurement of SrtA enzyme activity, compounds **16**–**23** displayed moderate to significant SrtA inhibition, comparable to berberine chloride and *p*HMB, against *S. aureus*-derived SrtA, a transpeptidase responsible for anchoring surface proteins to the peptidoglycan cell wall in Gram-positive bacteria. Further bioassays of compound **16** indicated that the underlying mechanism of action was associated with the inhibition of adhesion of *S. aureus* to fibronectin via fibronectin-binding protein. The results demonstrate the potential of these metabolites for the development of new agents to treat Gram-positive bacterial infections by inhibiting SrtA activity.

References

1. Clardy, J.; Fischbach, M. A. Polyketides, modular polyketide synthases. *Wiley Encyclopedia of Chemical Biology* **2008**.
2. Hu, G.-P.; Yuan, J.; Sun, L.; She, Z.-G.; Wu, J.-H.; Lan, X.-J.; Zhu, X.; Lin, Y.-C.; Chen, S.-P. Statistical research on marine natural products based on data obtained between 1985 and 2008. *Mar. Drugs* **2011**, *9*, 514−525.
3. Blunt, J. W.; Copp, B. R.; Keyzers, R. A.; Munro, M. H. G.; Prinsep, M. R. Marine natural products. *Nat. Prod. Rep*. **2014**, *31*, 160−258.
4. Hussain, H.; Al-Sadi, A.M.; Schulz, B.; Steinert, M.; Khan, A.; Green, I.R.; Ahmed, I. A fruitful decade for fungal polyketides from 2007 to 2016: Antimicrobial activity, chemotaxonomy and chemodiversity. *Future Med. Chem.* **2017**, *9*, 1631–1648.
5. Aldholmi, M.; Marchand, P.; Ourliac-Garnier, I.; Le Pape, P.; Ganesan, A. A decade of antifungal leads from natural products: 2010–2019. *Pharmaceuticals* **2019**, *12*, 182–202.
6. Weissman, K.J.; Leadlay, P.F. Combinatorial biosynthesis of reduced polyketides. *Nat. Rev. Microbiol.* **2005**, *3*, 925–936.
7. Albers-Schönberg, G.; Joshua, H.; Lopez, M.B.; Hensens, O.D.; Springer, J.P.; Chen, J.; Ostrove, S.; Hoffman, C.H.; Alberts, A.W.; Patchett, A.A. Dihydromevinolin, a potent hypocholesterolemic metabolite produced by *Aspergillus terreus*. *J. Antibiot*. **1981**, *34*, 507–512.
8. Oxford, A.E.; Raistrick, H.; Simonart, P. Studies in the biochemistry of micro-organisms: Griseofulvin, C(17)H(17)O(6)Cl, a metabolic

product of *Penicillium griseo-fulvum Dierckx. Biochem. J*. **1939**, *33*, 240–248.

9. Sanchez, J.F.; Chiang, Y.-M.; Szewczyk, E.; Davidson, A.D.; Ahuja, M.; Oakley, C.E.; Bok, J.W.; Keller, N.; Oakley, B.R.; Wang, C.C.C. Molecular genetic analysis of the orsellinic acid/F9775 gene cluster of *Aspergillus nidulans. Mol. Biosyst.* **2010**, *6*, 587–593.
10. Xu, X.; Yang, H.; Xu, H.; Yin, L.; Chen, Z.; Shen, H. Diphenyl ethers from a marine-derived isolate of *Aspergillus* sp. CUGB-F046 *Nat. Prod. Res.* **2018**, *32*, 821–825.
11. Zhang, Y.; Li, X.-M.; Shang, Z.; Li, C.-S.; Ji, N.-Y.; Wang, B.-G. Meroterpenoid and diphenyl ether derivatives from *Penicillium* sp. MA-37, a fungus isolated from marine mangrove rhizospheric soil. *J. Nat. Prod*. **2012**, *75*, 1888–1895.
12. Feng, C.; Wei, Q.; Hu, C.; Zou. Y. Biosynthesis of diphenyl ethers in fungi. *Org. Lett.* **2019**, *21*, 3114–3118.
13. Hwang, J.-Y.; Lee, J.-H.; Park, S.C.; Lee, J.; Oh, D.-C.; Oh, K.-B.; Shin, J. New peptides from the marine-derived fungi *Aspergillus allahabadii* and *Aspergillus ochraceopetaliformis*. *Mar. Drugs* **2019**, *17*, 488–500.
14. Park, Y.; Liu, Y.; Hong, J.; Lee, C.-O.; Cho, H.; Kim, D.-K.; Im, K.S.; Jung, J.H. New bromotyrosine derivatives from an association of two sponges, *Jaspis wondoensis* and *Poecillastra wondoensis. J. Nat. Prod.* **2003**, *66*, 1495–1498.
15. Shinde, P.B.; Lee, Y.M.; Dang, H.T.; Hong, J.; Lee, C.-O.; Jung, J.H. Cytotoxic bromotyrosine derivatives from a two-sponge association of *Jaspis* sp. and *Poecillastra* sp. *Bioorg. Med. Chem. Lett.* **2008**, *18*, 6414–6418.

16. Chang, Y.H.; Shin, D.; Na, Z.; Lee, H.-S.; Kim, D.-D.; Oh, K.-B.; Shin, J. Dihydroxystyrene metabolites from an association of sponges *Poecillastra wondoensis* and *Japis* sp. *J. Nat. Prod.* **2008**, *71*, 779–783.
17. Kimura, J.; Ishizuka, E.; Nakao, Y.; Yoshida, W.Y.; Scheuer, P.J.; Kelly-Borges, K. Isolation of 1-methylherbipoline salts of halisulfate-1 and of suvanine as serine protease inhibitors from a marine sponge, *Coscinoderma mathewsi*. *J. Nat. Prod*. **1998**, *61*, 248–250.
18. Wright, A.E.; McCarthy, P.J. Sulfircin: A new sesterterpene sulfate from a deep-water sponge of the genus *Ircinia. J. Org. Chem*. **1989**, *54*, 3472–3474.
19. Solano, G.; Motti, C.A.; Jaspars, M. New iodotyramine derivatives from *Didemnum rubeum. Tetrahedron* **2009**, *65*, 7482–7486.
20. Carroll, A.R.; Copp, B.R.; Davis, R.A.; Keyzers, R.A.; Prinsep, M.R. Marine natural products. *Nat. Prod. Rep*. **2021**, *38*, 362–413.
21. Huibers, M.; Manuzi, A.; Rutjes, F.P.J.T.; van Delft, F.L.J. A sulfitylation-oxidation protocol for the preparation of sulfates. *J. Org. Chem*. **2006**, *71*, 7473–7476.
22. Brandstorm, A.; Strandlund, G.; Lagerstrom, P.-O. Kinetic studies of the sulfonation of 2-*tert*-butylphenol with chlorosulfonic acid. *Acta Chem. Scand.* **1980**, *34*, 467–480.
23. Yabuuchi, T.; Kusumi, T. Phenylglycine methyl ester, a useful tool for absolute configuration determination of various chiral carboxylic acids. *J. Org. Chem.* **2000**, *65*, 397–404.
24. Tsuda, M.; Sasaki, M.; Mugishima, T.; Komatsu, K.; Sone, T.; Tanaka, M.; Mikami, Y.; Kobayashi, J. Scalusamides A-C, new

pyrrolidine alkaloids from the marine-derived fungus *Penicillium citrinum*. *J. Nat. Prod.* **2005**, *68*, 273–276.

25. Hua, S.-S.; Jiang, N.; Wanga, X.-L.; Chen, C.-J.; Fan, J.-Y.; Wurin, G.; Ge, H.-M.; Tan, R.-X.; Jiao, R.-H. Prenylated diphenyl ethers from the mantis-associated fungus *Aspergillus versicolor* GH-2. *Tetrahedron Lett.* **2015**, *56*, 3894–3897.
26. Li, Z.-X.; Wang, X.-F.; Ren, G.-W.; Yuan, X.-L.; Deng, N.; Ji, G.-X.; Li, W.; Zhang, P. Prenylated diphenyl ethers from the marine algal-derived endophytic fungus *Aspergillus tennesseensis*. *Molecules* **2018**, *23*, 2368–2374.
27. Bunyapaiboonsri, T.; Yoiprommarat, S.; Intereya, K.; Kocharin, K. New diphenyl ethers from the insect pathogenic fungus *Cordyceps* sp. BCC 1861. *Chem. Pharm. Bull.* **2007**, *55*, 304–307.
28. Oh, K.-B.; Lee, J.H.; Chung, S.-C.; Shin, J.; Shin, H.J.; Kim, H.-K.; Lee, H.-S. Antimicrobial activities of the bromophenols from the red alga *Odonthalia corymbifera* and some synthetic derivatives. *Bioorg. Med. Chem. Lett.* **2008**, *18*, 104–108.
29. Lee, H.-S.; Lee, T.-H.; Yang, S.H.; Shin, H.J.; Shin, J.; Oh, K.-B. Sesterterpene sulfates as isocitrate lyase inhibitors from tropical sponge *Hippospongia* sp. *Bioorg. Med. Chem. Lett.* **2007**, *17*, 2483–2486.
30. Kwon, O.-S.; Kim, C.-K.; Byun, W.S.; Oh, J.; Lee, Y.-J.; Lee, H.-S.; Sim, C.J.; Oh, D.-C.; Lee, S.K.; Oh, K.-B.; et al. Cyclopeptides from the sponge *Stylissa flabelliformis*. *J. Nat. Prod.* **2018**, *81*, 1462-1434.
31. Elsebai, M. F.; Saleem, M.; Tejesvi, M. V.; Kajula, M.; Mattila, S.; Mehiri, M.; Turpeinen, A.; Pirttila, A. M. Fungal phenalenones:

chemistry, biology, biosynthesis and phylogeny. *Nat. Prod. Rep*. **2014**, *31*, 628−645.

32. Nazir, M.; Maddah, F.; Kehraus, S.; Egereva, E.; Piel, J.; Brachmann, A. O.; König, G. M. Phenalenones: Insight into the biosynthesis of polyketides from the marine alga-derived fungus *Coniothyrium* cereal. *Org. Biomol. Chem.* **2015**, *13*, 8071−8079.
33. Galarraga, J. A.; Neill K. G.; Raistrick, H. Colouring matters of *Penicillium herquei. Biochem. J*. **1955**, *61*, 456–464.
34. Frost, D. A.; Halton, D. D.; Morrison, G. A. Naturally occurring compounds related to phenalenone. Part 8. Structure and synthesis of demethylherqueichrysin. *J. Chem. Soc. Perkin Trans. 1*. **1977**, 2443–2448.
35. Narasimhachari, N.; Vining, L. C. Herqueichrysin, a new phenalenone antibiotic from *Penicillium herquei. J. Antibiot*. **1972**, *25*, 155–162.
36. Julianti, E.; Lee, J.-H.; Liao, L.; Park, W.; Park, S.; Oh, D.-C.; Oh, K.-B.; Shin, J. New polyaromatic metabolites from a marine-derived fungus *Penicillium* sp. *Org. Lett*. **2013**, *15*, 1286−1289.
37. Furihata, K.; Seto, H. Decoupled HMBC (D-HMBC), an improved technique of HMBC. *Tetrahedron Lett*. **1995**, *36*, 2817−2820.
38. Tansakul, C.; Rukachaisirikul, V.; Maha, A.; Kongprapan, T.; Phongpaichit, S.; Hutadilok-Towatana, N.; Borwornwiriyapan, K.; Sakayaroj, J. A new phenalenone derivative from the soil fungus *Penicillium herquei* PSU-RSPG93. *J. Nat. Prod. Res*. **2014**, *28*, 1718−1724.

39. Barton, D. H. R.; Mayo, P.; Morrison, G. A.; Raistrick, H. The constitutions of atrovenetin and of some related herqueinone derivatives. *Tetrahedron*. **1959**, *6*, 48−62.
40. Brooks, J. S.; Morrison, G. A. The constitution of herqueinone and its relationship to isoherqueinone. *Tetrahedron Lett*. **1970**, *12*, 963−966.
41. Rani, B. R.; Ubukata, M.; Osada, H. Reduction of arylcarbonyl using zinc dust in acetic acid. *Bull. Chem. Soc. Jpn*. **1995**, *68*, 282−284.
42. Bonner, T. G.; McNamara, P. The pyridine-catalysed acetylation of phenols and alcohols by acetic anhydride. *J. Chem. Soc. B*. **1968**, 795−797.
43. Lugemwa, F. N.; Shaikh, K.; Hochstedt, E. Facile and efficient acetylation of primary alcohols and phenols with acetic anhydride catalyzed by dried sodium bicarbonate. *Catalysts* **2013**, *3*, 954−965.
44. Ayer, W. A.; Hoyano, Y.; Pedras M. S.; Altena, I. Metabolites produced by the Scleroderris canker fungus, *Gremmeniellaabietina*. Part 1. *Can. J. Chem*. **1986**, *64*, 1585−1589.
45. Krohn, K.; Sohrab, MD. H.; Aust, H.-J.; Draeger, S.; Schulz, B. Biologically active metabolites from fungi, 19: New isocoumarins and highly substituted benzoic acids from the endophytic fungus, *Scytalidium* sp. *Nat. Prod. Res*. **2004**, *18*, 277−285.
46. Homma, K.; Fukuyama, K.; Katsube, Y.; Kimura, Y.; Hamasaki, T. Structure and absolute configuration of an atrovenetin-like metabolite from *Aspergillus silvaticus*. *Agric. Biol. Chem*. **1980**, *44*, 1333−1337.

47. Stodola, F. H.; Raper, K. B.; Fennell, D. I. Pigments of *Penicillium herquei*. *Nature* **1951**, *167*, 773−774.
48. Suga, T.; Yoshioka, T.; Hirata, T.; Aoki, T. ^{13}C NMR signal assignments of herqueinone and its phenalenone derivatives. *Bull. Chem. Soc. Jpn*. **1983**, *56*, 3661−3666.
49. Harman, R. E.; Cason, J.; Stodola, F. H.; Adkins, A. Structural features of herqueinone, a red pigment from *Penicillium herquei. J. Org. Chem*. **1955**, *20*, 1260−1269.
50. Cason, J.; Koch, C. W.; Correia, J. S. Structures of herqueinone, isoherqueinone and norherqueinone. *J. Org. Chem*. **1970**, *35*, 179−186.
51. Ayer, W. A.; Hoyano, Y.; Pedras M. S.; Clardy, J.; Arnold, E. Metabolites produced by the scleroderris canker fungus, *Gremmeniellaabietina*. Part 2. The structure of scleroderolide. *Can. J. Chem*. **1987**, *65*, 748−753.
52. Ayer, W. A.; Kamada, M.; Ma, Y. T. Sclerodin and related compounds from a plant disease causing fungus, *Scleroderris yellow*. *Can. J. Chem*. **1989**, *67*, 2089–2094.
53. Shiomi, K.; Matsui, R.; Isozaki, M.; Chiba, H.; Sugai, T.; Yamaguchi, Y.; Masuma, R.; Tomoda, H.; Chiba, T.; Yan, H.; Kitamura, Y.; Sugiura, W.; Omura, S.; Tanaka, H. Fungal phenalenones inhibit HIV-1 Integrase. *J. Antibiot*. **2005**, *58*, 65–68.
54. Vichai, V.; Kirtikara, K. Sulforhodamine B colorimetric assay for cytotoxicity screening. *Nat. Protoc*. **2006**, *1*, 1112−1116.
55. Kim, C.-K.; Woo, J.-K.; Kim, S.-H.; Cho, E.; Lee, Y.-J.; Lee, H.-S.; Sim, C. J.; Oh, D.-C.; Oh, K.-B.; Shin, J. Meroterpenoids from a Tropical *Dysidea* sp. Sponge. *J. Nat. Prod.* **2015**, *78*, 2814−2821.

56. Nakane, M.; Klinghofer, V.; Kuk, J. E.; Donnelly, J. L.; Budzik, G. P.; Pollock, J. S.; Basha, F.; Carter, G. W. Novel potent and selective inhibitors of inducible nitric oxide synthase. *Mol. Pharmacol*. **1995**, *47*, 831−834.
57. Chung, H.-J.; Koh, W.; Kim, W. K.; Shin, J.-S.; Lee, J.; Lee, S. K.; Ha, I.-H. The anti-inflammatory effects of Shinbaro3 is mediated by downregulation of the TLR4 signalling pathway in LPS-stimulated RAW264.7 macrophages. *Mediators Inflamm*. **2018**.
58. Carmeliet, P.; Jain, R. K. Angiogenesis in cancer and other diseases. *Nature*. **2000**, *407*, 249–257.
59. Yu, S.; Oh, J.; Li, F.; Kwon, Y.; Cho, H.; Shin, J.; Lee, S. K.; Kim, S. New scaffold for angiogenesis inhibitors discovered by targeted chemical transformations of wondonin natural products. *ACS Med. Chem. Lett*. **2017**, *8*, 1066–1071.
60. Anh, S.; Lee, M.; An S.; Hyun, S.; Hwang, J.; Lee, J.; Noh, M. 2-Formyl-komarovicine promotes adiponectin production in human mesenchymal stem cells through PPARγ partial agonism. *Bioorg. Med. Chem*. **2018**, *26*, 1069−1075.
61. Gould, I.M. Antibiotic resistance: The perfect storm. *Int. J. Antimicrob Agents* **2009**, *34*, S2–S5.
62. Maresso, A.W.; Schneewind, O. Sortase as a target of anti-infective therapy. *Pharm. Rev*. **2008**, *60*, 128–141.
63. Cascioferro, S.; Totsika, M.; Schillaci, D. Sortase A: An ideal target for anti-virulence drug development. *Microb. Pathog*. **2014**, *77*, 105–112.

64. Rasko, D.A.; Sperandio, V. Anti-virulence strategies to combat bacteria-mediated disease. *Nat. Rev. Drug. Discov.* **2010**, *9*, 117–128.
65. Hendrickx, A.P.; Budzik, J.M.; Oh, S.Y.; Schneewind, O. Architects at the bacterial surface-sortases and the assembly of pili with isopeptide bonds. *Nat. Rev. Microbiol.* **2011**, *9*, 166–176.
66. Mazmanian, S.K.; Skaar, E.P.; Gaspar, A.H.; Humayun, M.; Gornicki, P.; Jelenska, J.; Joachmiak, A.; Missiakas, D.M.; Schneewind, O. Passage of heme-iron across the envelope of *Staphylococcus aureus*. *Science* **2003**, *299*, 906–909.
67. Clancy, K.W.; Melvin, J.A.; McCaerty, D.G. Sortase transpeptidases: Insights into mechanism, substrate specificity and inhibition. *Biopolymers* **2010**, *94*, 385–396.
68. Mazmanian, S.K.; Liu, G.; Jensen, E.R.; Lenoy, E.; Schneewind, O. *Staphylococcus aureus* sortase mutants defective in the display of surface proteins and in the pathogenesis of animal infections. *Proc. Natl. Acad. Sci. USA* **2000**, *97*, 5510–5515.
69. Mazmanian, S.K.; Ton-That, H.; Su, K.; Schneewind, O. An iron-regulated sortase anchors a class of surface protein during *Staphylococcus aureus* pathogenesis. *Proc. Natl. Acad. Sci. USA* **2002**, *99*, 2293–2298.
70. Weiss, W.J.; Lenoy, E.; Murphy, T.; Tardio, L.; Burgio, P.; Projan, S.J.; Schneewind, O.; Alksne, L. Effect of srtA and srtB gene expression on the virulence of *Staphylococcus aureus* in animal models of infection. *J. Antimicrob. Chemother* **2004**, *53*, 480–486.
71. Rateb, M.E.; Ebel, R. Secondary metabolites of fungi from marine habitats. *Nat. Prod. Rep*. **2011**, *28*, 290–344.

72. Jin, L.; Quan, C.; Hou, X.; Fan, S. Potential pharmacological resources: Natural bioactive compounds from marine-derived fungi. *Mar. Drugs* **2016**, *14*, 76.
73. Youssef, F.S.; Ashour, M.L.; Singab, A.N.B.; Wink, M. A comprehensive review of bioactive peptides from marine fungi and their biological significance. *Mar. Drugs* **2019**, *17*, 559.
74. Liao, L.; Bae, S.Y.;Won, T.H.; You, M.; Kim, S.-H.; Oh, D.-C.; Lee, S.K.; Oh, K.-B.; Shin, J. Asperphenins A and B, lipopeptidyl benzophenones from a marine-derived *Aspergillus* sp. fungus. *Org. Lett*. **2017**, *19*, 2066–2069.
75. Tsukamoto, S.; Miura, S.; Yamashita, Y.; Ohta, T. Aspermytin A: A new neurotrophic polyketide isolated from a marine-derived fungus of the genus *Aspergillus*. *Bioorg. Med. Chem. Lett.* **2004**, *14*, 417–420.
76. Pan, C.; Shi, Y.; Chen, X.; Chen, C.-T.A.; Tao, X.; Wu, B. New compounds from a hydrothermal vent crab-associated fungus *Aspergillus versicolor* XZ-4. *Org. Biomol. Chem.* **2017**, *15*, 1155–1163.
77. Wang, J.; He, W.; Huang, X.; Tian, X.; Liao, S.; Yang, B.; Wang, F.; Zhou, X.; Liu, Y. Antifungal new oxepine-containing alkaloids and xanthones from the deep-sea-derived fungus *Aspergillus versicolor* SCSIO 05879. *J. Agric. Food Chem*. **2016**, *64*, 2910–2916.
78. Liao, L.; You, M.; Chung, B.K.; Oh, D.-C.; Oh, K.-B.; Shin, J. Alkaloidal metabolites from a marine-derived *Aspergillus* sp. fungus. *J. Nat. Prod*. **2015**, *78*, 349–354.

79. Xie, F.; Li, X.-B.; Zhou, J.-C.; Xu, Q.-Q.; Wang, X.-N.; Yuan, H.-Q.; Lou, H.-X. Secondary metabolites from *Aspergillus fumigatus*, an endophytic fungus from the liverwort Heteroscyphus tener (Steph) Schiffn. *Chem. Biodivers.* **2015**, *12*, 1313–1321.
80. Heredia, M.L.; de la Cuesta, E.; Avendano, C. Acid-promoted reactions in 1-hydroxy, 1-dimethylaminomethyl and 1-methylene-4-arylmethyl-2,4-dihydro-1H-pyrazino[2,1-b]-quinazoline-3,6-diones. *Tetrahedron* **2002**, *58*, 6163–6170.
81. Oh, K.-B.; Kim, S.-H.; Lee, J.; Cho, W.-J.; Lee, T.; Kim, S. Discovery of diarylacrylonitriles as a novel series of small molecule sortase A inhibitors. *J. Med. Chem.* **2004**, *47*, 2418–2421.
82. Oh, K.-B.; Oh, M.-N.; Kim, J.-G.; Shin, D.-S.; Shin, J. Inhibition of sortase-mediated *Staphylococcus aureus* adhesion to fibronectin via fibronectin-binding protein by sortase inhibitors. *Appl. Microbiol. Biotechnol.* **2006**, *70*, 102–106.
83. Lineweaver, H.; Burk, D. The determination of enzyme dissociation constants. *J. Am. Chem. Soc*. **1934**, *56*, 658–666.
84. Alksne, L.E.; Projan, S.J. Bacterial virulence as a target for antimicrobial chemotherapy. *Curr. Opin. Biotechnol.* **2000**, *11*, 625–636.
85. Frankel, B.A.; Bentley, M.; Kruger, R.G.; McCaerty, D.G. Vinyl sulfones: Inhibitors of srtA, a transpeptidase required for cell wall protein anchoring and virulence in *Staphylococcus aureus. J. Am. Chem. Soc.* **2004**, *126*, 3404–3405.
86. Kim, T.S.; Shin, Y.-H.; Lee, H.-M.; Kim, J.K.; Choe, J.H.; Jang, J.-C.; Um, S.; Jin, H.S.; Komatsu, M.; Cha, G.-H. Ohmyungsamycins

promote antimicrobial responses through autophagy activation via AMP-activated protein kinase pathway. *Sci. Rep*. **2017**, *7*, 3431.

87. Elgalai, I.; Foster, H.A. Comparison of adhesion of wound isolates of *Staphylococcus aureus* to immobilized proteins. *J. Appl. Micrbiol.* **2003**, *94*, 413–420.

APPENDIX A:

NMR Spectroscopic data of Isolated Compounds

List of Figures

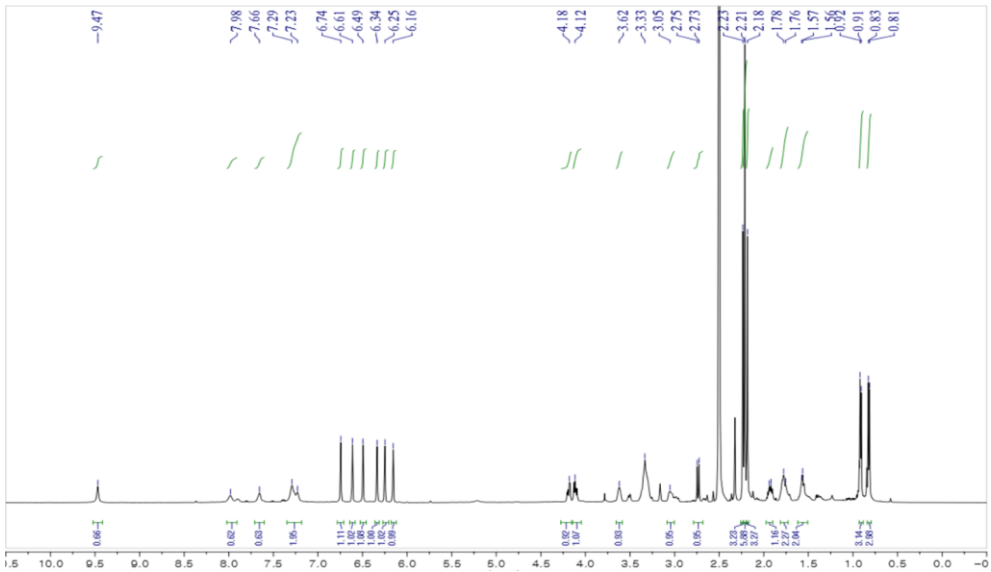

Figure A1. The ^{1}H NMR (500 MHz, DMSO-d_6) spectrum of **1**

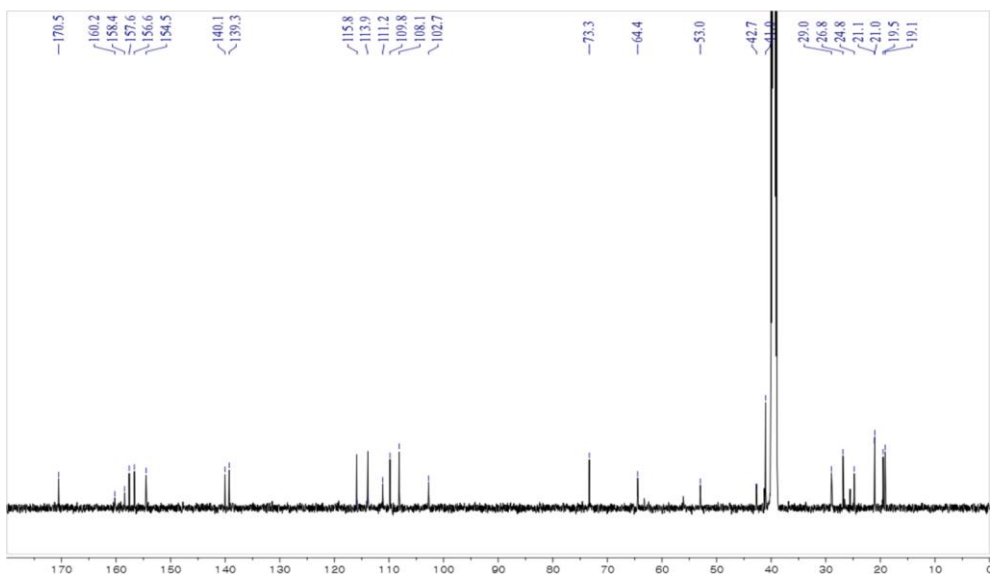

Figure A2. The ^{13}C NMR (125 MHz, DMSO-d_6) spectrum of **1**

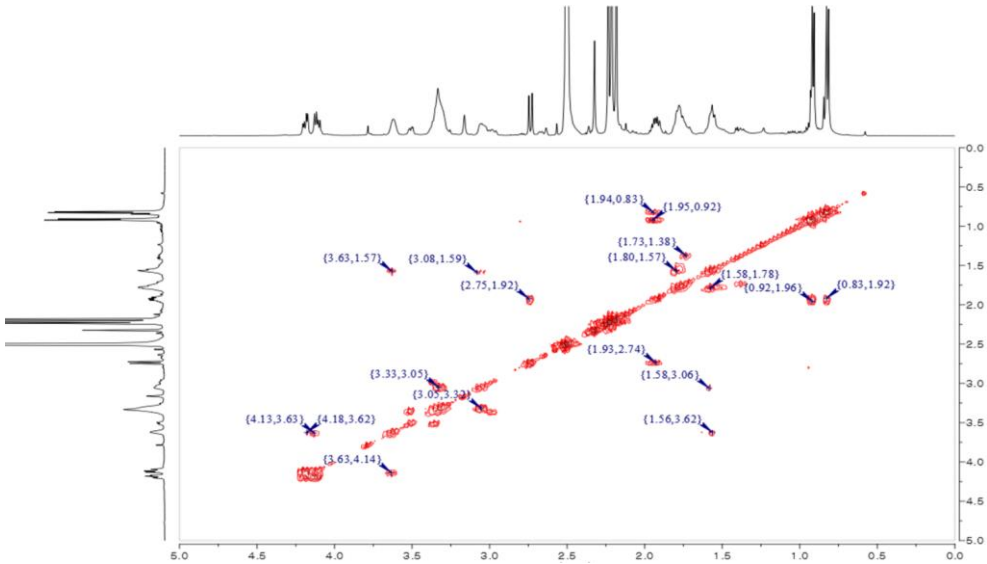

Figure A3. The COSY (500 MHz, DMSO-d_6) spectrum of **1**

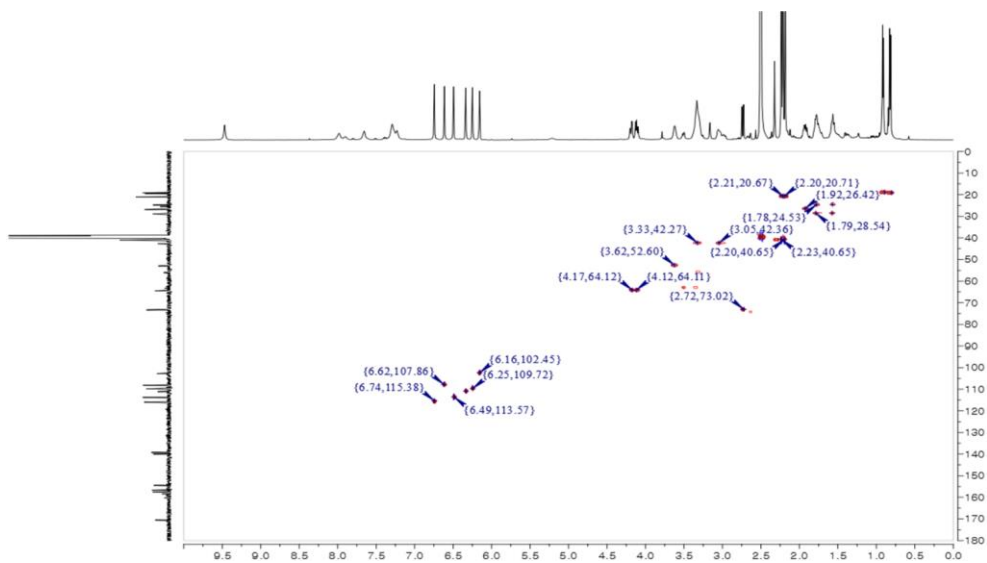

Figure A4. The HSQC (500 MHz, DMSO-d_6) spectrum of **1**

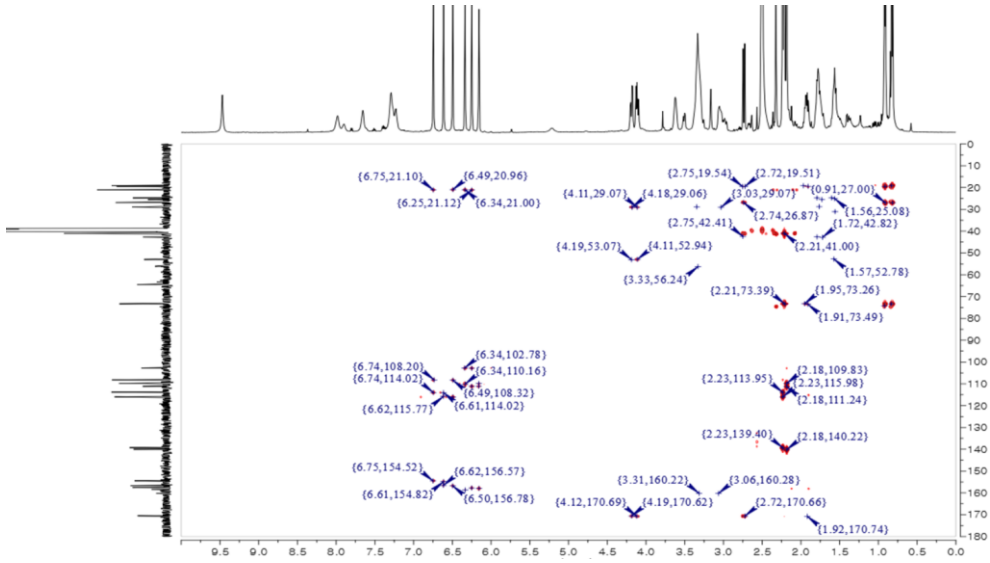

Figure A5. The HMBC (500 MHz, DMSO-d_6) spectrum of **1**

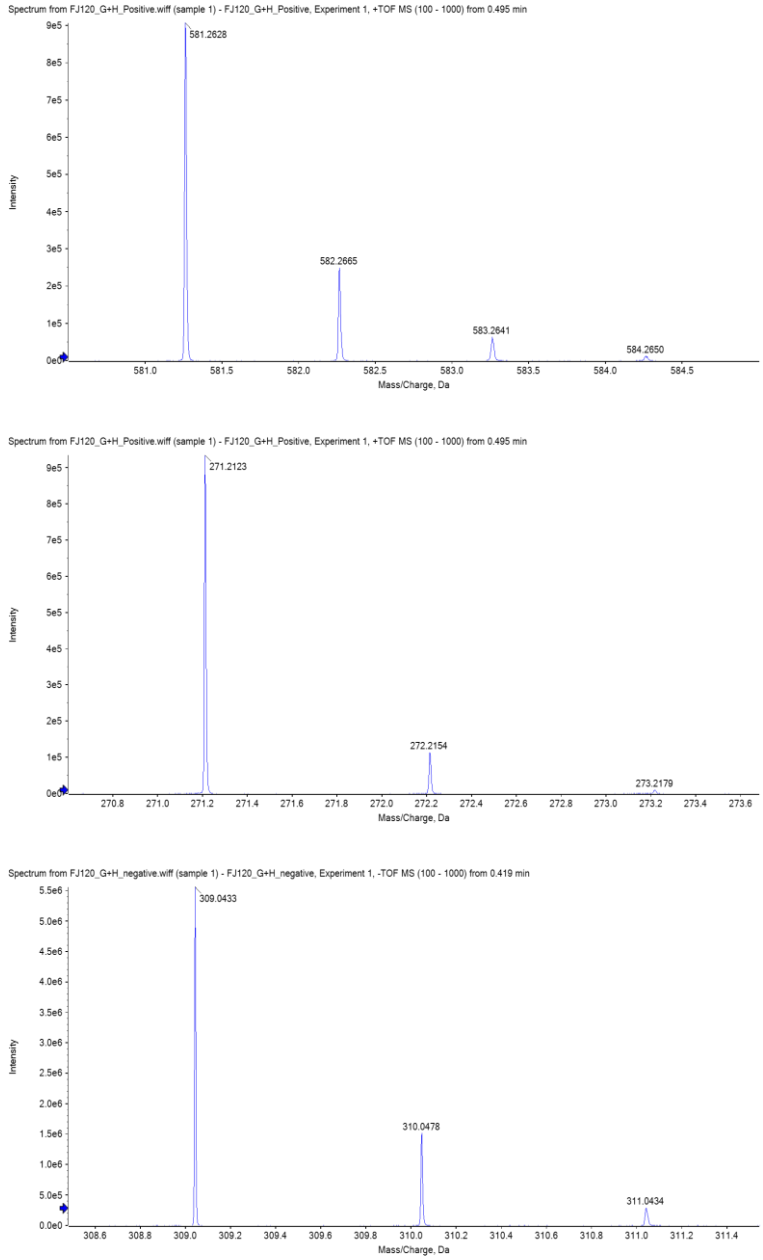

Figure A6. HR–ESI–MS data of **1**

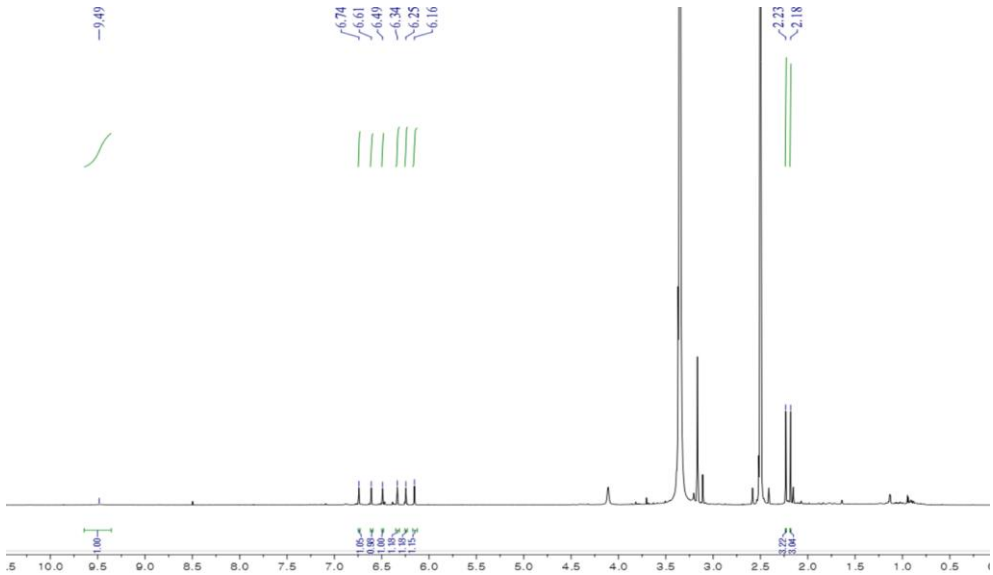

Figure A7. The ^{1}H NMR (600 MHz, DMSO- d_6) spectrum of **2**

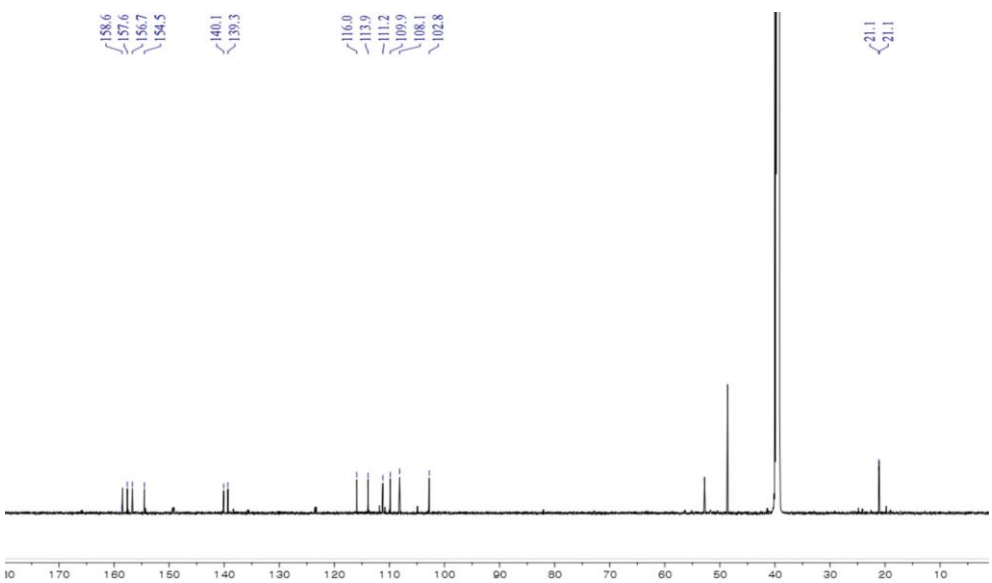

Figure A8. The ^{13}C NMR (150 MHz, DMSO- d_6) spectrum of **2**

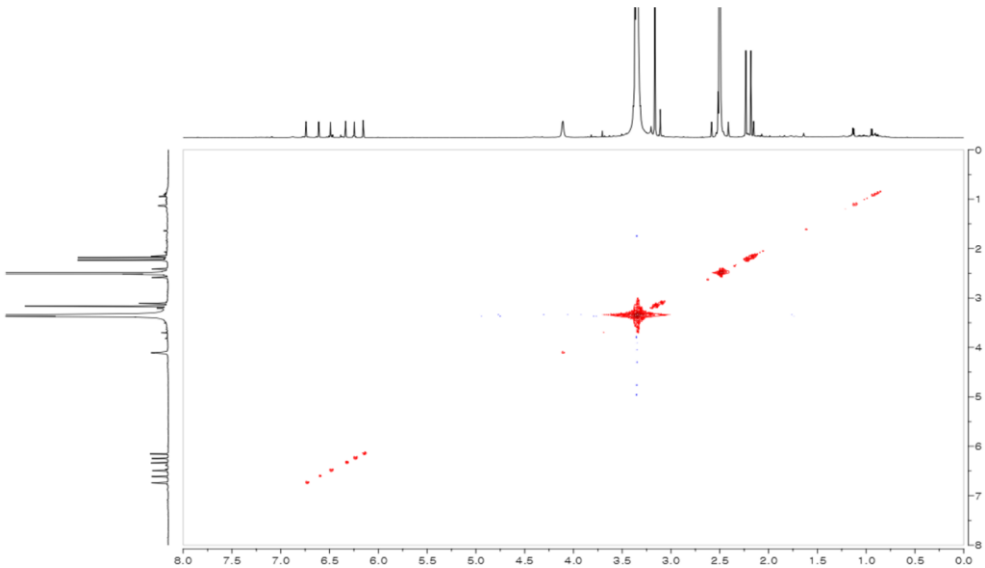

Figure A9. The COSY (600 MHz, DMSO- d_6) spectrum of **2**

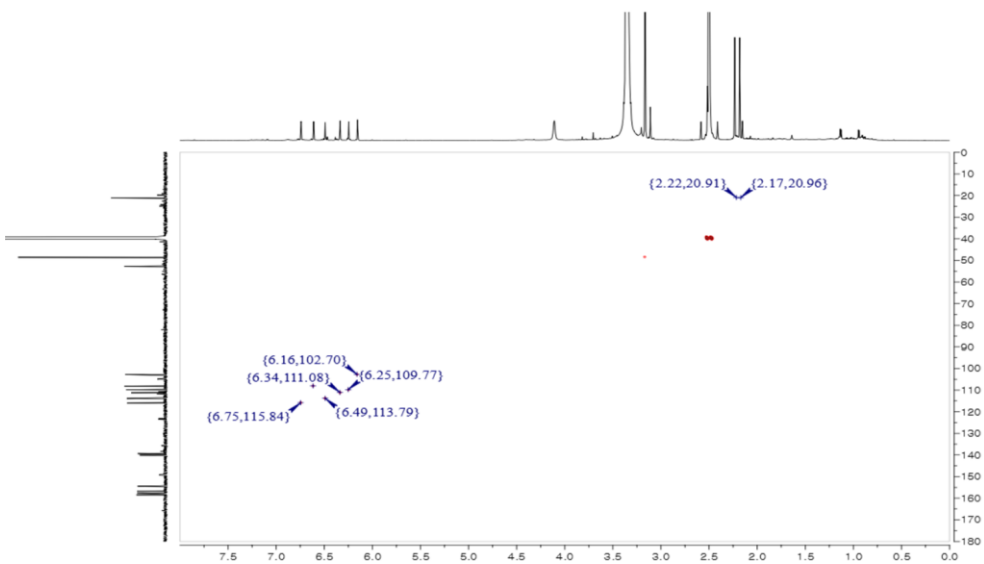

Figure A10. The HSQC (600 MHz, DMSO- d_6) spectrum of **2**

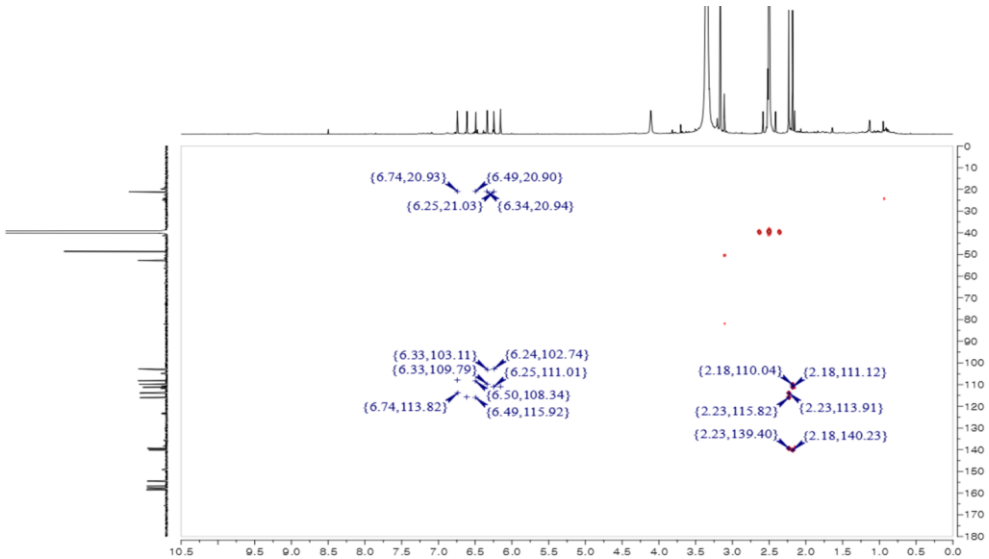

Figure A11. The HMBC (600 MHz, DMSO- d_6) spectrum of **2**

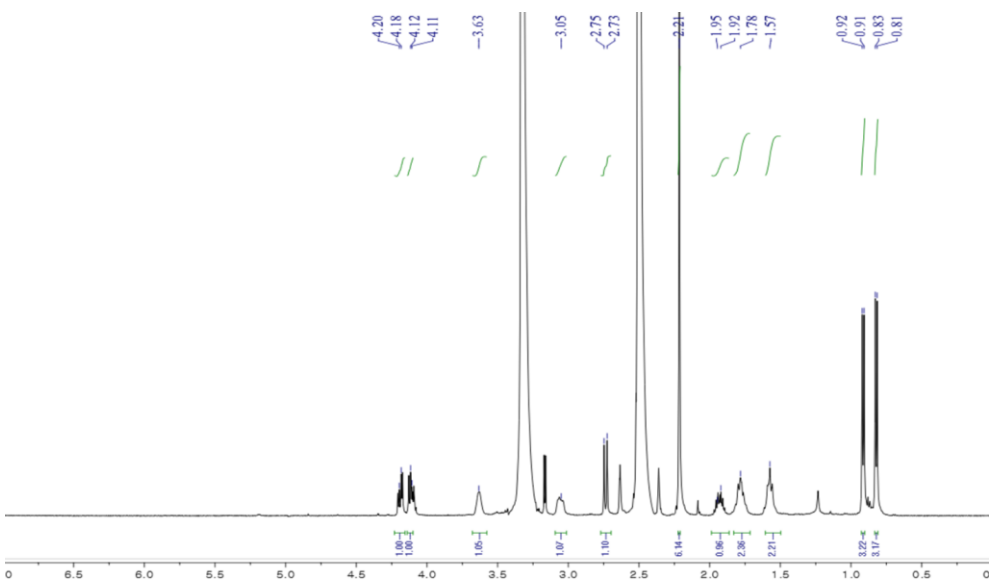

Figure A12. The ^{1}H NMR (600 MHz, DMSO-d_6) spectrum of **3**

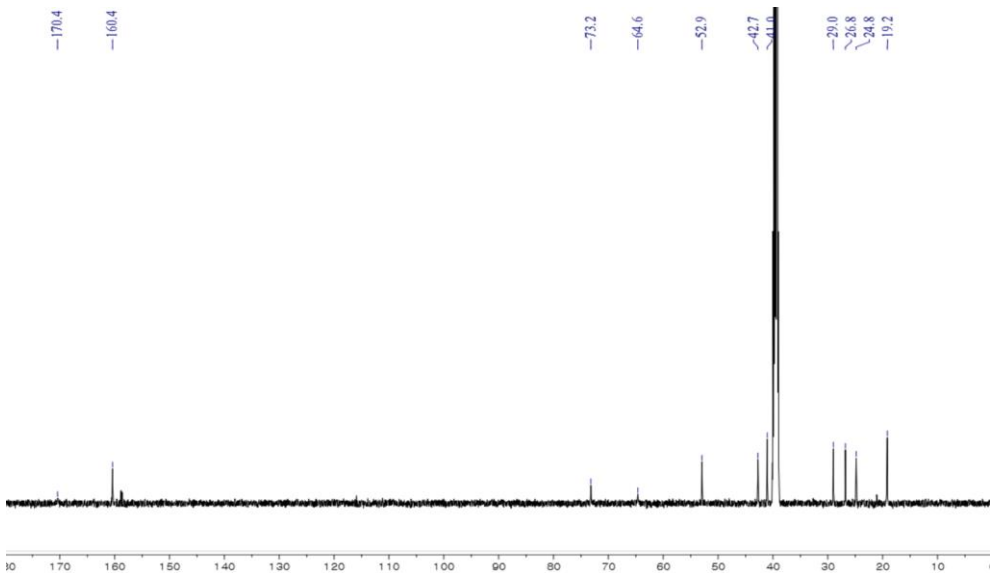

Figure A13. The ^{13}C NMR (150 MHz, DMSO-d_6) spectrum of **3**

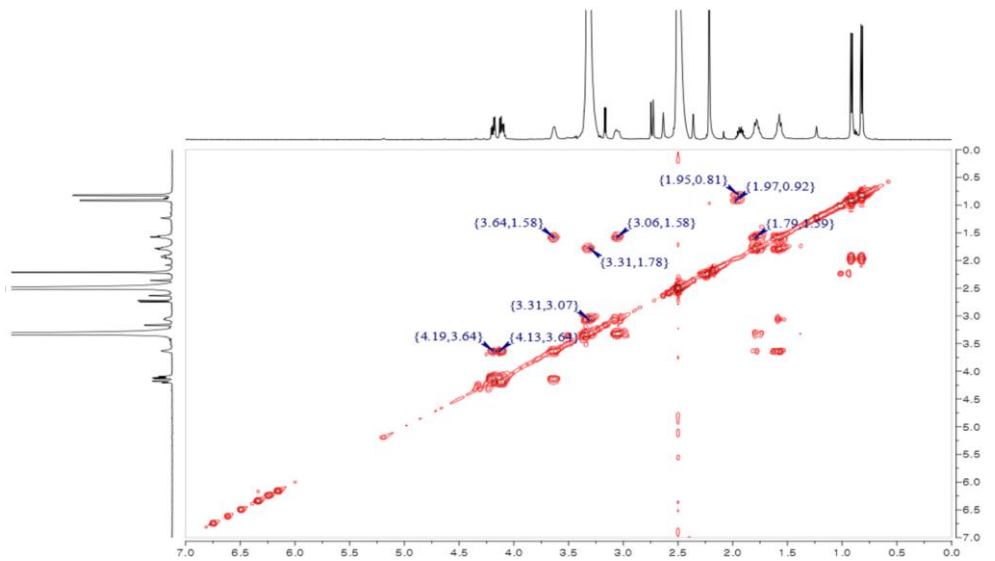

Figure A14. The COSY (600 MHz, DMSO-d_6) spectrum of **3**

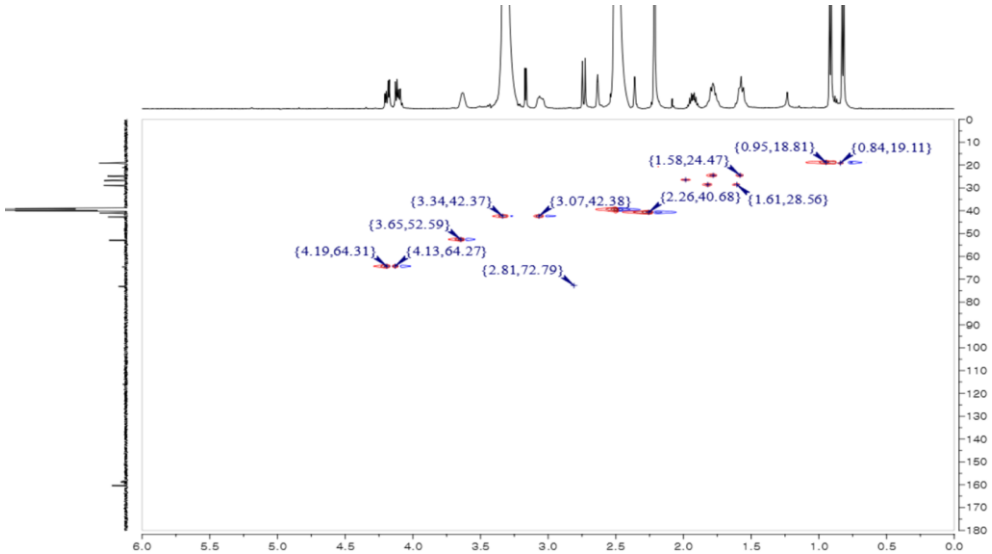

Figure A15. The HSQC (600 MHz, DMSO-d_6) spectrum of **3**

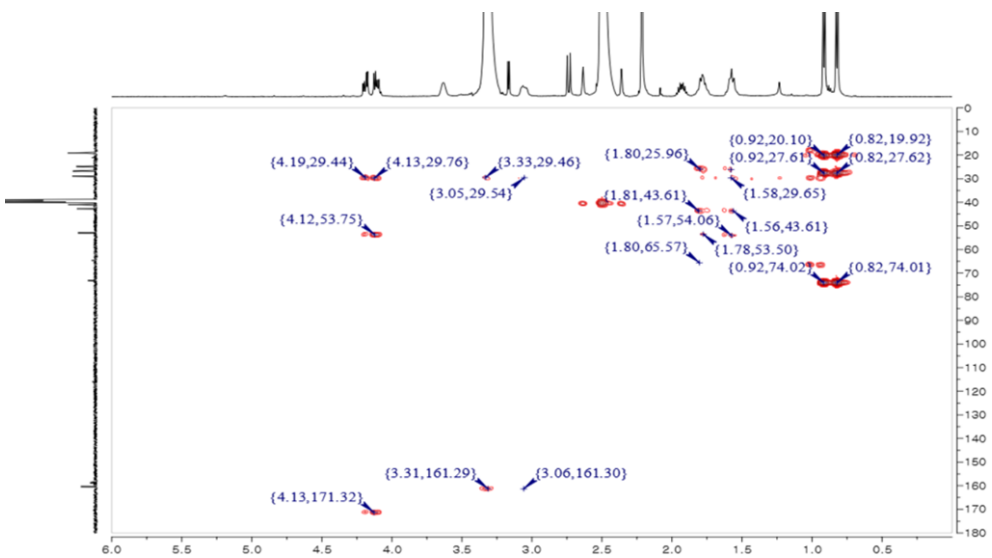

Figure A16. The HMBC (600 MHz, DMSO-d_6) spectrum of **3**

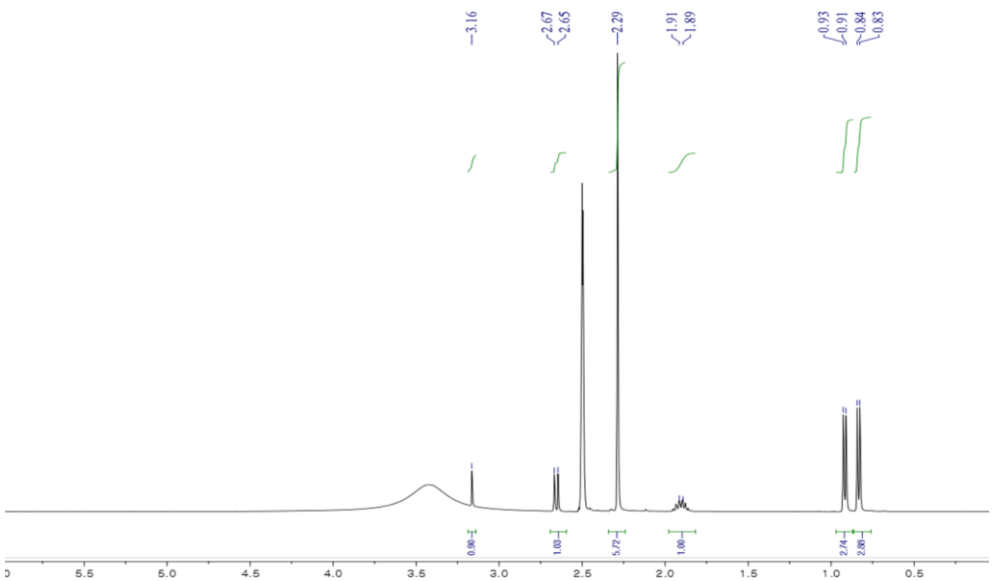

Figure A17. The ^{1}H NMR (400 MHz, DMSO-d_6) spectrum of **3a**

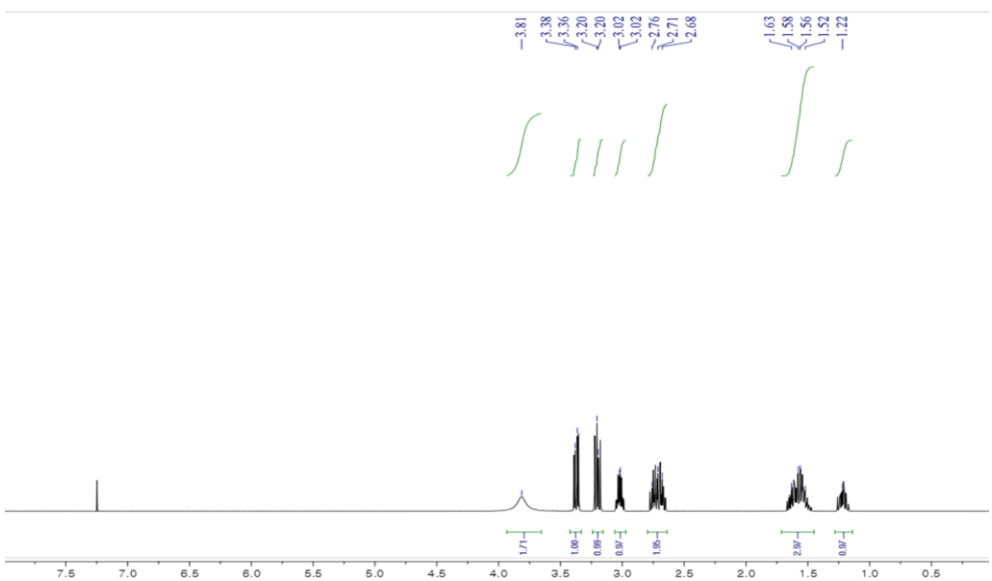

Figure A18. The ^{1}H NMR (400 MHz, $CDCl_3$) spectrum of **3b**

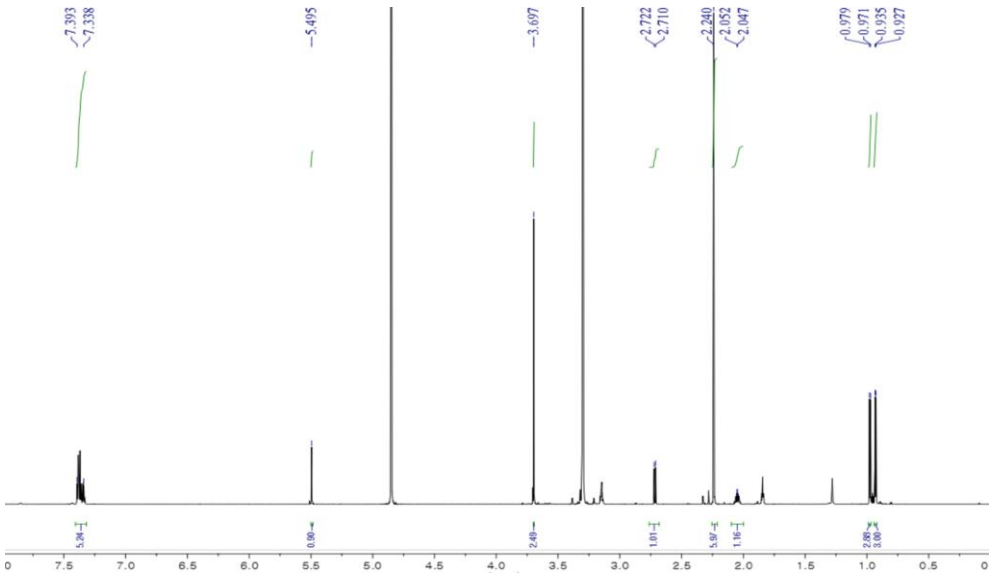

Figure A19. The ^{1}H NMR (800 MHz, Methanol-d_4) spectrum of **3a*S***

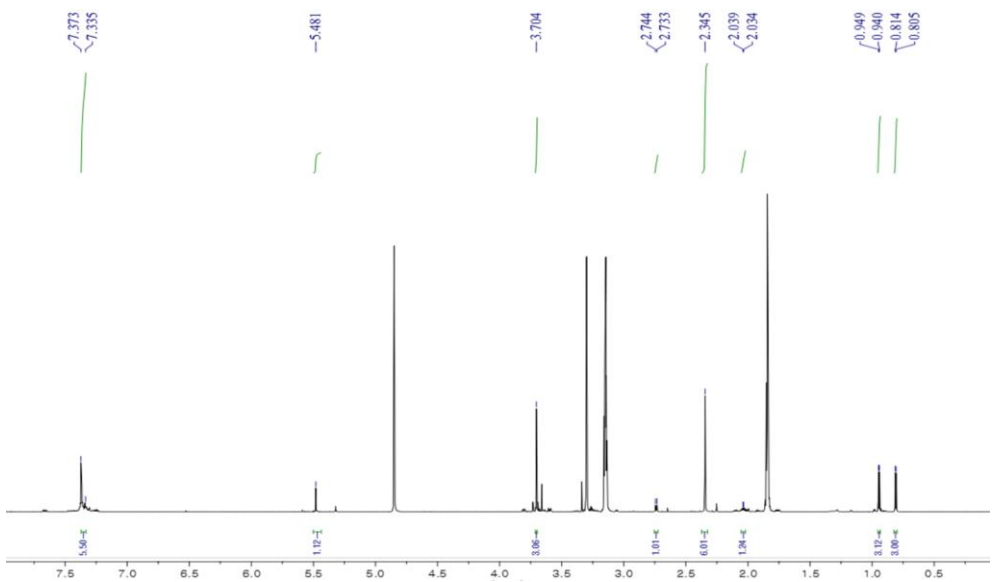

Figure A20. The ^{1}H NMR (800 MHz, Methanol-d_4) spectrum of **3a*R***

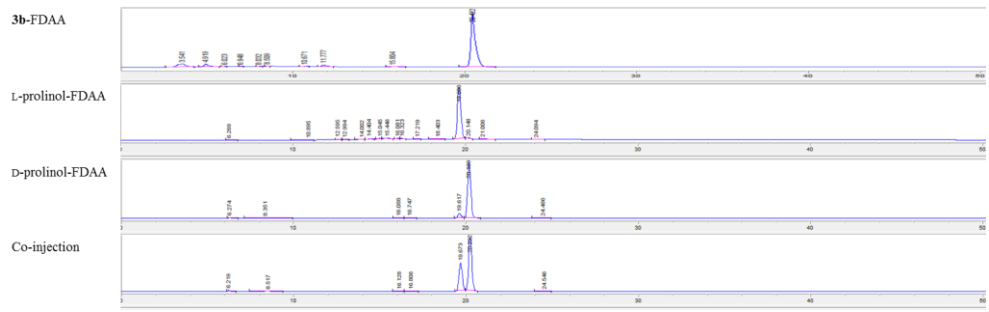

Figure A21. The LC/MS chromatogram data of **3b-L-FDAA** adduct

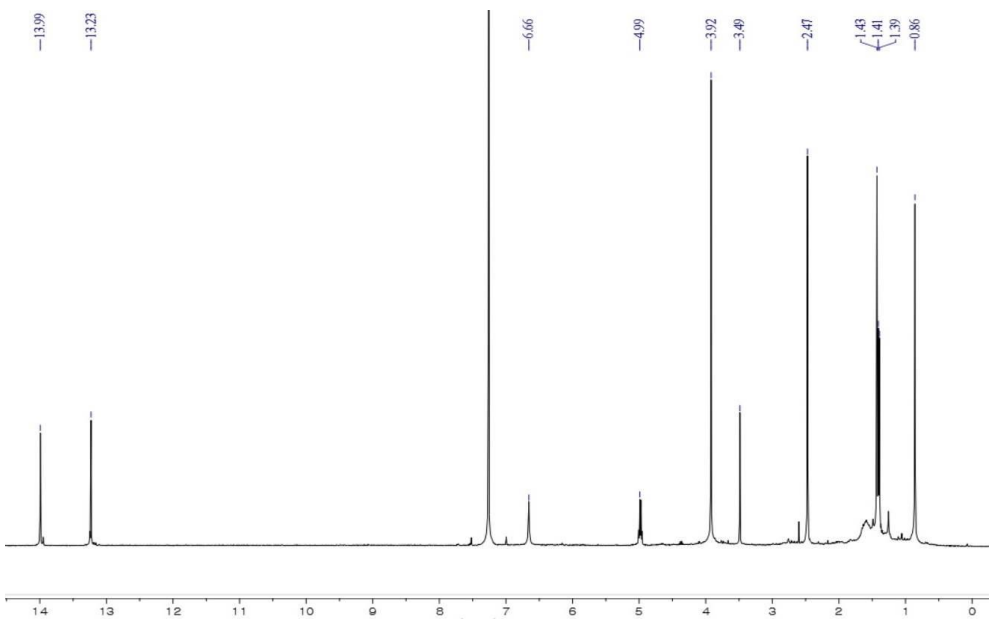

Figure A22. The ^{1}H NMR (400 MHz, $CDCl_3$) spectrum of **5**

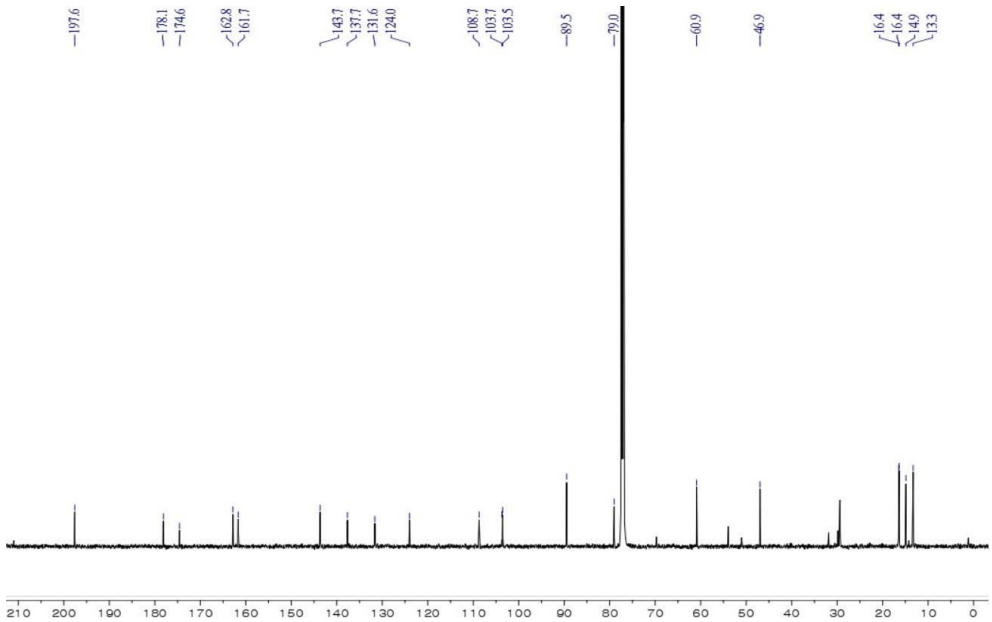

Figure A23. The ^{13}C NMR (125 MHz, $CDCl_3$) spectrum of **5**

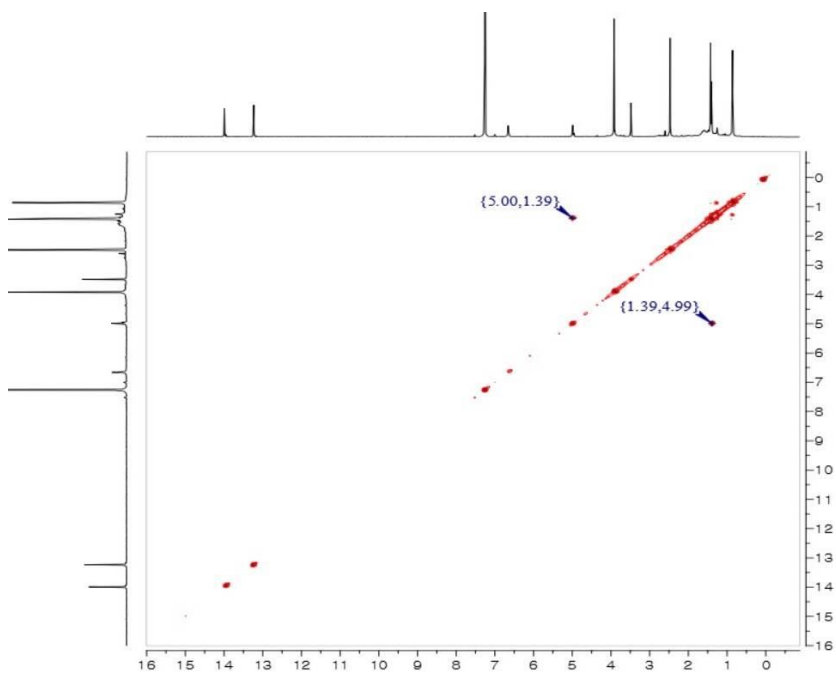

Figure A24. The COSY (400 MHz, $CDCl_3$) spectrum of **5**

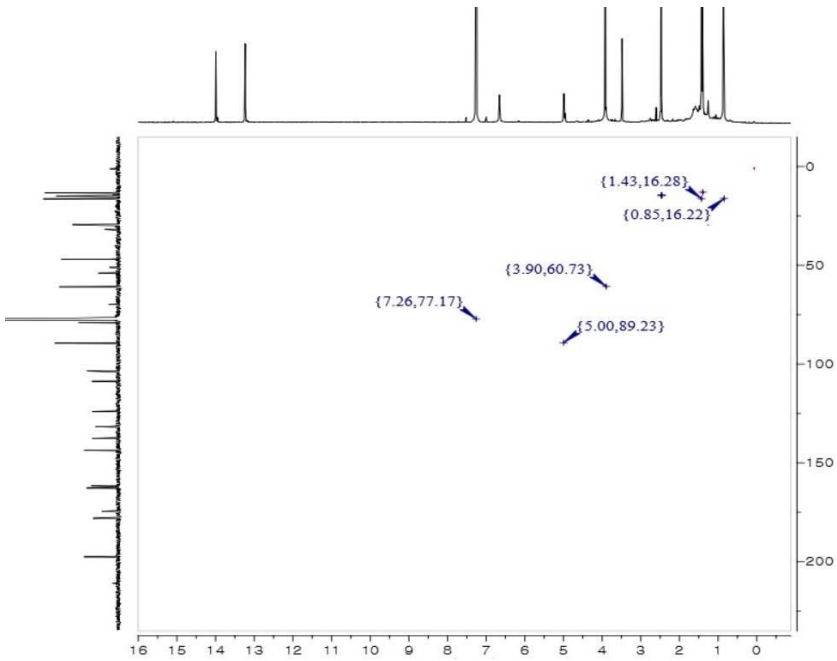

Figure A25. The HSQC (400 MHz, $CDCl_3$) spectrum of **5**

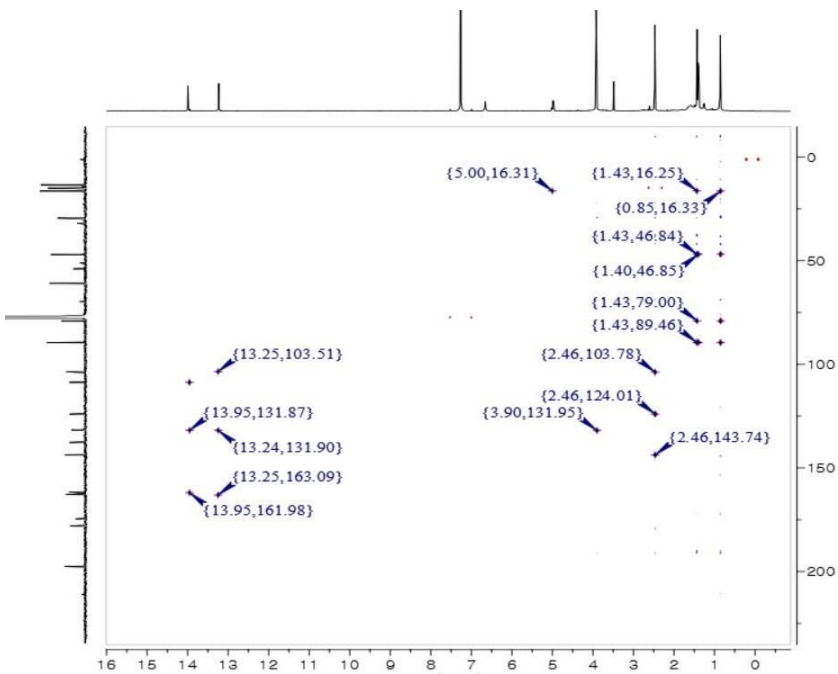

Figure A26. The HMBC (400 MHz, $CDCl_3$) spectrum of **5**

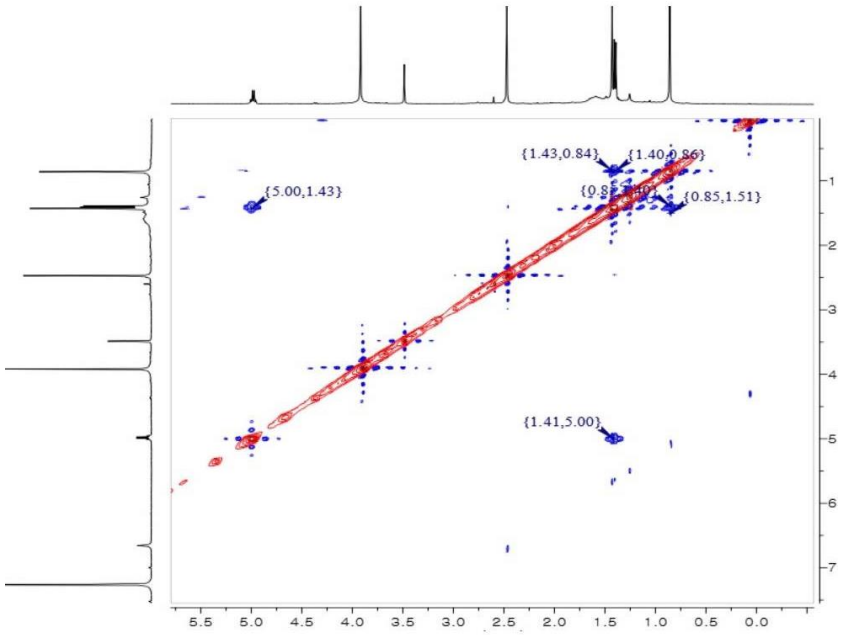

Figure A27. The NOESY (400 MHz, $CDCl_3$) spectrum of **5**

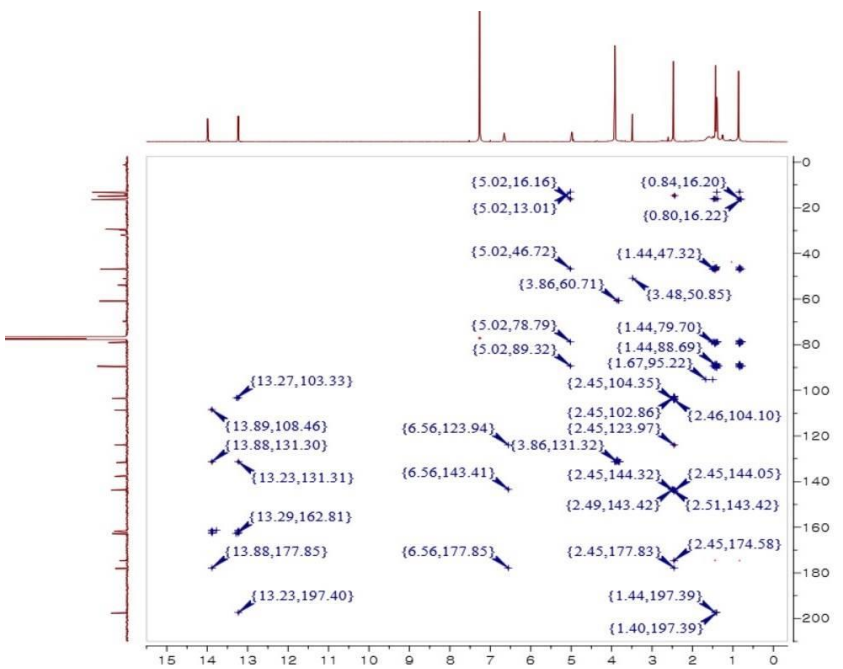

Figure A28. The D-HMBC (800 MHz, J_{CH} = 4 Hz, $CDCl_3$) spectrum of **5**

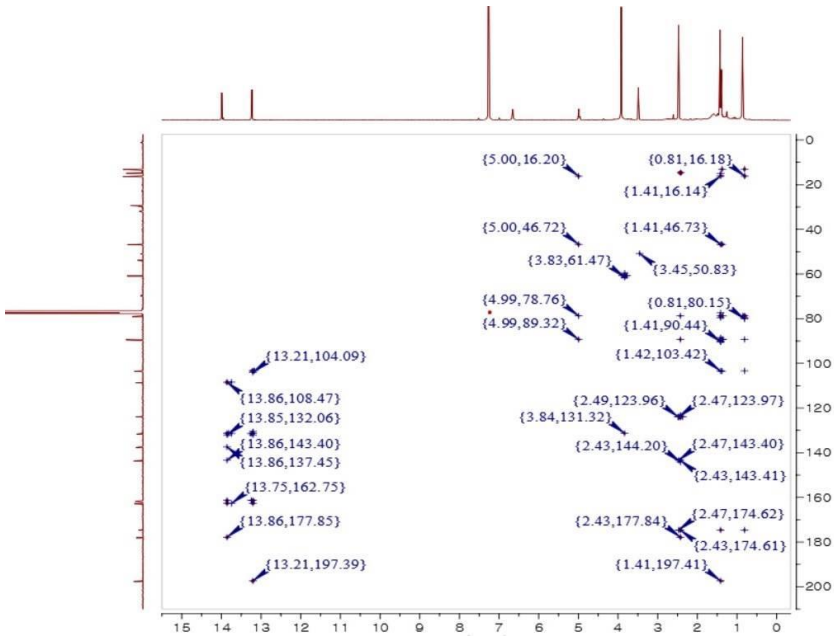

Figure A29. The D-HMBC (800 MHz, J_{CH} = 2 Hz, $CDCl_3$) spectrum of **5**

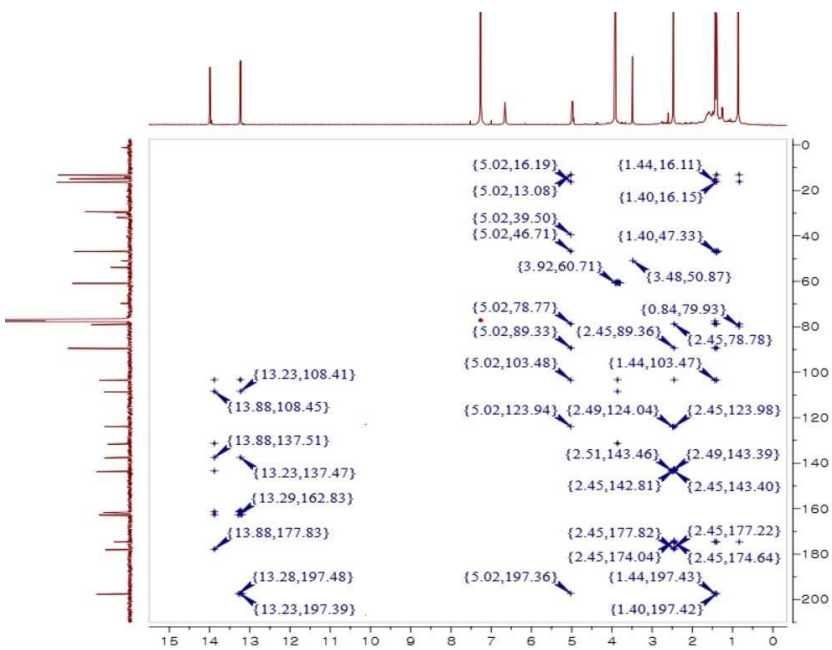

Figure A30. The D-HMBC (800 MHz, J_{CH} = 1 Hz, $CDCl_3$) spectrum of **5**

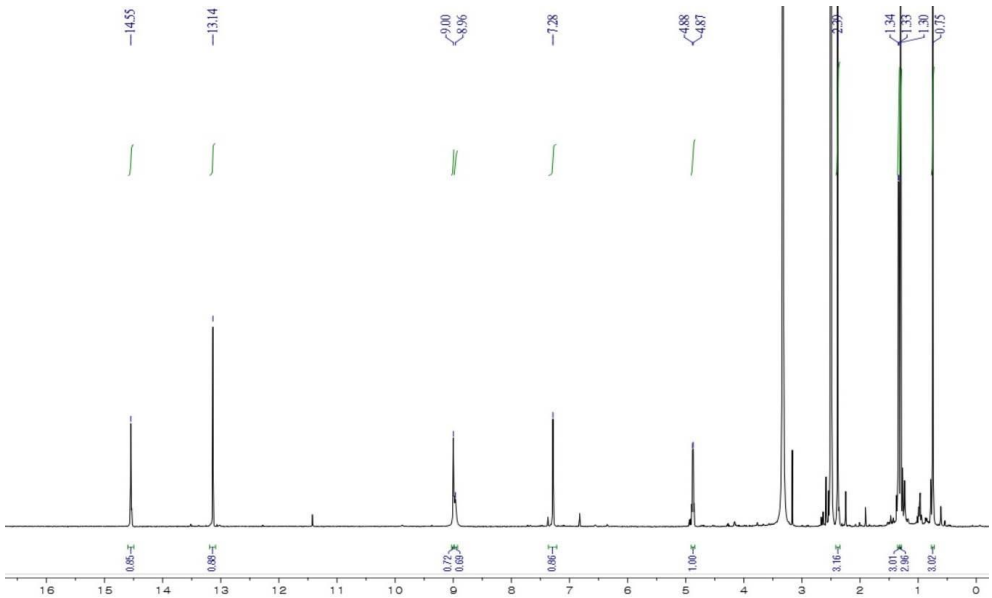

Figure A31. The ^{1}H NMR (600 MHz, DMSO-d_6) spectrum of **6**

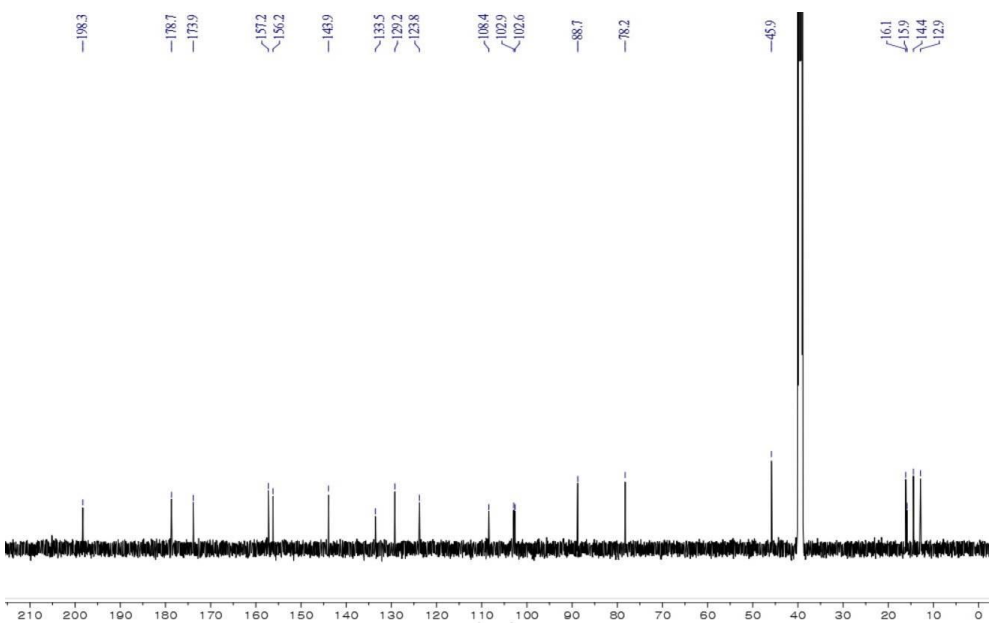

Figure A32. The ^{13}C NMR (150 MHz, DMSO-d_6) spectrum of **6**

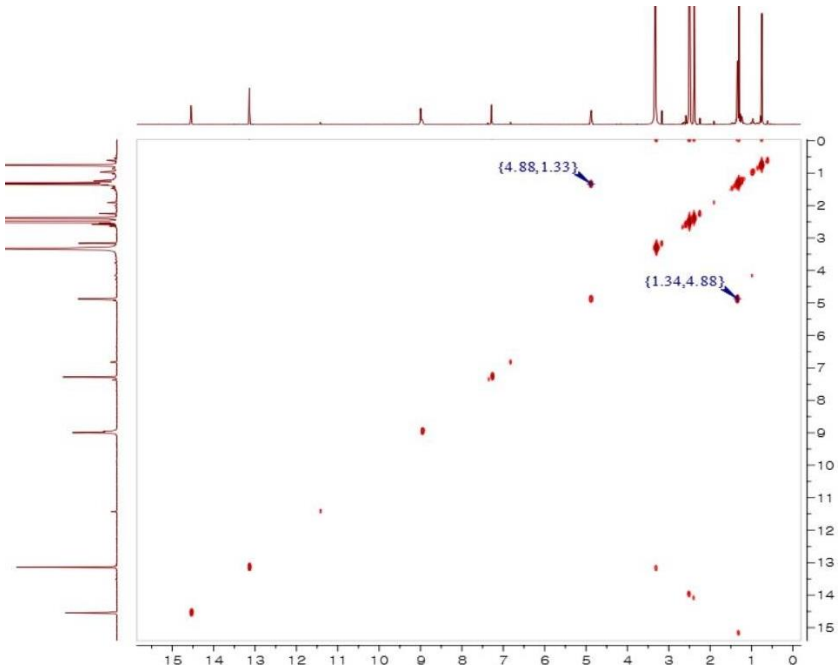

Figure A33. The COSY (600 MHz, DMSO-d_6) spectrum of **6**

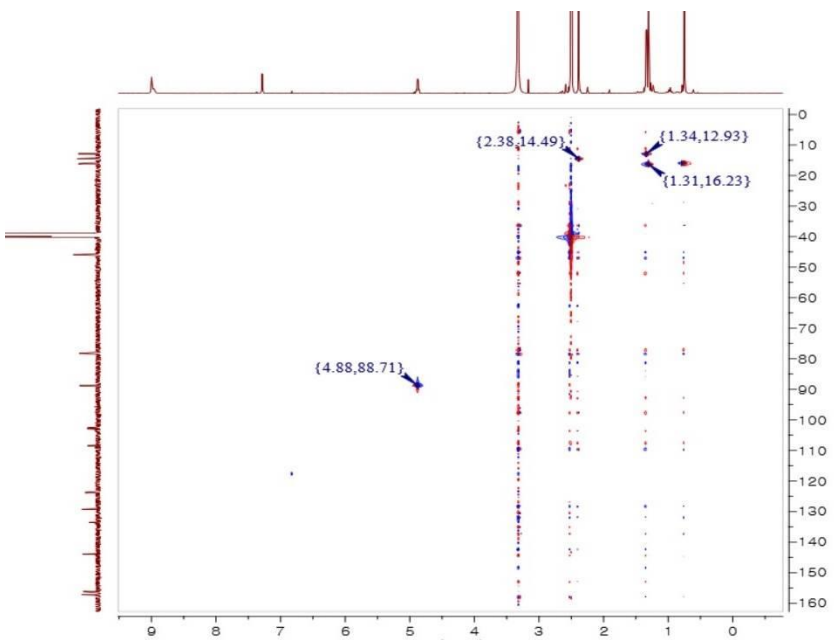

Figure A34. The HSQC (600 MHz, DMSO-d_6) spectrum of **6**

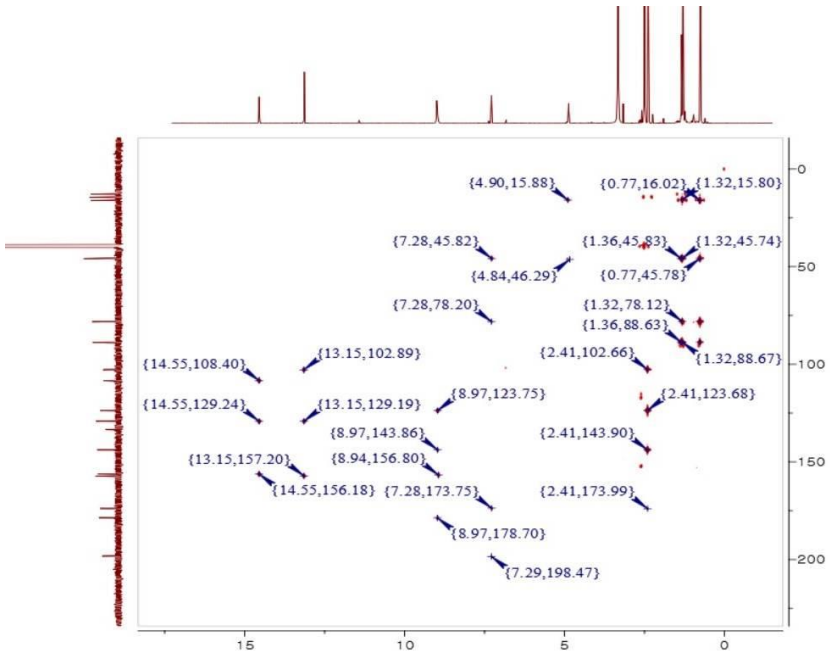

Figure A35. The HMBC (500 MHz, DMSO-d_6) spectrum of **6**

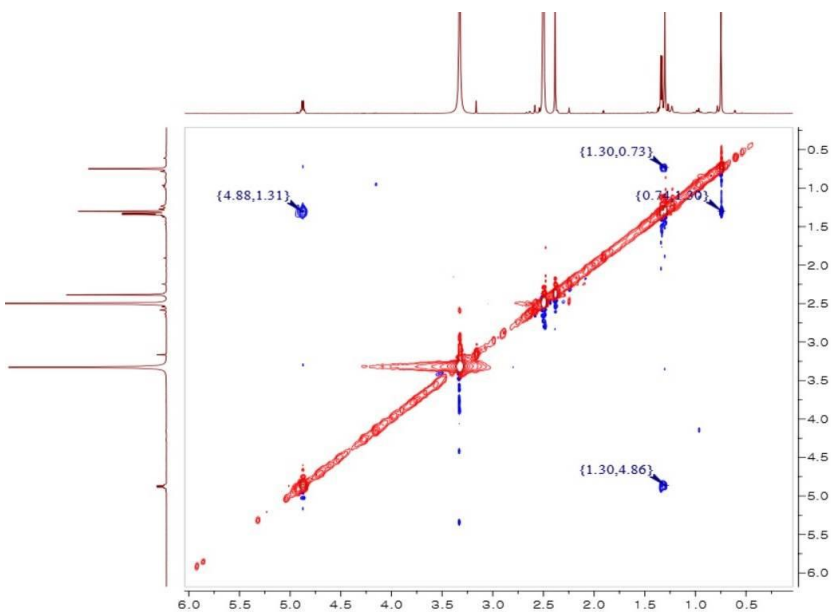

Figure A36. The NOESY (500 MHz, DMSO-d_6) spectrum of **6**

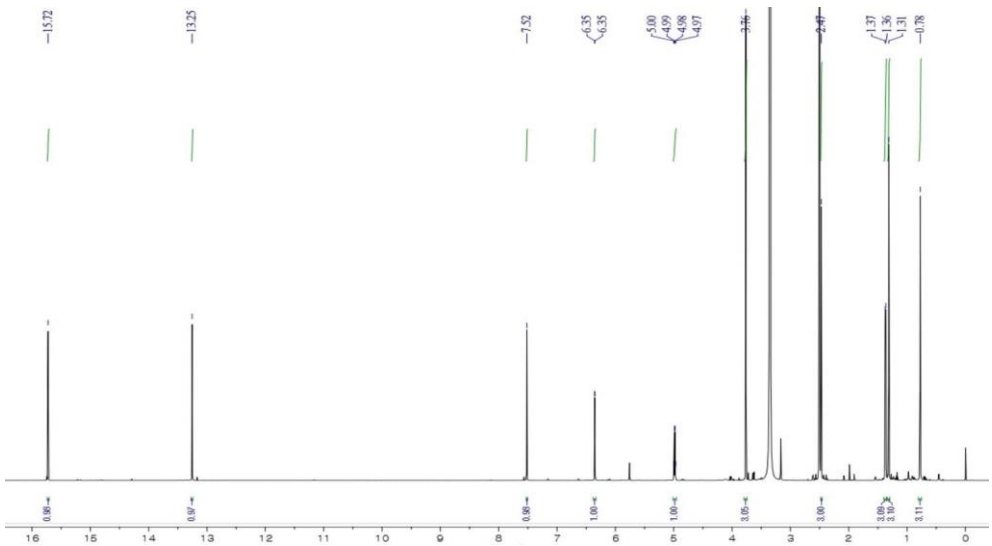

Figure A37. The ^{1}H NMR (600 MHz, DMSO-d_6) spectrum of **7**

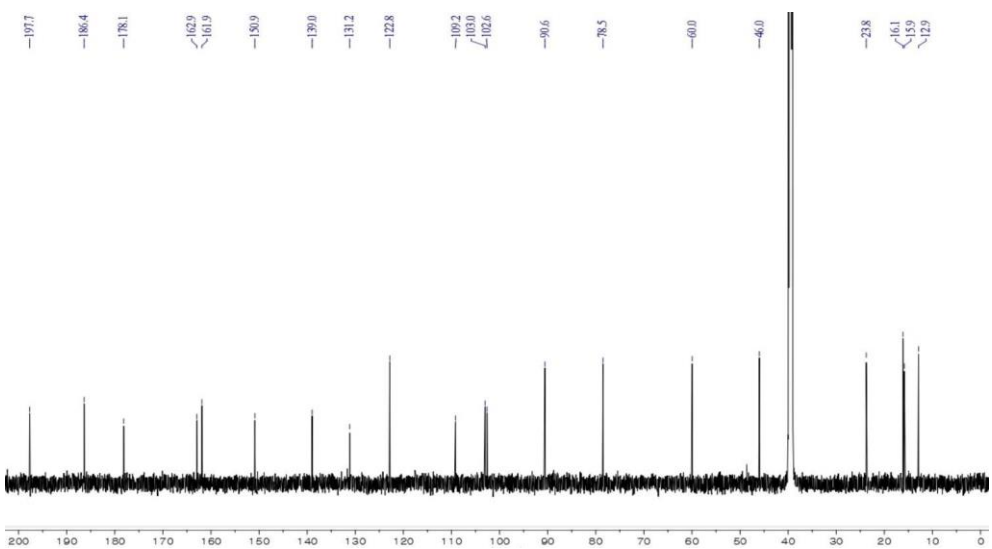

Figure A38. The ^{13}C NMR (150 MHz, DMSO-d_6) spectrum of **7**

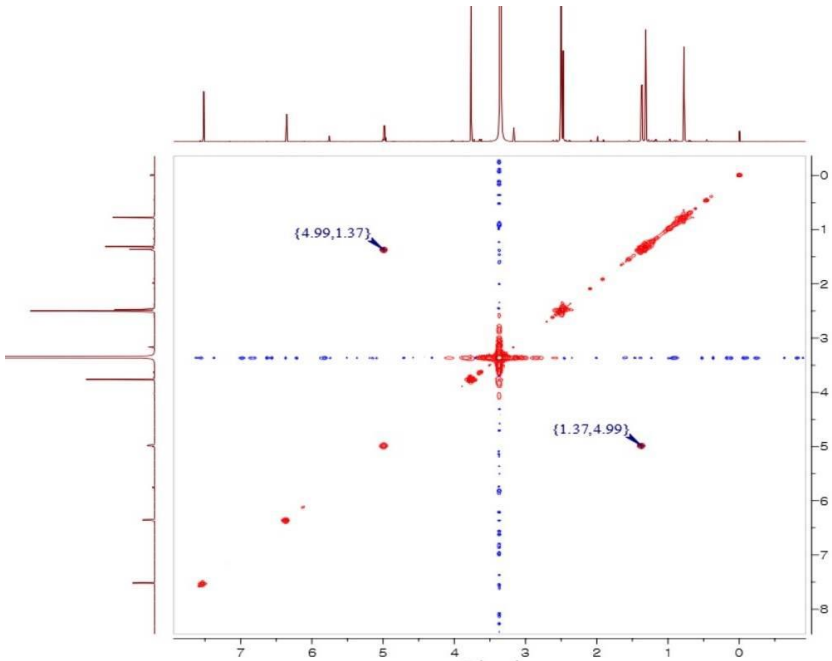

Figure A39. The COSY (600 MHz, DMSO-d_6) spectrum of **7**

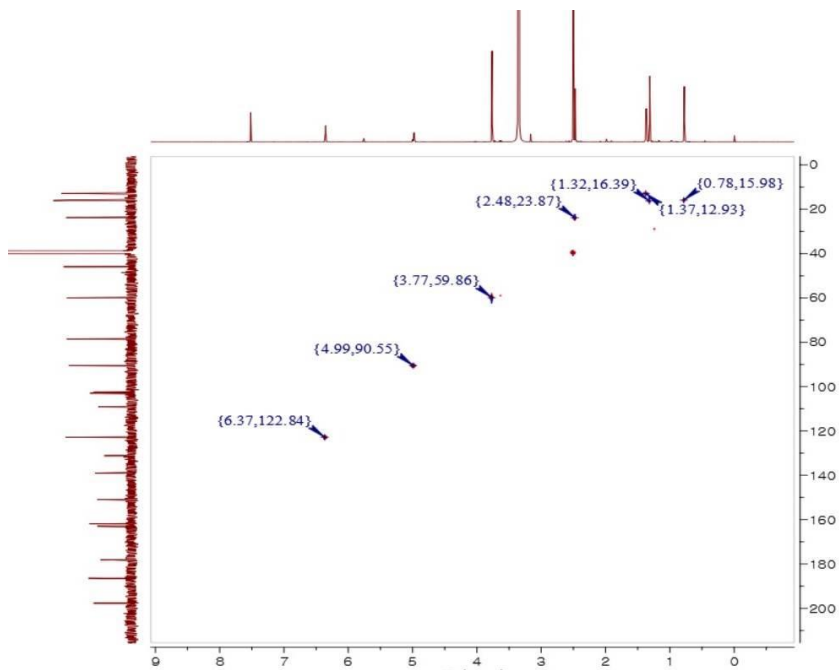

Figure A40. The HSQC (600 MHz, DMSO-d_6) spectrum of **7**

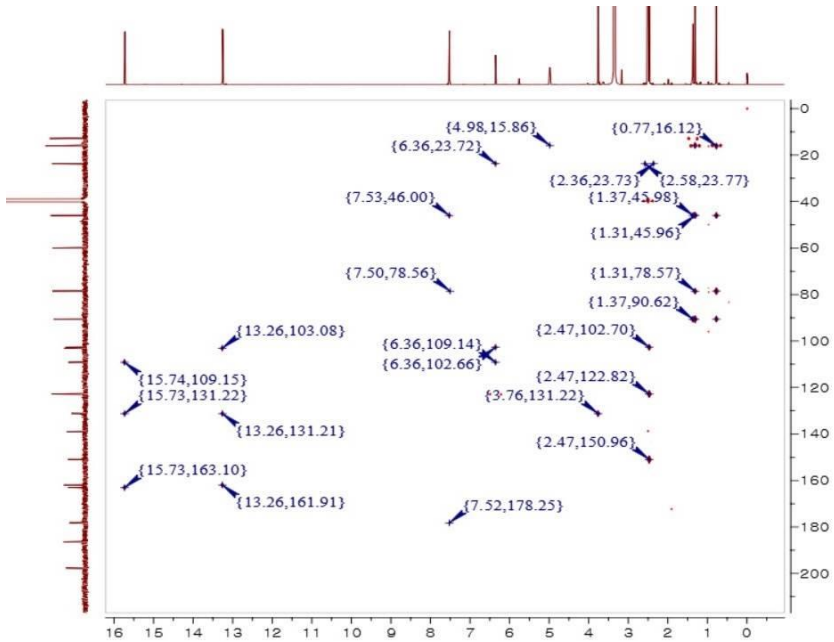

Figure A41. The HMBC (600 MHz, DMSO-d_6) spectrum of **7**

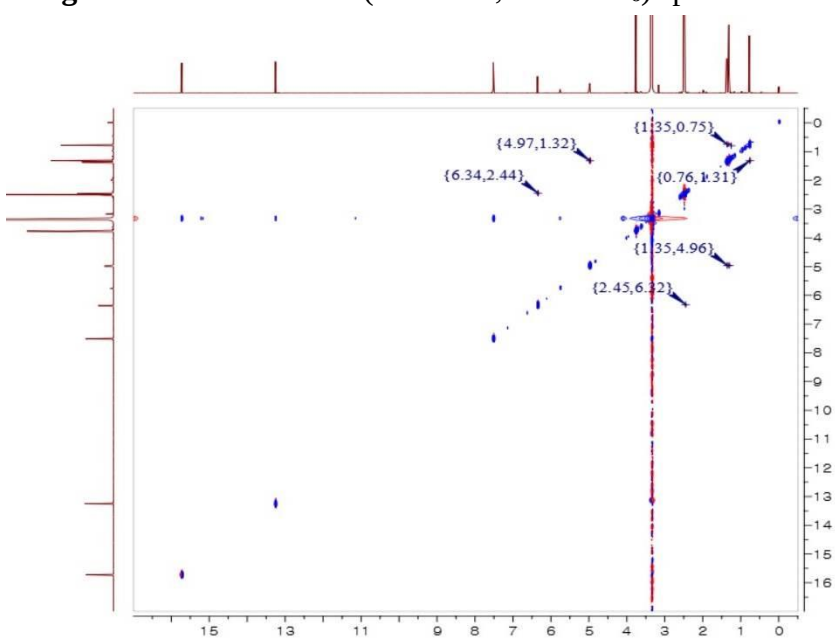

Figure A42. The NOESY (600 MHz, DMSO-d_6) spectrum of **7**

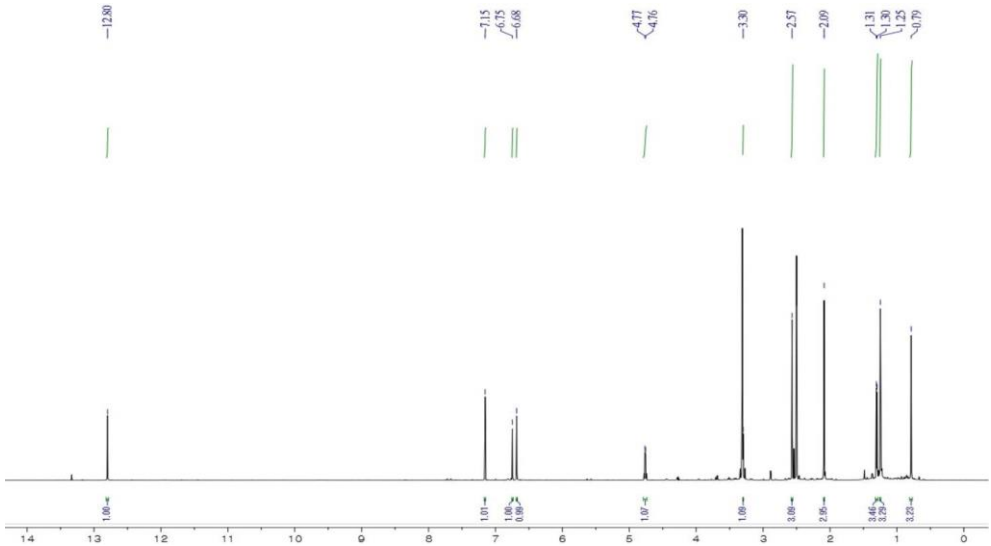

Figure A43. The ^{1}H NMR (600 MHz, DMSO-d_6) spectrum of **8**

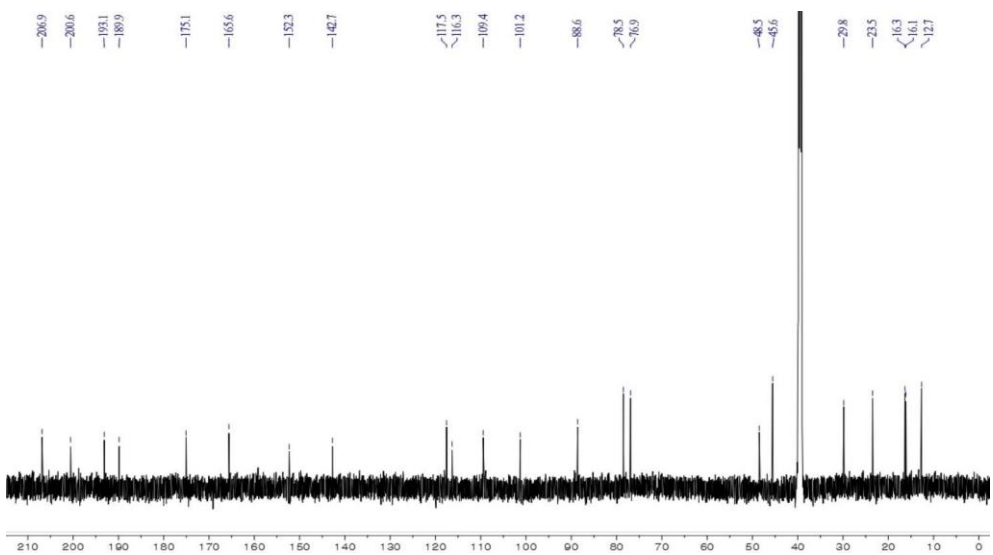

Figure A44. The ^{13}C NMR (150 MHz, DMSO-d_6) spectrum of **8**

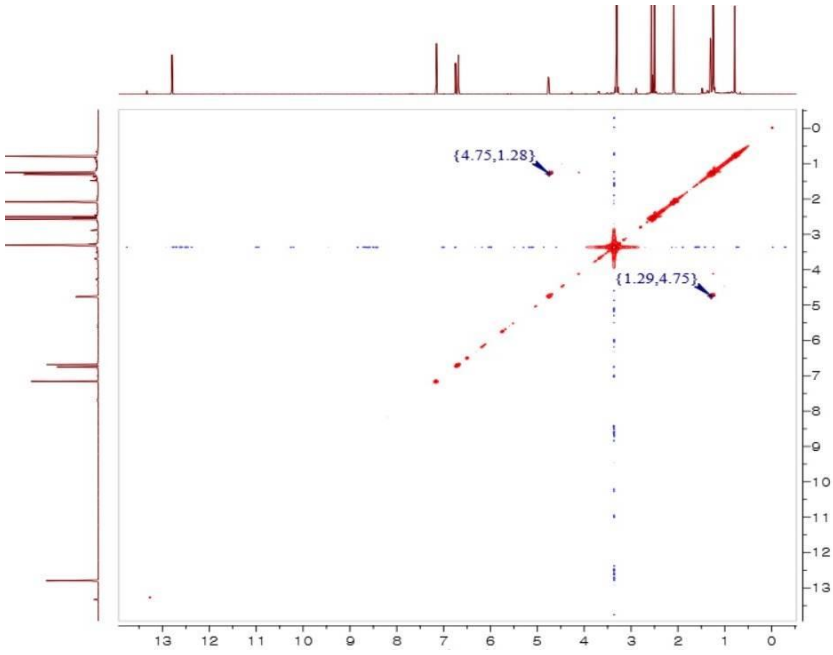

Figure A45. The COSY (600 MHz, DMSO-d_6) spectrum of **8**

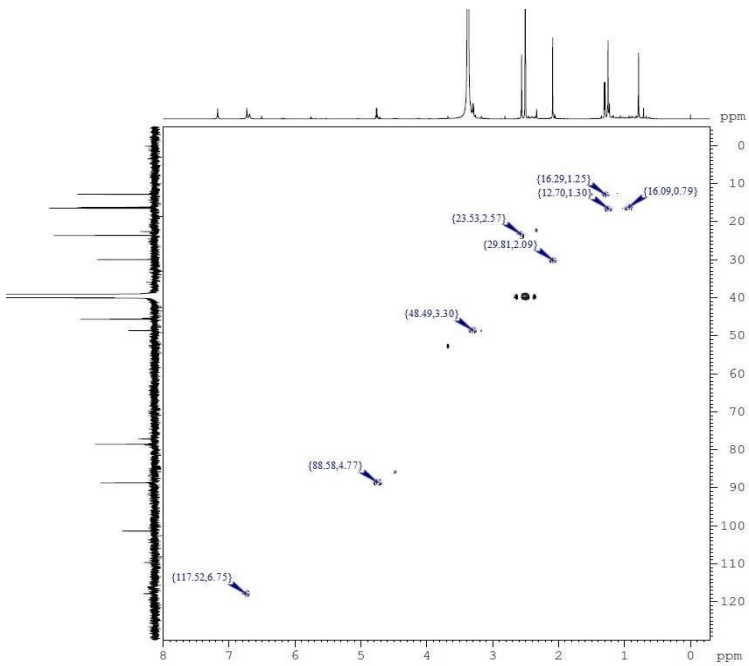

Figure A46. The HSQC (600 MHz, DMSO-d_6) spectrum of **8**

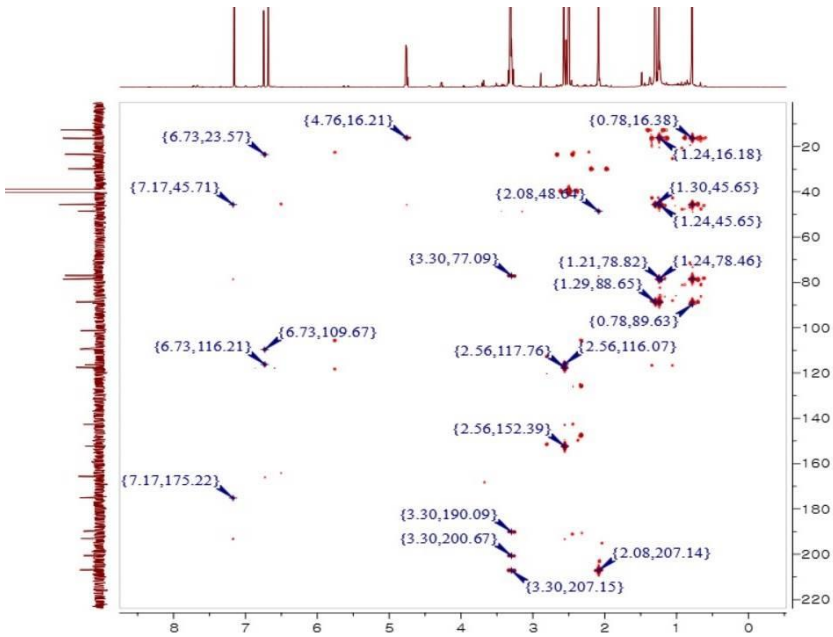

Figure A47. The HMBC (600 MHz, DMSO-d_6) spectrum of **8**

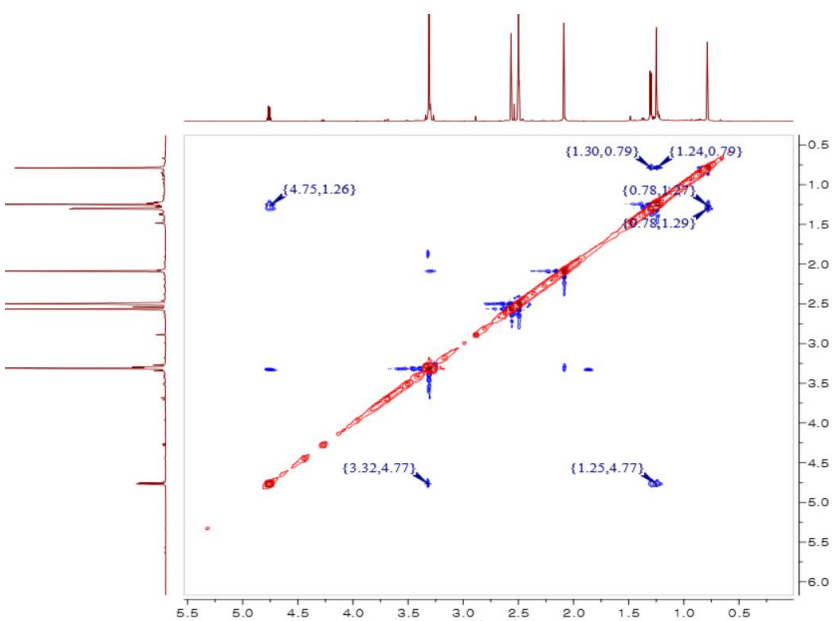

Figure A48. The NOESY (600 MHz, DMSO-d_6) spectrum of **8**

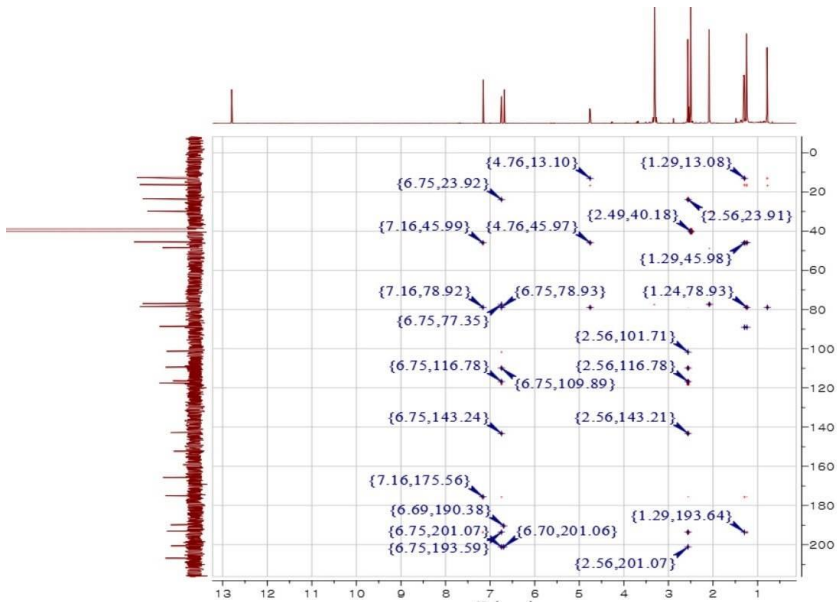

Figure A49. The D-HMBC (800 MHz, J_{CH} = 1 Hz, DMSO-d_6) spectrum of **8**

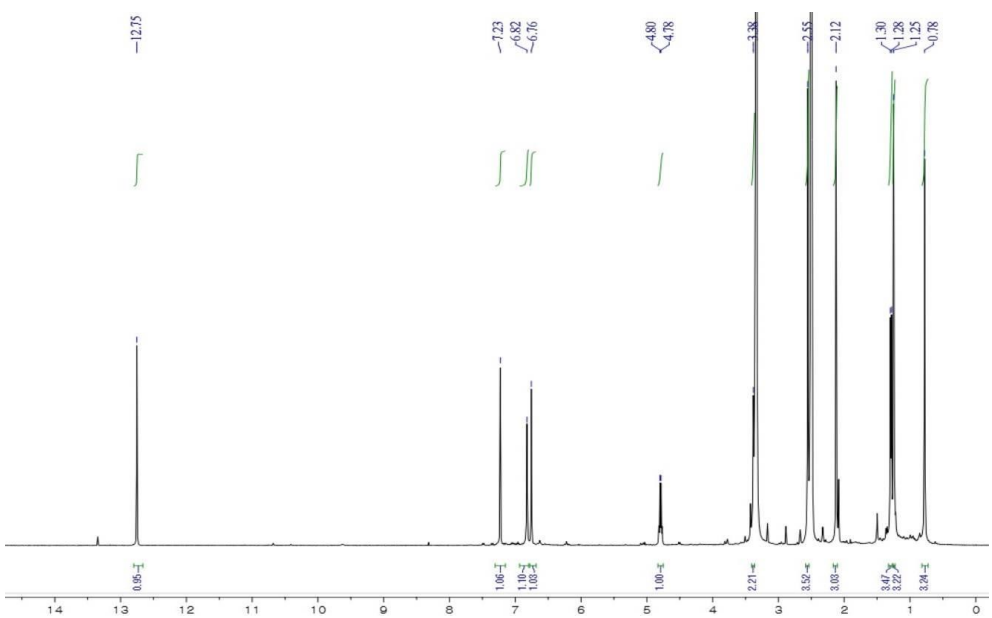

Figure A50. The ^{1}H NMR (600 MHz, DMSO-d_6) spectrum of **9**

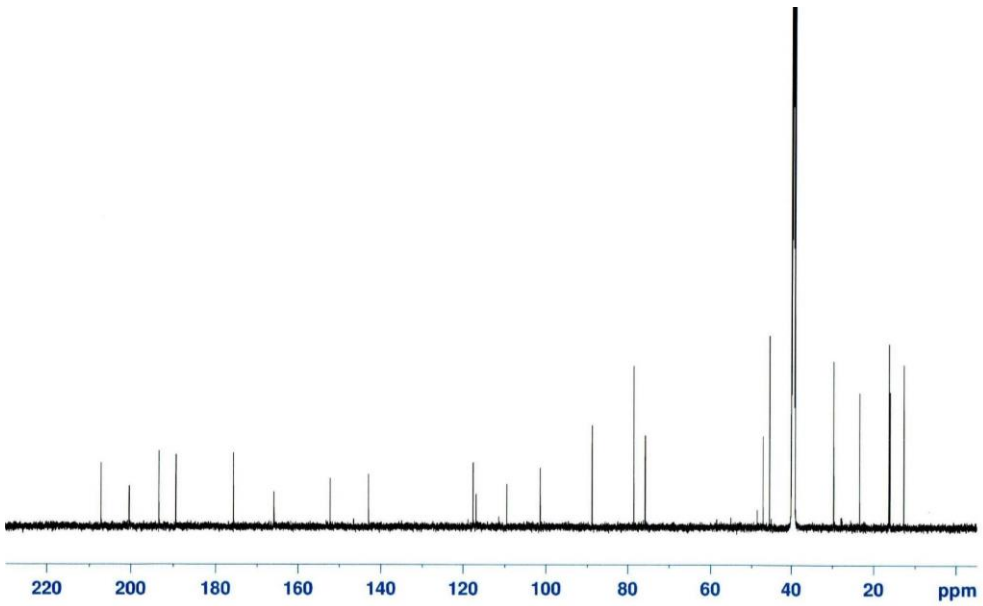

Figure A51. The ^{13}C NMR (150 MHz, DMSO-d_6) spectrum of **9**

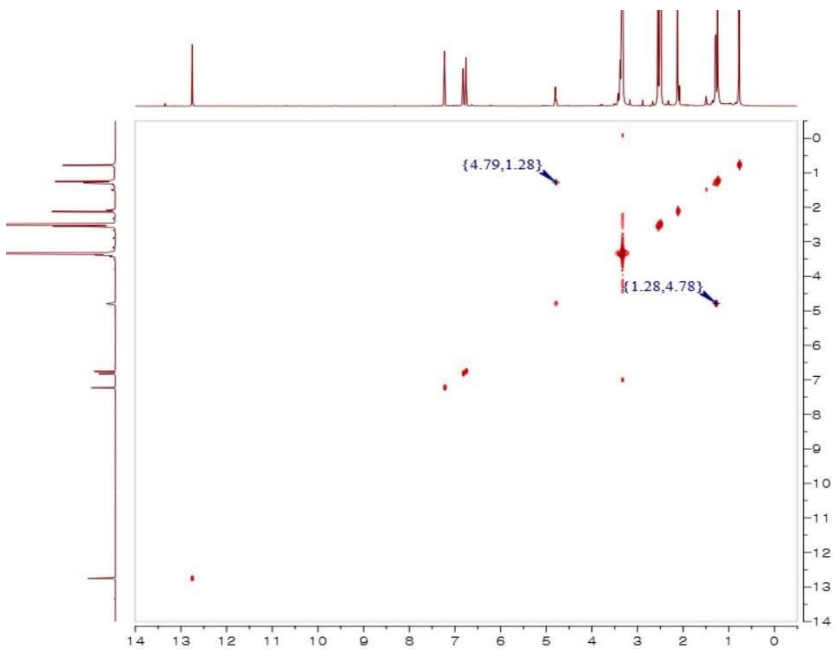

Figure A52. The COSY (600 MHz, DMSO-d_6) spectrum of **9**

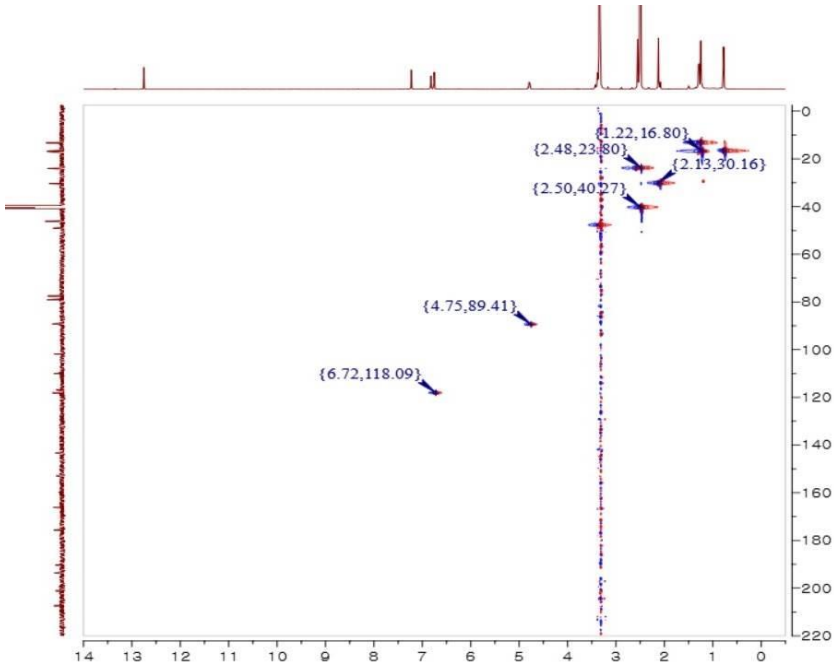

Figure A53. The HSQC (600 MHz, DMSO-d_6) spectrum of **9**

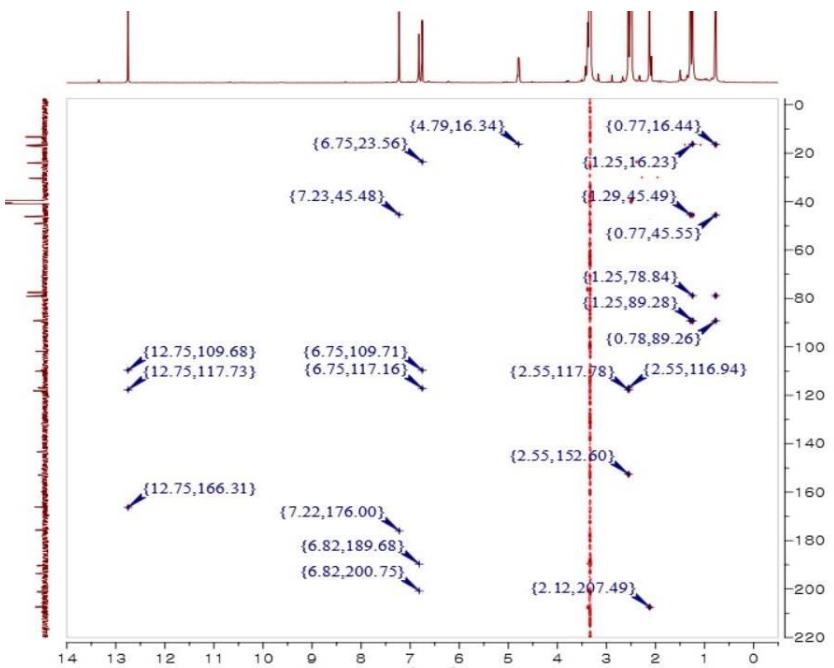

Figure A54. The HMBC (600 MHz, DMSO-d_6) spectrum of **9**

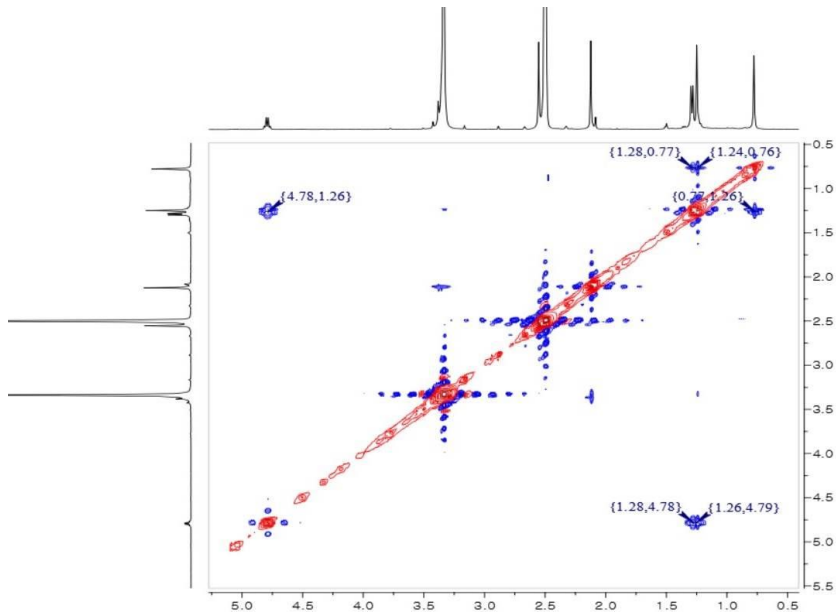

Figure A55. The NOESY (400 MHz, DMSO-d_6) spectrum of **9**

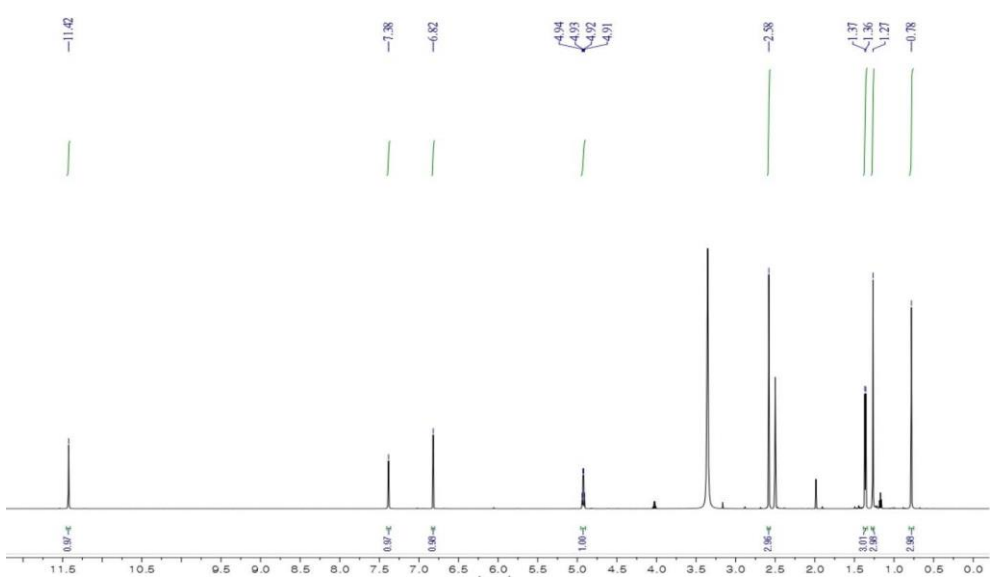

Figure A56. The ^{1}H NMR (600 MHz, DMSO-d_6) spectrum of **10**

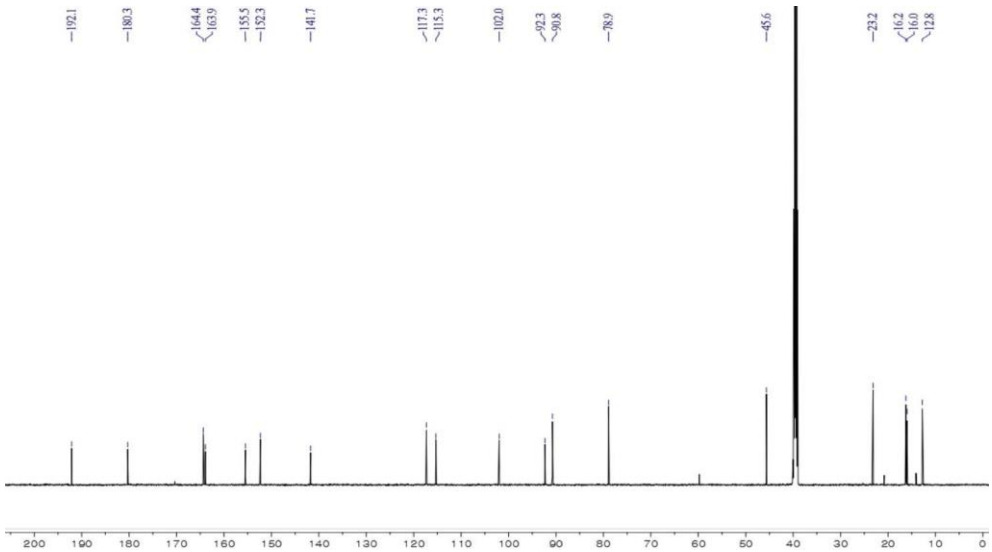

Figure A57. The ^{13}C NMR (150 MHz, DMSO-d_6) spectrum of **10**

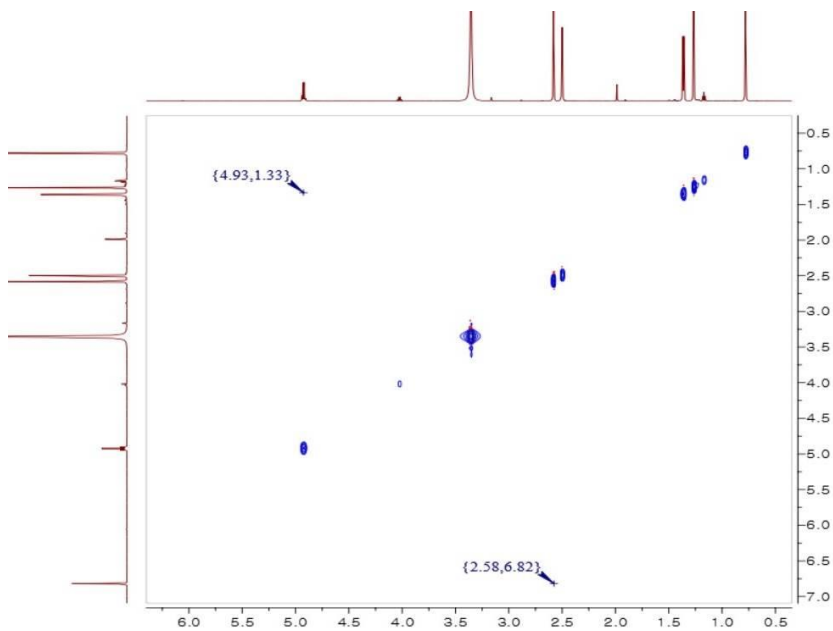

Figure A58. The COSY (600 MHz, DMSO-d_6) spectrum of **10**

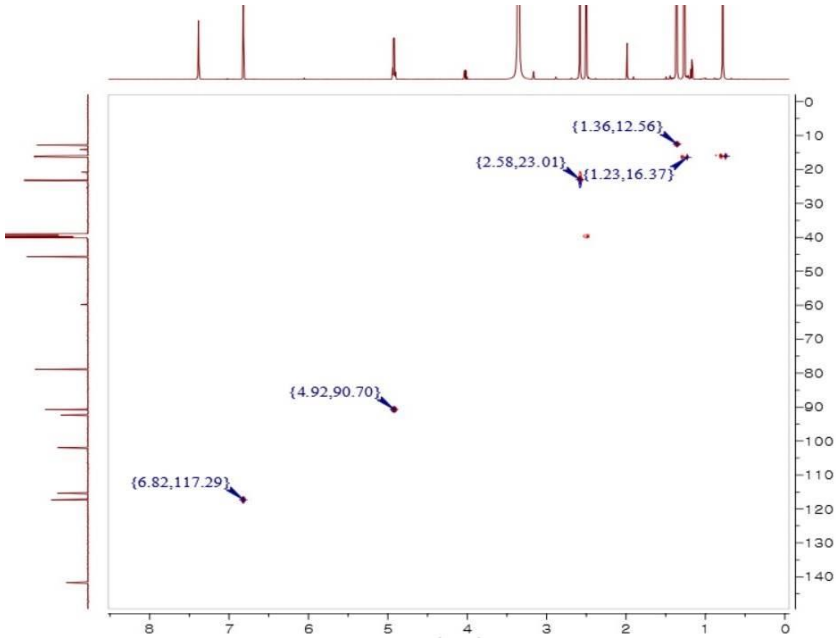

Figure A59. The HSQC (600 MHz, DMSO-d_6) spectrum of **10**

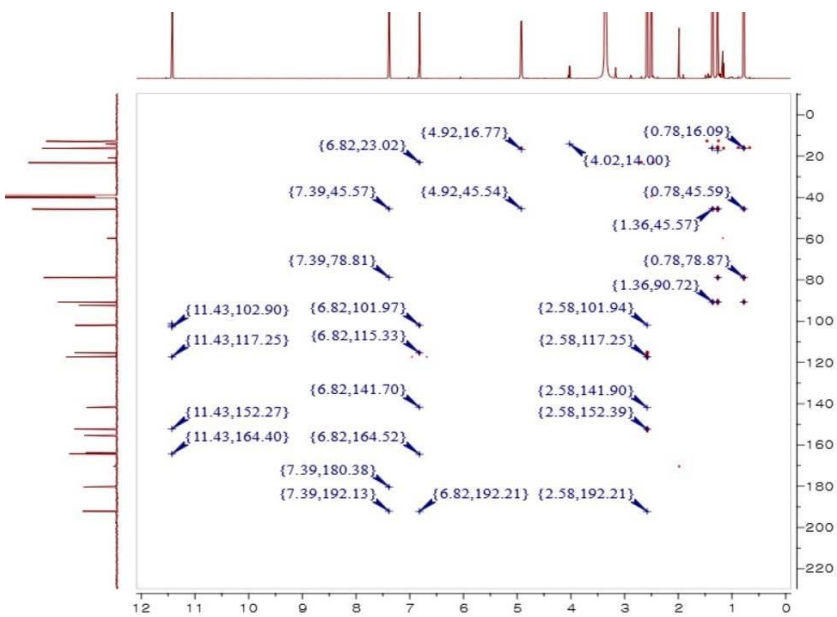

Figure A60. The HMBC (600 MHz, DMSO-d_6) spectrum of **10**

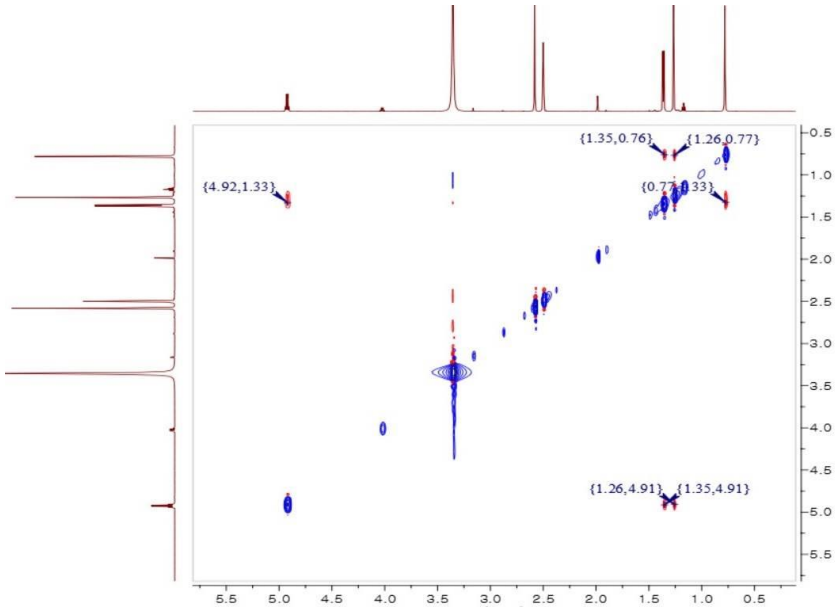

Figure A61. The NOESY (600 MHz, DMSO-d_6) spectrum of **10**

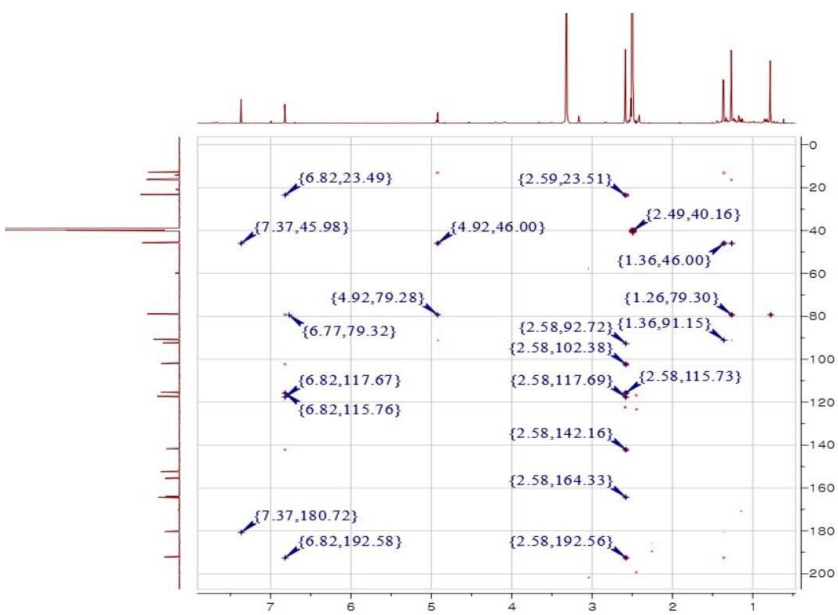

Figure A62. The D-HMBC (800 MHz, J_{CH} = 1 Hz, DMSO-d_6) spectrum of **10**

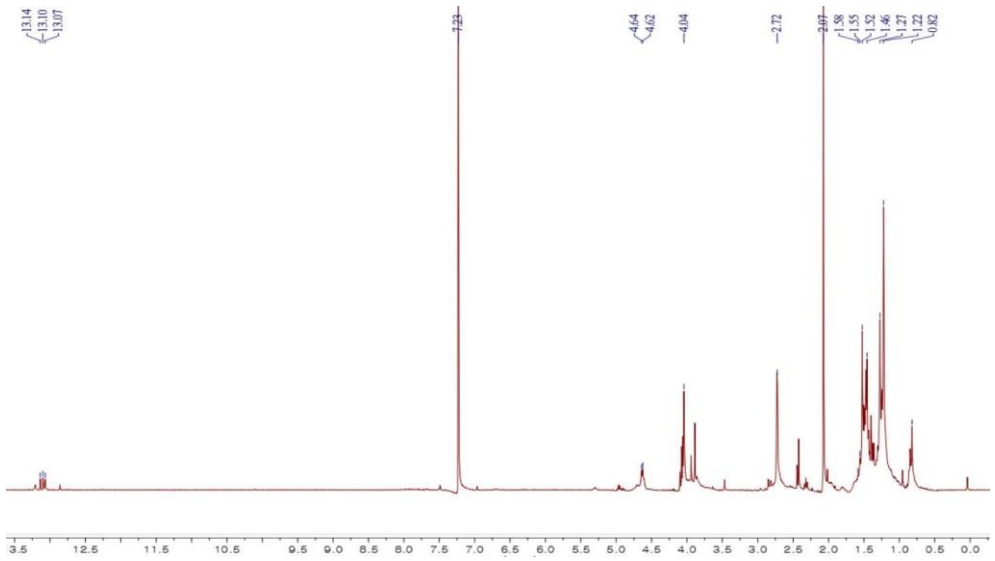

Figure A63. The ^{1}H NMR (400 MHz, $CDCl_3$) spectrum **5a**

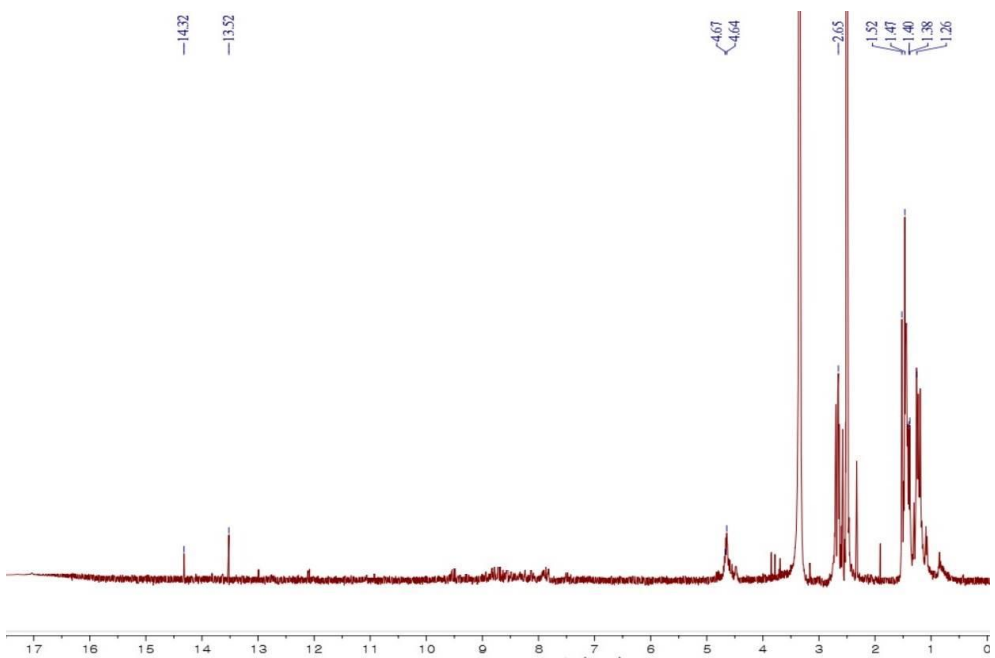

Figure A64. The ^{1}H NMR (400 MHz, DMSO-d_6) spectrum **6a**

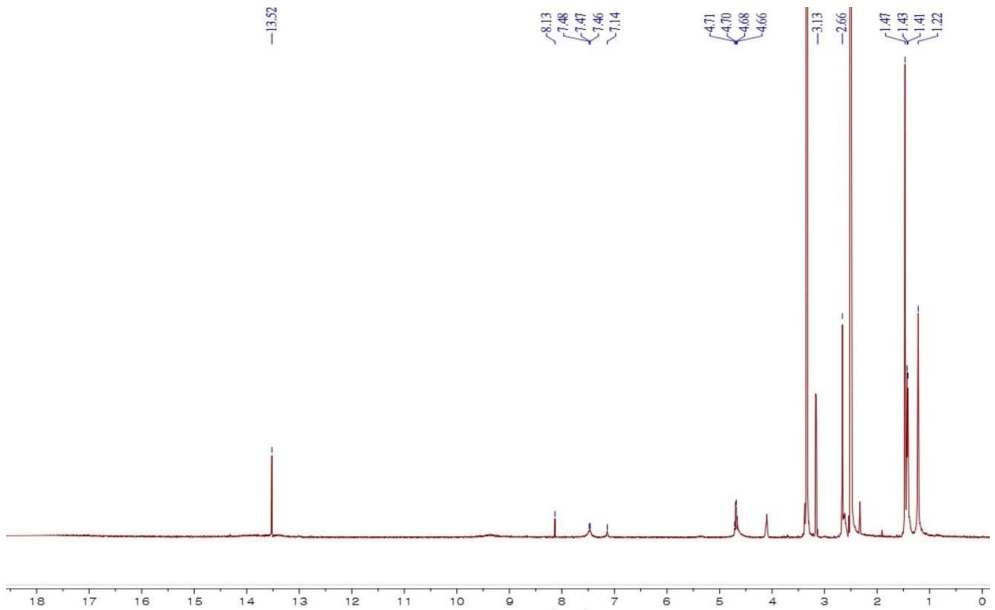

Figure A65. The ^{1}H NMR (400 MHz, DMSO-d_6) spectrum **7a**

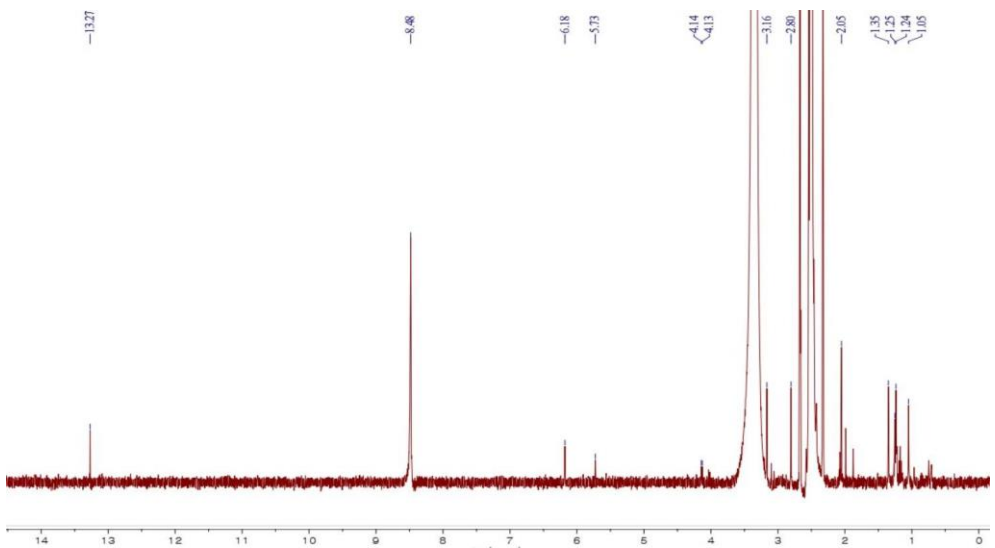

Figure A66. The ^{1}H NMR (400 MHz, DMSO-d_6) spectrum **8a**

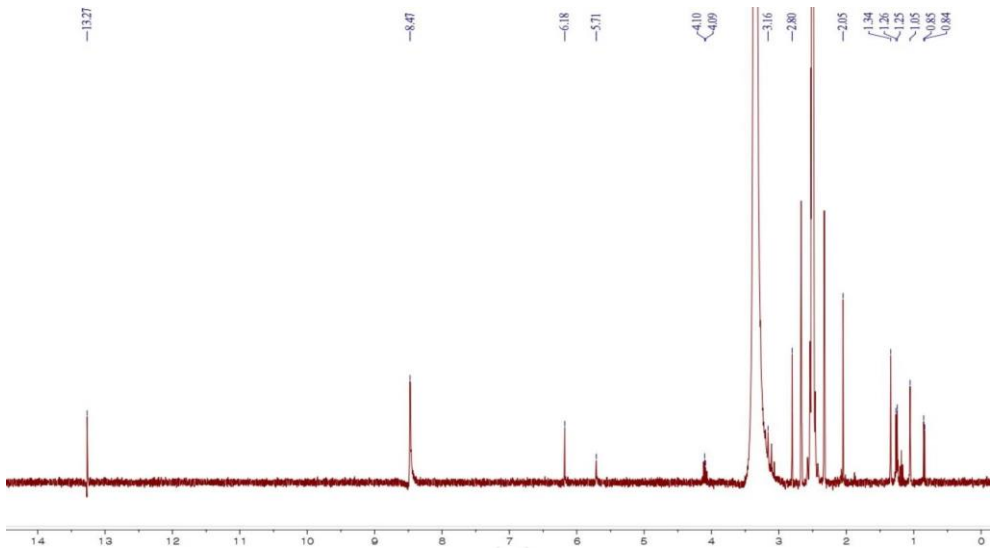

Figure A67. The ^{1}H NMR (400 MHz, DMSO-d_6) spectrum **9a**

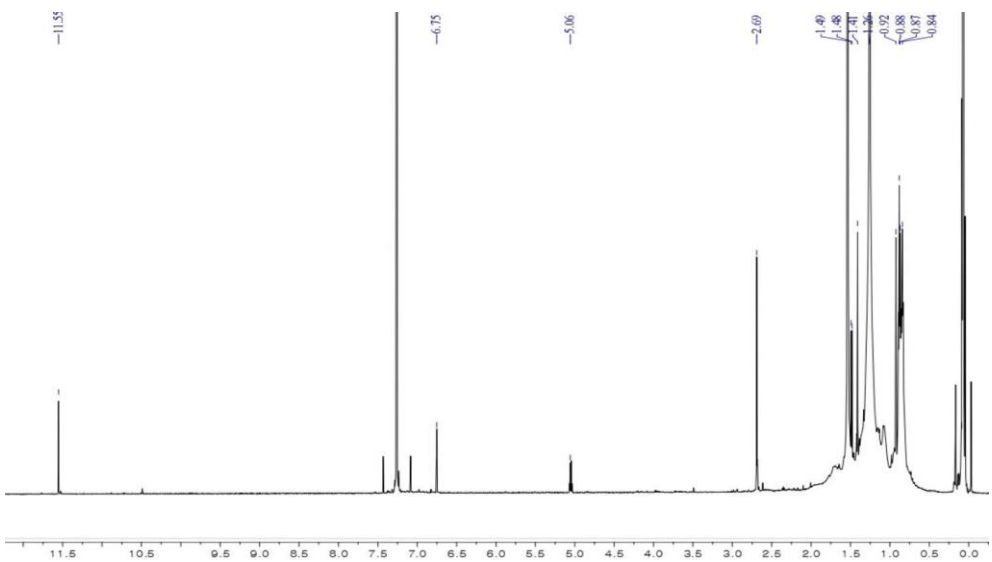

Figure A68. The ^{1}H NMR (400 MHz, $CDCl_3$) spectrum **10a**

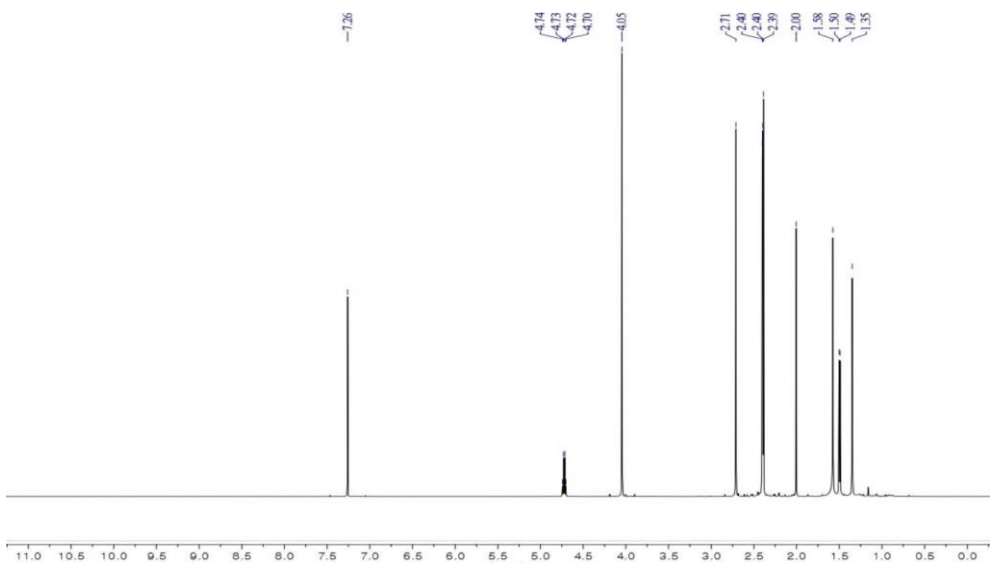

Figure A69. The ^{1}H NMR (600 MHz, $CDCl_3$) spectrum of **5b**

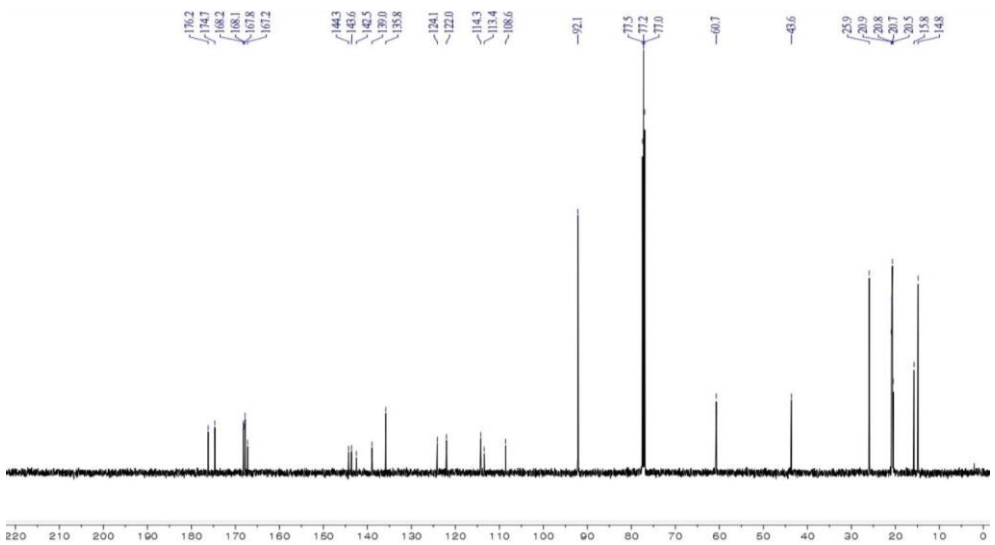

Figure A70. The ^{13}C NMR (150 MHz, $CDCl_3$) spectrum of **5b**

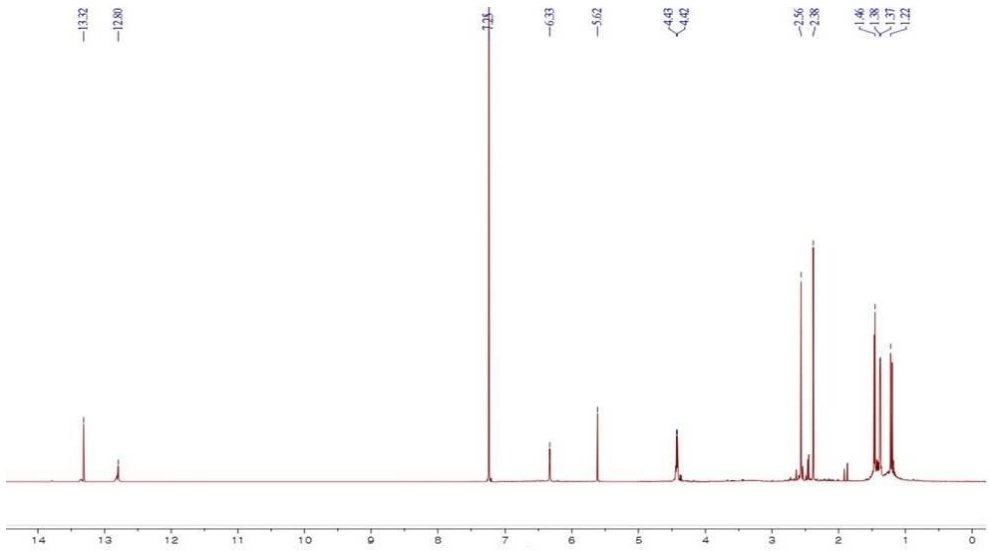

Figure A71. The ^{1}H NMR (400 MHz, $CDCl_3$) spectrum of **8b** (**9b**, **11a**)

APPENDIX B:

Supporting Information

List of Figures

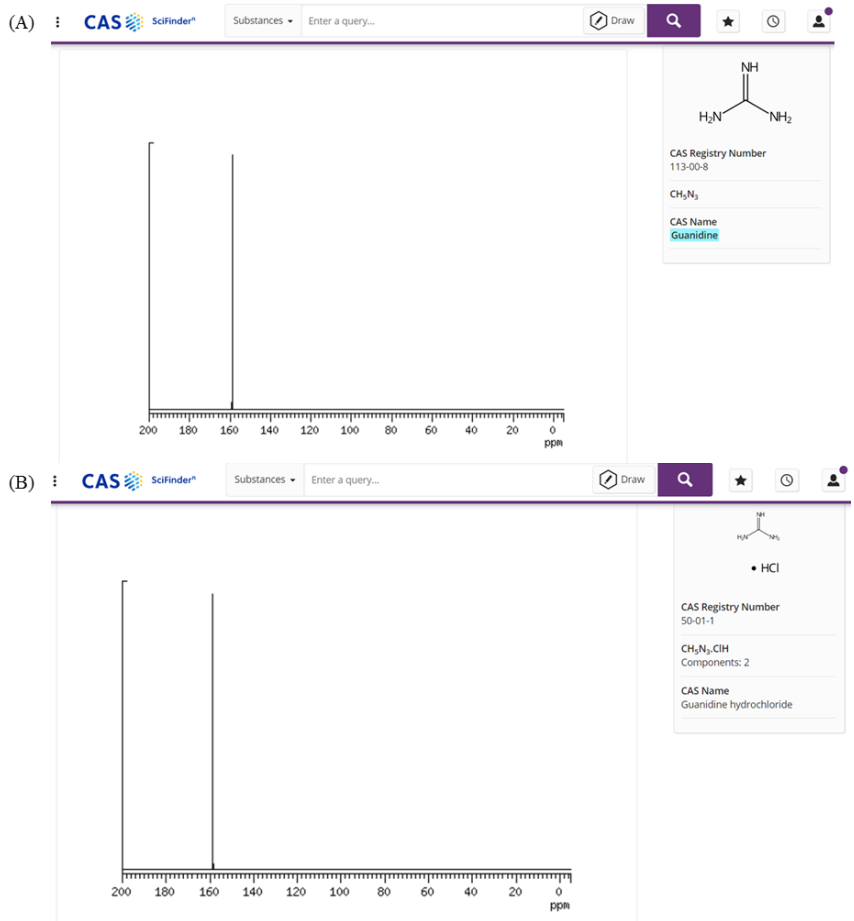

Figure B1. The ^{13}C NMR (25 MHz, D_2O) spectra of guanidine and guanidine hydrochloride. (A) The ^{13}C NMR (25 MHz, D_2O) spectrum of guanidine (CAS 113-00-8). The ^{13}C NMR (25 MHz, D_2O) spectrum of guanidine hydrochloride (CAS 50-01-1). The Scifinder provides experimental carbon NMR spectra of both guanidine (CAS 113-00-8) and guanidine hydrochloride (CAS 50-01-1) obtained from the National Institute of Advanced Industrial Science and Technology (Japan).

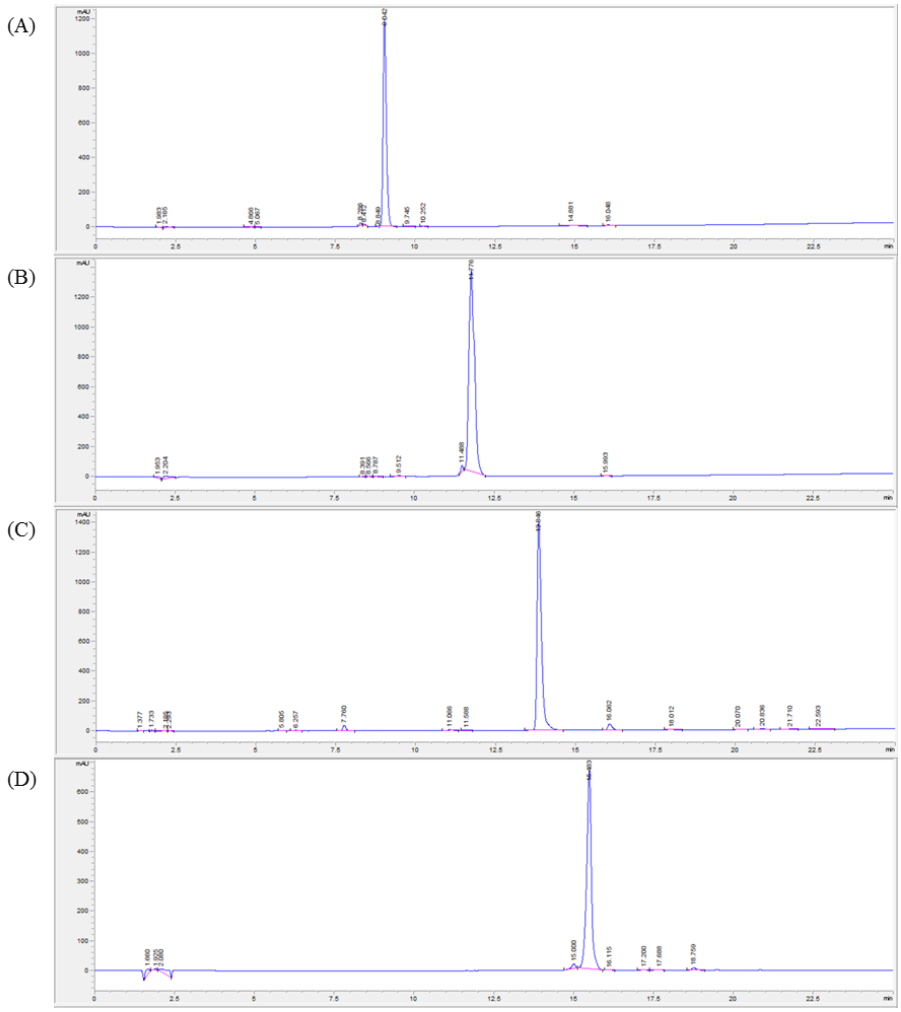

Figure B2. The HPLC analysis of **1**. *Condition*: (A) YMC-ODS-A column, 250 × 4.6 mm; 20–100% MeCN-H_2O gradient over 25 min; 0.5 mL/min; UV detection at 210 nm; t_R = 9.042 min. (B) YMC-ODS-A column, 250 × 4.6 mm; 10–100% MeCN-H_2O gradient over 25 min; 0.5 mL/min; UV detection at 210 nm; t_R = 11.776 min. (C) YMC-ODS-A column, 250 × 4.6 mm; H_2O-MeOH, 60:40; 0.5 mL/min; UV detection at 210 nm; t_R = 13.846 min. (D) YMC-ODS-A column, 250 × 4.6 mm; H_2O-MeCN, 69:31; 0.5 mL/min; UV detection at 210 nm; t_R = 15.483 min.

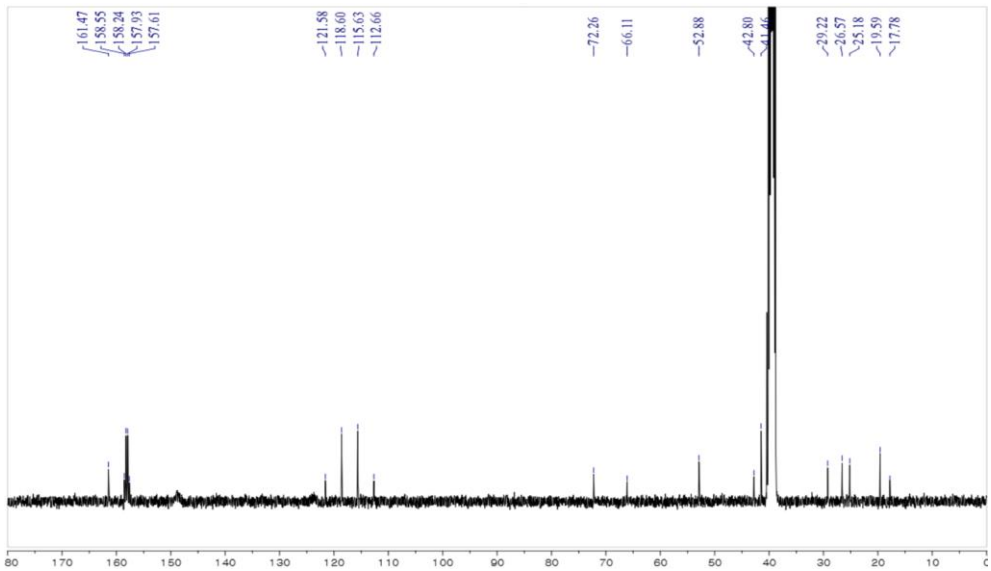

Figure B3. The ^{13}C NMR (100 MHz, DMSO-d_6) spectrum of **3c**

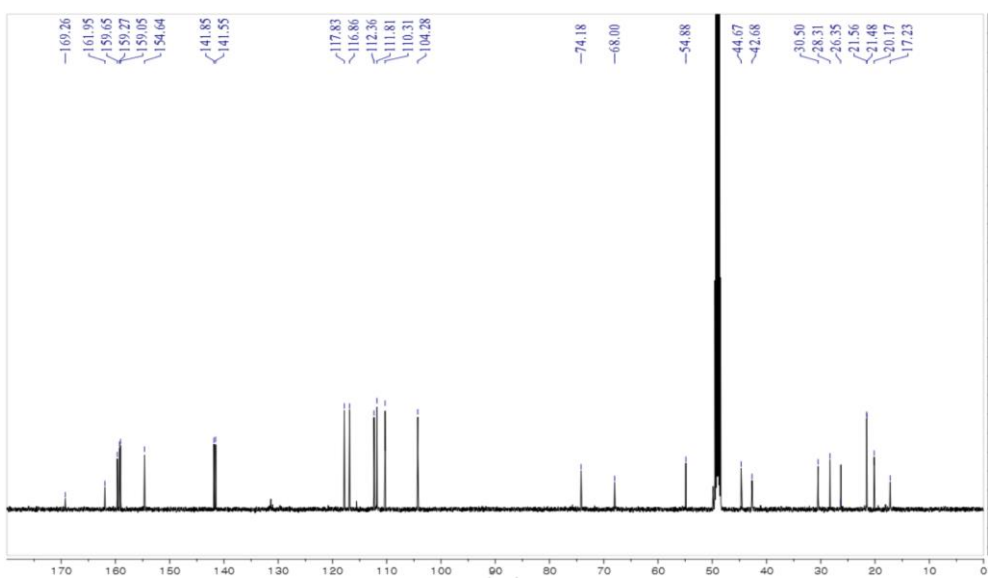

Figure B4. The ^{13}C NMR (125 MHz, MeOH-d_4) spectrum of **1**

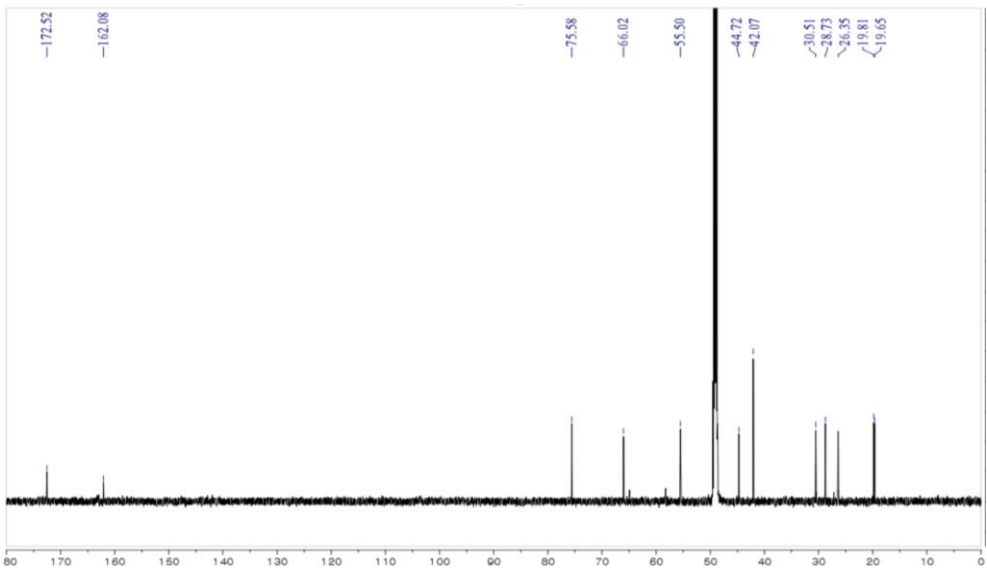

Figure B5. The ^{13}C NMR (200 MHz, MeOH-d_4) spectrum of **3**

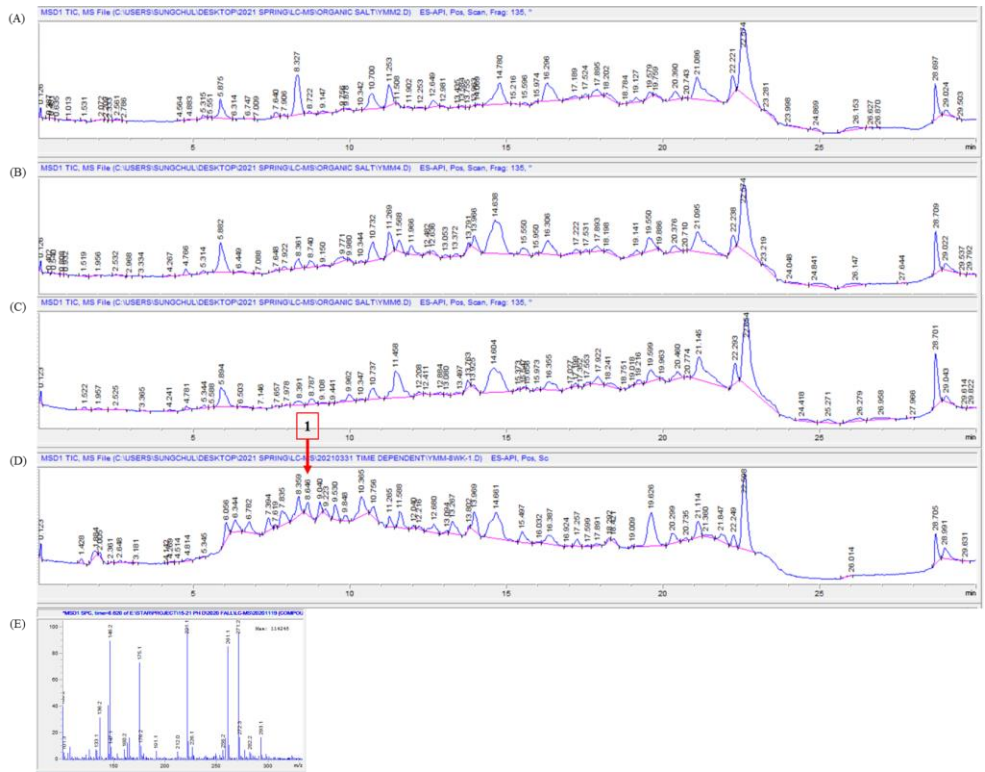

Figure B6. The time-scale LC–MS analysis of YMM liquid media extracts. (A)–(D) Extracts from 2, 4, 6, and 8 weeks of incubation, respectively. (E) The MS data on t_R = 8.641. *Condition*: YMC-ODS-A column, 250 × 4.6 mm; 10-100% MeCN-H_2O gradient over 20 min with 0.1% trifluoroacetic acid. Compound **1** (t_R = 8.646).

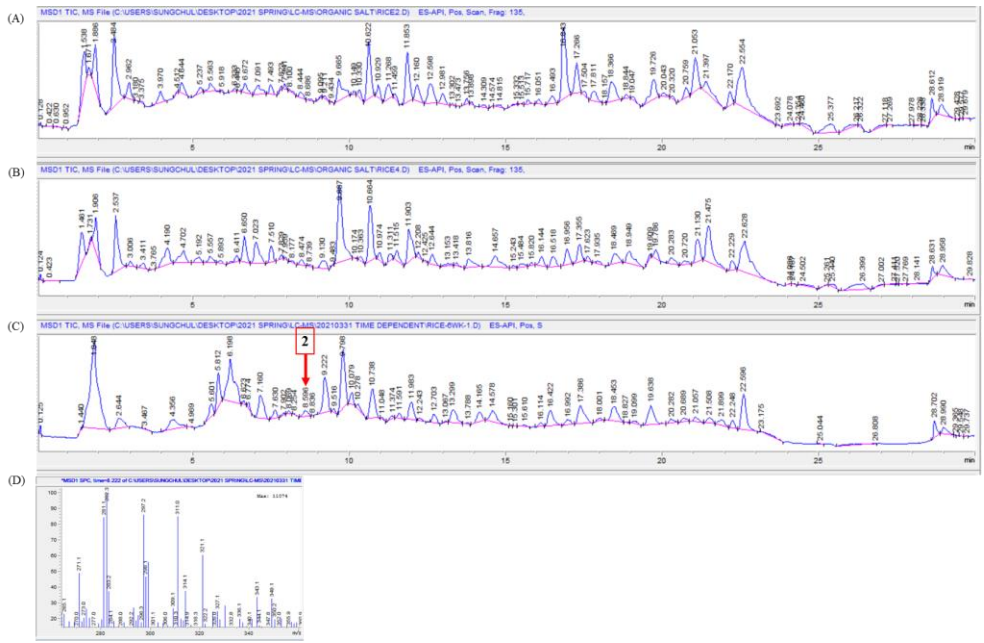

Figure B7. The time-scale LC–MS analysis of YMM-rice semi-solid media extracts. (A)–(C) Extracts from 2, 4 and 6 weeks of incubation, respectively. (D) The MS data on t_R = 8.596. *Condition*: YMC-ODS-A column, 250 × 4.6 mm; 10-100% MeCN-H_2O gradient over 20 min with 0.1% trifluoroacetic acid. Compound **2** (t_R = 8.596).

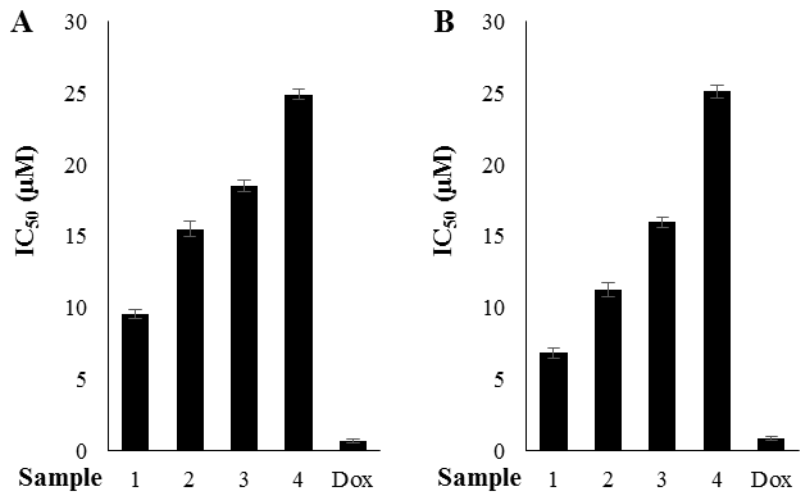

Figure B8. The MTT assay against K562 and A549 cancer cells. (A) IC_{50} values were calculated by MTT assay results against K562 cancer cell. (B) IC_{50} values were calculated by MTT assay results against A549 cancer cell. Doxorubicin was used as a positive control. The values are expressed as the mean ± SD of triplicate tests.

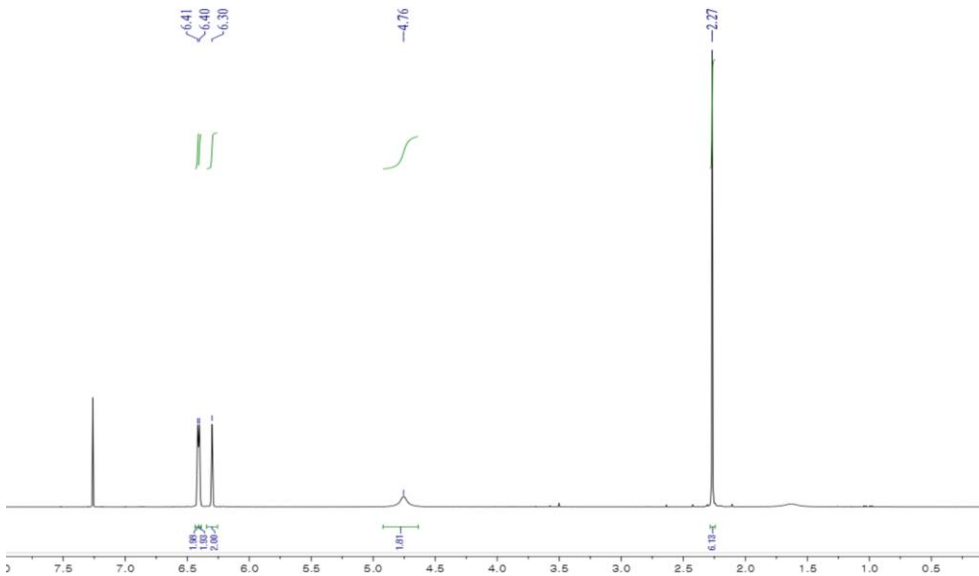

Figure B9. The ^{1}H NMR (400 MHz, $CDCl_3$) spectrum of **4**

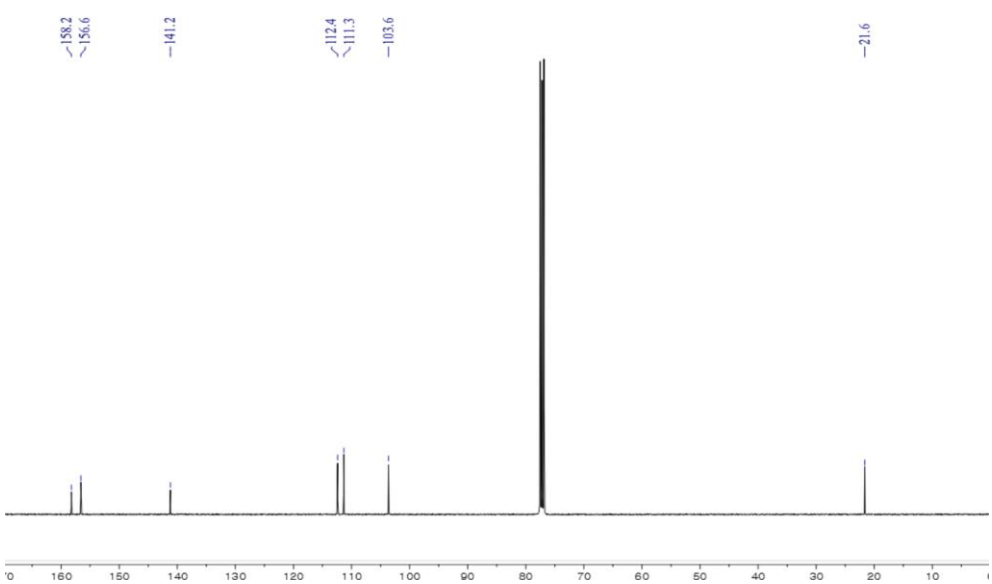

Figure B10. The ^{13}C NMR (100 MHz, $CDCl_3$) spectrum of **4**

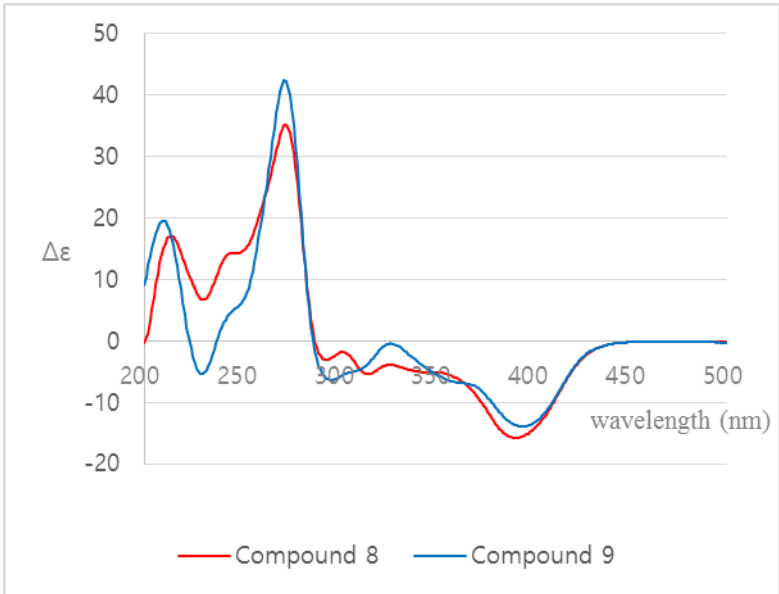

Figure B10. The CD spectra of **8** and **9**

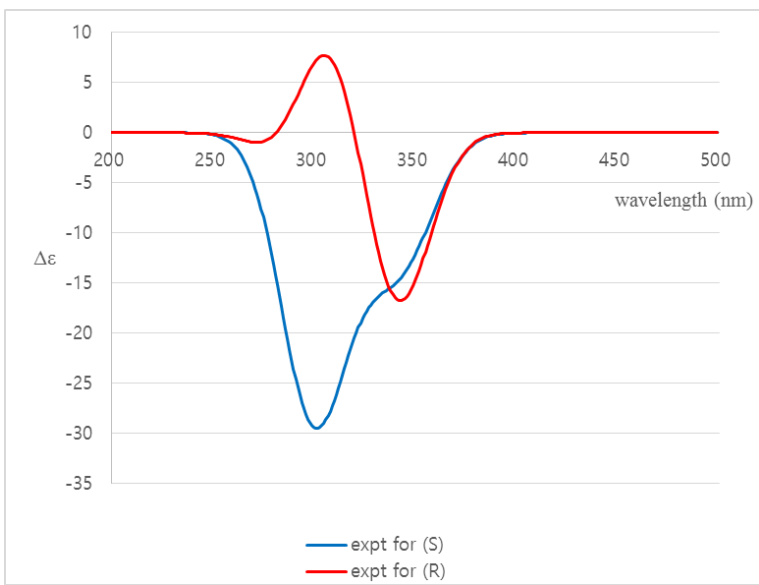

Figure B11. The ECD spectra of **8** and **9**

Table B1. The ^{13}C NMR data of **1–3** and **3c**

No	1[a]	2[a]	3[a]	3c[a]	1[b]	3[b]
	δ_C, type	δ_C, type	δ_C, type	δ_C, type	δ_C, type	δ_C, type
1	154.50, C	154.50, C			154.64, C	
2	108.13, CH	108.15, CH			110.31, CH	
3	156.65, C	156.69, C			154.64, C	
4	113.93, CH	113.89, CH			116.86, CH	
5	139.28, C	139.34, C			141.55, C	
6	115.83, CH	115.95, CH			117.83, CH	
7	157.59, C	157.60, C			159.05, C	
8	102.74, CH	102.79, CH			104.28, CH	
9	158.43, C	158.47, C			159.27, C	
10	109.82, CH	109.85, CH			111.81, CH	
11	140.05, C	140.10, C			141.85, C	
12	111.15, CH	111.21, CH			112.36, CH	
13	21.02, CH_3	21.13, CH_3			21.48, CH_3	
14	21.09, CH_3	21.06, CH_3			21.56, CH_3	
1′	42.67, CH_2		42.74, CH_2	42.80, CH_2	44.67, CH_2	44.72, CH_2
2′	24.78, CH_2		24.82, CH_2	25.18, CH_2	26.35, CH_2	26.35, CH_2
3′	28.96, CH_2		28.98, CH_2	29.22, CH_2	30.50, CH_2	30.51, CH_2
4′	52.98, CH		52.95, CH	52.88, CH	54.88, CH	55.50, CH
5′	64.45, CH_2		64.64, CH_2	66.11, CH_2	68.00, CH_2	66.02, CH_2
6′	170.53, C		170.37, C	ND	169.26, C	172.52, C
7′	73.31, CH		73.19, CH	72.26, CH	74.18, CH	75.58, CH
8′	26.84, CH		26.80, CH	26.57, CH	28.31, CH	28.73, CH
9′	19.13, CH_3		19.16, CH_3	17.78, CH_3	17.23, CH_3	19.65, CH_3
10′	19.51, CH_3		19.16, CH_3	19.57, CH_3	20.17, CH_3	19.81, CH_3
11′	41.01, CH_3		41.05, CH_3	41.46, CH_3	42.68, CH_3	42.07, CH_3
12′	41.01, CH_3		41.05, CH_3	41.46, CH_3	42.68, CH_3	42.07, CH_3
13′	160.24, C		160.39, C	161.47, C	161.95, C	162.08, C

[a] Data were obtained in DMSO-d_6. [b] Data were obtained in MeOH-d_4.

Table B2. Results of cytotoxicity tests

	IC_{50} (μM)	
Compounds	K562	A549
1	9.5	6.8
2	16	11
3	19	16
4	25	25
Doxorubicin	0.72	0.90

국문초록

해양 유래 진균 *Aspergillus*와 *Penicillium*의 이차대사물질에 대한 연구

서울대학교 대학원

약학과

천연물과학 전공

박 성 철

미생물 유래 생리 활성 천연물은 신약 개발 과정에 있어 핵심적인 역할을 해 왔다. 이와 동시에, 전통적 약물의 내성 증가로 인해 새로운 탄소 골격을 가진 생리 활성 화합물의 공급이 시급한 상황이다. 오늘날, 가장 인상적인 생리활성 천연물의 보고는 주로 미생물이며, 적절하게 개선된 미생물 및 화학 분석 관련 기술들로 독특하고 아직 조사되지 않은 미지 환경의 미생물 탐사가

가능해졌다.

그 중 해양 유래 진균은 1990년대부터 생리활성 이차 대사물질의 새로운 공급원으로 인식되어 왔다. 최근, 진균은 새로운 화합물의 주요 생산원 중 하나로 각광받고 있다. 기술적인 접근에서 미생물과 화학 관련 분석 기법들이 시대의 흐름에 맞춰 개선되고 발전함에 따라, 이전에는 탐사할 수 없던 독특하고 조사되지 않은 환경이 탐구되고 있다. 해양은 다양한 환경 조건을 가지고 있기 때문에, 해양에서 유래한 미생물들은 환경에 적응하기 위해 독특하고 흥미로운 생리활성 이차 대사물질을 생산한다. 따라서, 해양 유래 진균은 구조적으로 새로운 생리활성 천연물의 유망한 원천이 된다.

현재까지 해양 유래 진균으로부터 파생된 생리활성 천연물을 살펴보자면 다음과 같다. 세균감염을 치료하기 위한 페니실린의 대체품으로 널리 알려진 항생제인 *Acremonium chrysogenum* 유래 cephalosporin C, 비소세포 폐암에 대한 항암

활성으로 임상 3상을 진행중인 *Aspergillus* 유래 plinabulin, HSV-1과 HSV-2에 대한 항바이러스 활성을 가진 *Scytalidium* 유래 halovir A, 대장암 세포에 대한 항종양 활성을 가진 *Aspergillus* 유래 asperphenin A 등 다양한 활성과 구조를 갖는 해양 진균 유래 물질들이 있다.

이와 같은 이유로, 박사학위 기간 동안 해양 유래 진균이 생산하는 생리활성 이차대사물질의 연구를 진행하였다. 600 종 이상의 해양 유래 진균을 다양한 해양 환경에서 분리하였고, 그 중 *Aspergillus ochraceopetalifumis*, *Penicillium herquei*, *Aspergillus* sp. (F452)로부터 생리활성 이차 대사물질의 분리, 구조결정 연구를 진행하였다.

1. 해양 유래 진균 *Aspergillus ochraceopetaliformis*로부터 분리된 폴리케타이드와 아미노산 기원 유기 염, ochraceopetalin 연구.

제주도 인근 해안 해저에서 채집한 토양에서 *Aspergillus ochraceopetaliformis*를 분리하였다. 해당 해양 유래 진균에서 두 가지 생물유전자 기원 화합물이 혼합된 형태의 화합물인 ochraceopetalin (**1**)을 분리하였다. 화합물 **1**의 구조는 NMR, 고해상 ESI–MS, RI 등 분광학적 데이터의 다각적 분석에 기초해 폴리케타이드와 아미노산 생물유전자 기원의 천연물이 혼합된 형태의 새로운 유기 염 구조로 확립되었다. 비록 유기 염에서 음이온과 양이온 부분이 모두 유기물의 형태를 갖는 천연물들이 가끔 해양 유기체에서 발견되지만, 문헌조사 결과를 토대로, 화합물 **1**은 해양에서 유래한 진균에서 첫 번째로 발견된 음이온과 양이온이 유기물의 형태를 갖는 유기 염 화합물이다.

분광학적 분석과 화학적 분석을 종합한 결과, **1**의 구조는 전례 없는 구조 계열의 황화 디페닐에테르-아미놀아미노산 에스터 구아니디늄 소금으로 결정되었고, 1-sulfoxy-diorcinol (**2**)은 화합물 **1**의 음이온 부분에 상응하는 황화 디페닐에테르로 결정되었다. 화합물 1과 2는 각각 YMM 액체 배지 배양액과 쌀을 이용한 고체 배지 배양액에서 분리되었다. 화합물 1의 절대 구조는 연속적인 pH 의존적 물질 분해를 통하여 확인하였다. pH를 변화시킴으로써, 화합물**1**을 diorcinol (**4**)과 두 개의 입체 중심을 가진 ochraceopetaguanidine (**3**)으로 분리했다. 화합물**3**은 기본적인 가수 분해를 통하여 *N,N*-dimethaylvaline (**3a**)와 prolinol (**3b**)로 분리하였다. 화합물**3a**의 절대 구조는 PGME 방법에 의해 결정되었고, 화합물 **3b**의 절대 구성은 Marfey 반응을 사용하여 고정되었다. Ochraceopetalin (**1**)은 K562와 A549 세포에 대해 유의미한 세포독성을 보였다.

2. 해양 유래 진균 *Penicillium sp.*로부터 분리된 페날레논 계열 물질 구조 결정.

여섯 개의 신규 페날레논 유도체 (**5–10**)와 5개의 herqueinone 계열의 알려진 화합물은 해양에서 유래한 진균 *Penicillium* sp.로부터 분리되었다. 여섯 개의 신규 페날레논 유도체의 평면 구조는 NMR, MS 및 UV 분광기 등을 통해 얻은 분광학적 데이터의 결합 분석에 의해 구조 동정되었다. 신규 천연물 내 하이드로푸란 부분의 두 개의 입체 중심 (C-4 및 C-2')의 상대적 입체구조는 NOESY NMR 분석에 의해 규명되었다. 이러한 화합물의 절대 구조는 화학반응과 화학반응에 따른 반응물의 고유 광회전도에 기초하여 규명되었다. 화학반응에 대하여 조금 더 구체적으로 이야기 하자면, *ent*-peniciherqueinone (**5**)는 화학반응을 통하여 4-deoxy-*ent*-peniciherqueinone (**5a**)로 환원되었고, 다시 4-deoxy-9,11,12-

triacetyl-*ent*-peniciherqueinone (**5b**)로 아세틸화 되었다. 기지물질인 herqueinone (**12**)과 isoherqueinone (**13**) 역시 같은 화학반응을 통하여 환원 이후 아세틸화 되었다. 아세틸화된 기지물질 화합물**12**과 **13**의 고유 광회전도와 화합물 **5b**의 고유 광회전도를 비교하여 입체중심 C-2'의 절대구조를 규명하였다. 다른 화합물들과는 달리, oxopropylisoherqueinone A–B (**8–9**)와 triketone의 아세톤 첨가물 (**11**) 은 C-8 위치에서 2-케토-프로필 작용기를 가진다. C-4의 절대 구조는 화학 반응을 통하여 C-2'와 C-8에서 두 개의 입체 중심부를 제거한 뒤에 고유 광회전도를 비교하여 결정되었다. 4-hydroxysclerodin (**10**)과 화합물 11은 각각 중간 정도의 항혈관형성 및 항염증 활성을 나타냈으며, *ent*-peniciherqueinone (**5**)와 isoherqueinone (**13**) 은 독성을 나타내지 않는 동시에 중간 정도의 adipogenesis 유도 활성을 나타냈다.

3. 해양 유래 진균 *Aspergillus sp.*로부터 분리된 sortase-A 억제 활성 물질 연구.

SrtA 억제 활성 분석 결과를 토대로 해양 유래 진균 *Aspergillus* sp. (F452)로부터 8개의 기지 물질을 분리하였다. 균주 *Aspergillus* sp. (F452)는 제주도 인근 해안의 물에 잠긴 나무조각으로부터 분리되었다. 해당 균주는 쌀을 이용한 고체 배지 (쌀 200 g, 펩톤 2 g, 효모 추출물 2 g, 소금물 200 mL)에서 정적 상태로 6 주간 30℃ 조건으로 배양했다. 분리된 기지 물질은 다음과 같다: aspermytin A (**16**), versicomide A (**17**), versicoloid A (**18**), isochaetominines A–C (**19**–**21**), 14-*epi*-isochaetominine C (**22**), fumiquinazoline K (**23**). 알칼로이드 계열 화합물 (2–8)은 포도상구균에서 파생된 SrtA에 대하여 세포 생존성에 영향을 미치지 않은 동시에 약하거나 중간 정도의 억제 활성을 보였다. 반면, aspermytin A (**1**)는 146.0 μM의 IC_{50} 값을

보이며 SrtA에 대한 강력한 억제 활성을 보였다. 또한, 화합물 **1**은 섬유소 코팅된 표면에 대한 세균 밀착을 현저하게 감소시켰다. 현재의 결과로 보아, aspermytin A (**1**)의 기능적 메커니즘이 피브로넥틴에 대한 SrtA 매개 포도상구균 접착 억제와 밀접한 관련이 있음을 보이며, 결론적으로 해양 진균 유래 천연물 aspermytin A (**1**)는 잠재적 SrtA 억제제로 작용할 수 있음을 나타낸다.

주요어: 해양천연물, 해양유래 진균, *Aspergillus*, *Penicillium*, 구조결정

학번: 2015-23182

Publication List

1. Park, S. C.*; Lee, J.-H.*; Hwang, J.-Y.; Kwon, O.-S.; Liao, L.; Oh, D.-C.; Oh, K.-B.; Shin, J. Ochraceopetalin, a mixed biogenetic salt of polyketide and amino acid origins from a marine-derived *Aspergillus ochraceopetaliformis* fungus. *Mar Drugs*, **2021**, *19*, 413−423. *co-first author
2. Park, S. C.; Chung, B.; Lee, J.; Cho, E.; Hwang, J.-Y.; Oh, D.-C.; Shin, J.; Oh, K.-B. Sortase A-inhibitory metabolites from a marine-derived fungus *Aspergillus* sp. *Marine Drugs*, **2020**, *18*, 359−367.
3. Park, S. C.; Julianti, E.; Ahn, S.; Kim, D.; Lee, S. K.; Noh, M.; Oh, D.-C.; Oh, K.-B.; Shin J. Phenalenones from a marine-derived fungus *Penicillium* sp. *Marine Drugs*, **2019**, *17*, 176−191.
4. Hwang, J.-Y.; Chung, B.; Kwon, O.-S.; Park, S. C.; Cho, E.; Oh, D.-C.; Shin, J.; Oh, K.-B. Inhibitory effects of epipolythiodioxopiperazine fungal metabolites on isocitrate lyase in the glyoxylate cycle of *Candida albicans*. *Marine Drugs*, **2021**, *19*, 295−304.
5. Byun, W. S.; Bae, E. S.; Park, S. C.; Kim, W. K.; Shin, J.; Lee, S. K. Antitumor activity of asperphenin B by induction of apoptosis and regulation of glyceraldehyde-3-phosphate dehydrogenase in human colorectal cancer cells. *Journal of Natural Products*, **2021**, *84*,

683−693.

6. Park, J. S.; Cho, E.; Hwang, J.-Y.; Park, S. C.; Chung, B.; Kwon, O.-S.; Sim, C. J.; Oh, D.-C.; Oh, K.-B.; Shin, J. Bioactive bis(indole) alkaloids from a *Spongosorites* sp. sponge. *Marine Drugs*, **2021**, *19*, 3−16.
7. Hwang, J.-Y.; Park, S. C.; Byun, W. S.; Oh, D.-C.; Lee, S. K.; Oh, K.-B.; Shin, J. Bioactive bianthraquinones and meroterpenoids from a marine-derived *Stemphylium* sp. fungus. *Marine Drugs*, **2020**, *18*, 436−454.
8. Ahn, S.; Jang D. M.; Park, S. C.; An, S.; Shin, J.; Han, B. W.; Noh, M. Cyclin-dependent kinase 5 inhibitor butyrolactone I elicits a partial agonist activity of peroxisome proliferator-activated receptor γ. *Biomolecules*, **2020**, *10*, 275−291.
9. Hwang, J.-Y.; Lee, J.-H.; Park, S. C.; Lee, J.; Oh, D.-C.; Oh, K.-B.; Shin, J. New peptides from the marine-derived fungi *Aspergillus allahabadii* and *Aspergillus ochraceopetaliformis*. *Marine Drugs*, **2019**, *17*, 488−500.